UNIVERSITY OF CINCINNATI

FINAL REPORT

AN INVESTIGATION OF BLEED CONFIGURATIONS AND THEIR EFFECT ON SHOCK WAVE/BOUNDARY LAYER INTERACTIONS

Awatef Hamed
Principal Investigator

NASA Grant NAG3-1213LE
10 October 1990 - 26 June 1995

Submitted to

Dr. John D. Saunders, Project Monitor
NASA Lewis Research Center, MS 86-7
12000 Brookpark Avenue
Cleveland, OH 44135

September 7, 1995

TABLE OF CONTENTS

AN INVESTIGATION OF BLEED CONFIGURATIONS AND THEIR EFFECT ON SHOCK WAVE/BOUNDARY LAYER INTERACTIONS

ABSTRACT

The design of high efficiency supersonic inlets is a complex task involving the optimization of a number of performance parameters such as pressure recovery, spillage, drag, and exit distortion profile, over the flight Mach number range. Computational techniques must be capable of accurately simulating the physics of shock/boundary layer interactions, secondary corner flows, flow separation, and bleed if they are to be useful in the design. In particular, bleed and flow separation, play an important role in inlet unstart, and the associated pressure oscillations. Numerical simulations were conducted to investigate some of the basic physical phenomena associated with bleed in oblique shock wave boundary layer interactions that affect the inlet performance.

INTRODUCTION

The experimental measurements in most mixed compression inlet tests are limited to the static pressures over the inner surfaces and total pressure recovery at the engine face [1]. In a few experimental studies, some boundary layer profile measurements were obtained from pitot pressure rakes ahead and behind the shock/boundary layer/bleed regions [2-5]. Comparisons of flow computational results with the experimental measurements in supersonic inlets revealed discrepancies in the prediction of shock locations, and velocity profiles after the interactions [6-8]. A better understanding of these interactions is essential to improving inlet performance predictions.

The purpose of the present investigation is to characterize the flow field in the oblique shock wave/boundary layer/bleed interaction region and to develop a basic understanding of flow separation control mechanisms. The flow computations were carried out for different bleed configurations, and shock strengths. The solution domain extended across the interaction, and inside the bleed slots. A systematic investigation was conducted to determine the effects of the bleed location relative to the shock, slot width, depth and slot angle, on the flow characteristics and the bleed performance parameters at different bleed mass flow rates [9-13]. The obtained flow characteristics inside the bleed port were compared with the recently obtained experimental measurements [14, 15] with and without incident shock at NASA Lewis Research Center.

The results of the bleed investigation were presented in two formats, one giving the flow details in order to understand the nature of the interaction, and another giving the bleed performance parameters such as the discharge coefficient and total pressure recovery which are useful to the designer. The detailed pressure and Mach number contours as well as velocity profiles within the interaction zone and inside the bleed slots revealed the

important flow physics and the mechanisms affecting the flow separation and demonstrated the variation in the bleed flow velocities, and pressure gradient distribution across the bleed port. On the other hand, the bleed performance results in the form of bleed efficiency and pressure recovery at different plenum pressures and for different bleed configurations is useful in selecting the optimum bleed configuration in inlet designs.

ANALYSIS

The solution domain for the compressible Navier-Stokes equations extended inside the bleed slot and upstream and downstream the interaction region. The change in bleed (suction) mass flow was accomplished in the numerical investigation through changing the static pressure at the bottom of the bleed slot over a wide range covering choked and unchoked flow conditions. The PARC code [16] was selected after it was validated [10] for the case of separated SWTBLI at Mach 2.96 through comparison with Law's [17] experimental data. The mesh spacing was varied in both the streamwise, and normal directions to capture the important flow characteristics in the shock wave boundary layer interactions and inside the bleed port.

SUMMARY

1. Effect of Normal Bleed Slot Location in Laminar Boundary Layer/Shock Interaction

A study was conducted for bleed through a normal slot at three locations upstream, across and downstream the shock [9]. The external flow conditions were $M_\infty = 2.0$, $Re_\infty = 1.812\times10^6$/ft., and an impingement oblique shock angle of 32.585 deg., corresponding to the experimental test conditions of Hakinen et al. [18] without bleed. The bleed slot width of D = 0.011 inch was equal to the boundary layer displacement thickness δ^*before the interaction at x = 1.96 inch from the flat plate leading edge ($D/\delta^*=1$) and the slot depth was three times its width (L/D = 3.0). For a given plenum pressure at the slot exit, it was found that the shock induced flow separation on the plate surface was eliminated in the across the shock bleed configuration, but only reduced for the other two bleed locations. The results of this investigation were published in the Journal of Propulsion and Power, Vol. 11, No. 1, pp. 42-48, Jan.-Feb. 1995, and presented as AIAA Paper 91-2014 entitled "The Effect of Bleed Configuration on Shock Laminar Boundary Layer Interaction," at the Joint Propulsion Conference in Pasadena, CA, June 14-16, 1991 (Appendix A).

2. Effect of Bleed Mass Flow Through a Normal Slot in Shock-Wave/Turbulent-Boundary-Layer Interaction

A study was completed to investigate the effect of bleed mass flow in a normal slot across the incident oblique shock impingement point. The external flow conditions were

$M_\infty = 2.96$, $Re_\infty = 1.2\times10^7$/ft., and impinging oblique shock angle of 25.84 degree, corresponding to the experimental test conditions of Law [17] without bleed. The bleed slot width was D = 0.0213 ft. which is equal to 1.617 times the boundary layer thickness δ upstream of the interaction at x = 0.9 ft. ($D/\delta = 1.617$), and the bleed mass flow varied up to choked conditions (30% of the incoming boundary layer mass flow). The computed bleed results [10] indicated a complex expansion and compression wave structure across the slot opening due to bleed flow entrainment. The net effect of the bleed on the flow downstream is to reduce the momentum and displacement thickness and to move the reflected shock closer to the surface. The reduction in the momentum thickness downstream of the interaction increased with the increase in bleed mass flow, but eventually plateaud. This work was published in the Journal of Propulsion and Power, Vol. 10, No. 1, pp. 79-81, Jan.-Feb. 1995, and presented as AIAA Paper 92-3085 entitled "An Investigation of Shock/Turbulent Boundary Layer/Bleed Interaction," at the Joint Propulsion Conference in Nashville, Tennessee, July 6-8, 1992 (Appendix B).

3. Effect of Normal Bleed Configuration

A parametric study was conducted to determine the effect of normal bleed slot configuration on shock wave turbulent boundary layer interactions [11]. The external flow conditions were $M_\infty = 2.96$, $Re_\infty = 1.2\times10^7$/ft. and oblique shock impingement angle of 25.84 degree. Different slot width, depth and inclination were investigated. The results of the parametric investigation of the normal bleed slot configuration in STBLI were presented as AIAA Paper 93-0294 entitled "A Parametric Study of Bleed in Shock Wave Boundary Layer Interactions," at the 31st Aerospace Sciences Meeting in Reno, Nevada, January 11-14, 1993 (Appendix C).

(a) Slot Width

Flow computational results were obtained over a wide range of bleed mass flows for three different slot widths 0.8, 1.6 and 3.2 times the boundary layer thickness upstream of the interaction [14]. The results indicate that the bleed discharge coefficient and total pressure recovery are not very sensitive to the bleed slot width.

(b) Slot Aspect Ratio

Two slot aspect ratios = 3 and 6 were investigated for the intermediate slot width. Both the discharge coefficient and the momentum thickness downstream of the interaction were sensitive to changes in L/D and both improved as the aspect ratio increased.

(c) Slot Location

Additional flow computations were performed for three different bleed locations relative to the shock impingement point for the widest bleed slot ($D/\delta = 3.2$) over a range of bleed mass flows up to choked conditions. The upstream, across, and downstream bleed slot locations corresponded to the slot center at -D, 0 and +D relative to the shock impingement point. The results indicate that across the shock bleed gives the largest reduction in the momentum thickness downstream of the interaction at all bleed mass flows.

However, the total pressure recovery at the bleed slot exit was higher for downstream bleed.

4. Effect of Bleed Slot Angle and Location

Detailed flow computations [12] were performed for 20° slanted and 90° normal slots at three different locations upstream, across and downstream of the inviscid shock impingement location relative to the flat plate surface at $M_\infty = 2.96$, $Re_\infty = 1.2\times10^7$/ft. and oblique shock impingement angle of 25.84 deg. The slot opening was kept the same for both slots with $D/\delta = 0.8085$ for the normal slot and 0.2766 for the 20° slanted slot. The results indicate a large recirculating flow region inside the normal slot but not in the 20° slanted slot causing the choked discharge coefficient to more than triple. Bleed through the slanted slot produced redeveloping boundary layer downstream, with a higher friction coefficient. The largest reduction in the boundary layer momentum and displacement thickness downstream of the interaction were associated with the normal slot bleed across the shock.

The slanted bleed discharge coefficient was found to be more sensitive to bleed location and had the highest value when the bleed slot was located upstream of the shock. Normal bleed across the shock resulted in the largest reductions in both boundary layer displacement and momentum thickness downstream of the interaction. The results of this investigation will appear in Journal of Propulsion and Power, Vol. 11, No. 6, Nov.-Dec.. 1995 entitled "Shock-Wave Boundary-Layer Interactions with Bleed, Part 2: Effect of Slot Location," and were presented as AIAA Paper 93-2992 entitled "An Investigation of Shock Wave Turbulent Boundary Layer Interaction with Bleed Through Slanted Slots," in Orlando, Florida, July 1993 (Appendix D).

5. Plenum Interactions

The numerical investigation of shock-wave/turbulent boundary-layer/bleed interactions was conducted with a plenum at the end of the bleed slot [13]. The results were compared with the experimental data obtained by Willis et al. [14] and Davis et al. [15] in the 1'x1' supersonic tunnel at NASA Lewis Research Center. In this study the external flow conditions were $M_\infty = 2.46$, $Re_\infty = 1.81\times10^7$/ft., and the ratio of the slot width was one third the incoming boundary layer thickness before the interaction (D/δ = 1/3). The flow simulations were performed over a range of plenum pressures to simulate increased bleed mass flow rates up to choking for two shock strengths corresponding to shock generator wedge angle of 0° and 8°. The computational results with and without the plenum indicated that the interaction between the plenum and the recirculating flow inside the slot caused fluctuations in the bleed mass flow at the slot exit. These variations were associated with the changes in the size of the separated flow regions over both slot walls at exit. However, the bleed mass flow at the slot opening did not fluctuate and remained steady at the mean value of the exit mass flow. The computed bleed mass flow at the slot inlet were in good agreement with the experimental measurements. These results were presented in AIAA Paper 95-0033, "Flow Characteristics is in Boundary Layer Bleed Slots

with Plenum," at the 33rd Aerospace Sciences Meeting, in Reno, Nevada, January 9-12, 1995 (Appendix E).

REFERENCES

1. Hamed, A. and Shang, J., "Survey and Assessment of Validation Data Base for Shock-Wave/Boundary-Layer Interactions in Supersonic Inlets," AIAA Paper 89-2939, July 1989. To appear in the Journal of Propulsion and Power, October 1991.

2. Hingst, W.R. and Johnson, D.F., "Experimental Investigation of Boundary Layers in an Axisymmetric, Mach 2.5 Mixed Compression Inlet," NASA TMX-2903, 1973.

3. Fukuda, M.K., Hingst, W.G. and Reshotko, E., "Control of Shock Boundary Layer Interactions by Bleed in Mixed Compression Inlets," NASA CR 2595, 1975.

4. Fukuda, M.K., Hingst, W.G. and Reshotko, E., "Bleed Effects on Shock/Boundary-Layer Interactions in Supersonic Mixed Compression Inlets," Journal of Aircraft, Vol. 14, No. 2, February 1977, pp. 151-156.

5. Carter, T.D. and Spong, E.D., "High-Speed Inlet Investigation. Vol. I - Description of Program and Results; Vol. II - Data Summary," AFFDL-TR-77-105, November 1977.

6. Knight, D.D., "Calculation of High Speed Inlet Flows Using the Navier-Stokes Equations," Vol. I: Description of Results," AFFDL-TR-79-3138, February 1980.

7. Knight, D.D., "Improved Calculation of High Speed Inlet Flows. Part I - Numerical Algorithm," AIAA Journal, Vol. 19, No. 1, January 1981, pp. 34-41, and "Part II - Results," AIAA Journal, Vol. 19, No. 2, February 1981, pp. 172-179.

8. Saunders, J.D. and Keith, T.G. Jr., "Results from Computational Analysis of a Mixed Compression Supersonic Inlet," AIAA Paper 91-2581, 1991.

9. Hamed, A. and Lehnig, T., "An Investigation of Oblique Shock/Boundary Layer/Bleed Interaction," Journal of Propulsion and Power, Vol. 8, No. 2, 1992, pp. 418-424.

10. Hamed, A., Shih, S. and Yeuan, J.J., "Investigation of Shock/Turbulent Boundary Layer/Bleed Interactions," Journal of Propulsion and Power, Vol. 10, No. 1, Jan.-Feb. 1995, pp. 79-81.

11. Hamed, A., Shih, S.H. and Yeuan, J.J., "A Parametric Study of Bleed in Shock Boundary Layer Interactions," AIAA Paper 93-0294, Cincinnati, Ohio, January 1993.

12. Hamed, A., Yeuan, J.J. and Shih, S.H., "Shock-Wave Boundary-Layer Interactions with Bleed, Part 2: Effect of Slot Location," to appear in Journal of Propulsion and Power, Vol. 11, No. 6, November-December 1995.

13. Hamed, A., Yeuan, J.J. and Jun, Y.D., "Flow Characteristics in Boundary Layer Bleed Slots with Plenum," AIAA Paper 95-003, 33rd Aerospace Sciences Meeting and Exhibit, Reno, Nevada, January 9-12, 1995.

14. Willis, B., Davis, D. and Hingst, W., "Flow Coefficient Behavior for Boundary-Layer Bleed Holes and Slots," AIAA Paper 95-0031, 33rd Aerospace Sciences Meeting, Reno, Nevada, January 9-13, 1995.

15. Davis, D., Willis, B. and Hingst, W., "Flowfield Measurements in Slot-Bleed Oblique Shock-Wave and Turbulent Boundary-Layer Interaction," AIAA Paper 95-0032, 33rd Aerospace Sciences Meeting, Reno, Nevada, January 9-13, 1995.

16. Cooper, G.K. and Sirbaugh, J.R., "PARC Code: Theory and Usage," AEDC-TR-89-15, 1989.

17. Law, C.H., "Supersonic Turbulent Boundary-Layer Separation," AIAA Journal, Vol. 12, June 1974, pp. 794-797.

18. Hakkinen, R.J., Greber, I., Trilling, L. and Aberbanel, S.S., "The Interaction of an Oblique Shock Wave with a Laminar Boundary Layer," NASA Memo 2-18-58W, March 1959.

APPENDIX A

JOURNAL OF PROPULSION AND POWER
Vol. 11, No. 1, January–February 1995

Effect of Bleed Configuration on Shock/Laminar Boundary-Layer Interactions

A. Hamed*
University of Cincinnati, Cincinnati, Ohio 45221
and
T. Lehnigt†
Cold Jet, Inc., Loveland, Ohio 45140

The flowfield characteristics are simulated numerically in an oblique shock wave/laminar boundary-layer interaction for three different bleed configurations. The numerical solution for the flowfield is obtained for the strong conservation-law form of the two-dimensional compressible Navier-Stokes equations using an implicit scheme. The computations model the flow in the interaction region and inside the bleed slot for an impinging oblique shock of sufficient strength to cause boundary-layer separation on a flat plate boundary layer. The computed results are presented for a normal bleed slot at three different locations: 1) upstream, 2) across, and 3) downstream of the shock impingement point. The detailed flow characteristics in the interaction zone and inside the bleed slot are compared for the three cases. The resulting surface pressure and shear stress and boundary-layer displacement and momentum thickness distributions are also compared for the three bleed cases and for the shock wave/boundary-layer interaction without bleed.

Introduction

AIR bleed systems are used for controlling the shock wave/boundary-layer interactions when operating at supersonic speeds. Proper bleed system design is particularly important for the efficient and stable operation of mixed compression supersonic inlets.[1] The fundamental objectives of supersonic inlet bleed system design are to provide good aerodynamic flow characteristics with minimum boundary-layer bleed.[2,3] The elimination or reduction of separation in shock wave/boundary-layer interactions[4] is essential for controlling the pressure loss and maintaining a stable flowfield in supersonic inlets. Minimizing the bleed required to achieve boundary-layer control allows the penalties associated with incorporation of a supersonic inlet bleed system to be minimized as well. These penalties include a loss of inlet mass flow and an increase in drag due to venting of the bleed air into the freestream. Ideally, removal of only that portion of the low-momentum boundary layer needed to inhibit separation is desired.

Comparisons of internal flow computational results[5-7] with the experimental measurements in supersonic inlets[4,8] revealed reasonable agreement between the computed and measured surface pressures upstream of the ramp bleed. However, discrepancies in the predicted shock locations and velocity profiles were observed downstream of shock/boundary-layer interactions with bleed.

Hamed and Shang[1] reviewed the existing experimental data base for shock wave/boundary-layer interactions in supersonic inlets and other related configurations. According to this survey, there is enough experimental evidence[9-14] to indicate that local bleed can control flow separation in shock wave/boundary-layer interactions. There are disagreements,[1] however, among the different experimental results regarding the effects of bleed hole size,[13,14] and location relative to the shock.[9-12] Strike and Rippy[9] measured the surface pressure in the interaction zone of an oblique shock wave impinging a turbulent boundary layer over a flat plate, with suction. They determined that less suction is required to control separation, when applied upstream of the shock. Seebaugh and Childs[10] investigated experimentally the axisymmetric flow in the interaction region of the boundary layer inside a duct. Contrary to the conclusions of Strike and Rippy,[9] suction within the interaction region was found to be more effective in suppressing the effects of separation.

The purpose of this study is to clarify the effect of bleed location on controlling flow separation in shock wave/boundary-layer interactions. Numerical computations are performed to determine the flow characteristics in the interaction zone of an oblique shock wave/boundary layer, and within a normal bleed slot, upstream, downstream, and across the oblique shock impingement point.

Computational Details

The bleed study is conducted initially for laminar flow, in order to allow the flowfield characterization to be accomplished without the uncertainties associated with turbulence modeling. The partial differential equations used to describe the flow are the time-dependent compressible Navier-Stokes equations in strong conservation law form. The flow is treated as a perfect gas with molecular dynamic viscosity given by Sutherland's law, and a gas conductivity based on a constant Prandtl number. An implicit approximate factorization technique[15] is used in the numerical solution of the governing equations. Prior to the bleed investigation, the code[16,17] has been validated for laminar shock wave/boundary-layer interactions both for separated and unseparated flows[18] by comparing the computational results with Hakkinen's experimental data.[19]

The solution is obtained in a domain that includes the interaction region and the interior of the bleed port as shown schematically in Fig. 1. The specified static pressure at the bottom of the bleed slot simulates the plenum pressure that controls the bleed level for a given slot and flow configuration. Zero-order interpolations are applied for the rest of the flow variables at the bottom of the bleed slot. The no-slip condi-

Presented as Paper 91-2014 at the AIAA/SAE/ASME/ASEE 27th Joint Propulsion Conference, Sacramento, CA, June 24–26, 1991; received Aug. 2, 1991; revision received May 4, 1993; accepted for publication May 9, 1994.

*Professor, Department of Aerospace Engineering and Engineering Mechanics. Fellow AIAA.
†Senior Project Engineer. Member AIAA.

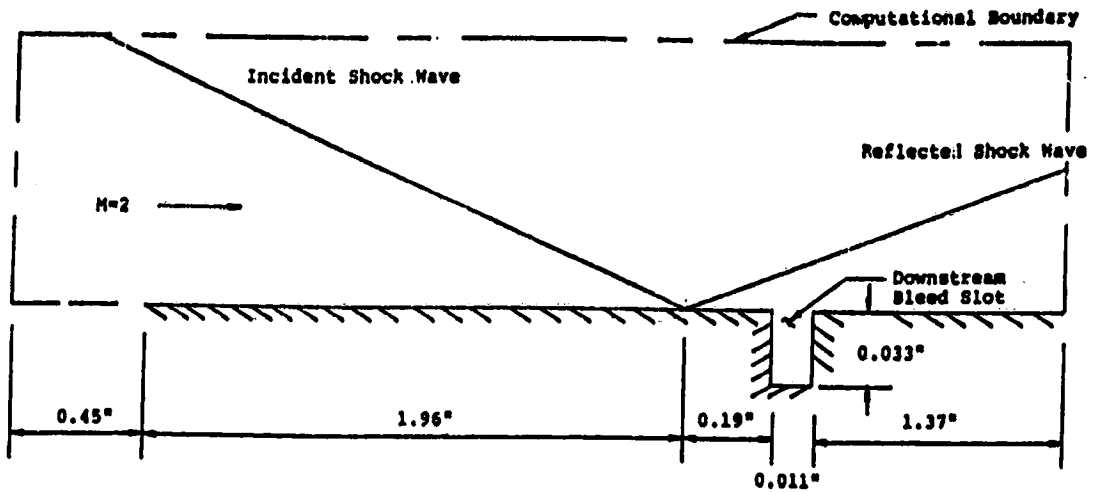

Fig. 1 Schematic of the solution domain for the shock-wave/boundary-layer/bleed interaction.

tion, adiabatic wall, and zero normal pressure gradients are specified at the solid surfaces. The impinging shock wave is explicitly introduced at the upper boundary using the Rankine-Hugoniot relations. Zero-order extrapolation of the flow variables is enforced at the downstream boundary, which is carefully positioned such that all generated or reflected shocks exit through it.

The orthogonal grid spacing was varied in both the streamwise and normal directions to capture the important flow characteristics in the shock wave/boundary-layer interaction zone and inside the bleed slot.[18] The computational grid consisted of (243 × 107) mesh points in the streamwise and normal directions, respectively, with grid clustering at the plate and around the slot walls. The following grid distribution was implemented in the solution of the shock-wave/laminar boundary-layer interactions with bleed:

$$\Delta Y_j = 0.0375 \qquad 77 \le j \le 107 \tag{1}$$

$$\Delta Y_j = 1.125\Delta Y \qquad 36 \ge j \ge 76 \tag{2}$$

$$\Delta Y_j = 1.5625 \times 10^{-4} \qquad 28 \le j \le 35 \tag{3}$$

$$\Delta Y_j = 1.125\Delta Y_{j-1} \qquad 1 \le j \le 27 \tag{4}$$

where $j = 1$ represents the bottom, and $j = 32$ the top of the bleed slot.

The grid inside the bleed slot consisted of (34 × 32) mesh points in the streamwise and normal direction, respectively. Stretching was used in the streamwise direction, in order to cluster the grid points inside, and near the slot as follows:

$$\Delta X_i = 0.03 \qquad i \le I - 64, \quad I + 63 \le i \tag{5}$$

$$\Delta X_i = 1.5625 \times 10^{-4} \qquad I - 20 \le i \le I - 13, \quad I + 13 \le i \le I + 20 \tag{6}$$

$$\Delta X_i = 1.125\Delta X_{i+1} \qquad I - 21 \ge i \ge I - 63, \quad I + 12 \ge i \ge I + 1 \tag{7}$$

$$\Delta X_i = 1.125\Delta X_{i-1} \qquad I - 12 \le i \le I, \quad I + 21 \le i \le I + 62 \tag{8}$$

where $i = I$ represents the grid at the center of the bleed slot.

The flow solution convergence monitoring was based on the shear stress at the plate surface τ_w, as follows:

$$\epsilon = \left| \frac{\tau_w^n - \tau_w^{n-1}}{\tau_w^n} \right|$$

The specified convergence criterion was $\epsilon \le 10^{-4}$ for the evaluation points at $X < X_{sh}$, and $\epsilon \le 10^{-5}$ for the evaluation points located at $X > X_{sh}$ to account for the different rates for convergence at the different locations from the plate leading edge (where X_{sh} is the tested shock impingement point location).

Results and Discussion

Results are presented for the computed flowfield in the interaction zone of an oblique shock/laminar boundary-layer interaction with bleed applied through a normal slot at three different locations relative to the shock impingement point. The freestream conditions are 2.0 Mach number and 2.96×10^5 Reynolds number, based on the shock impingement location, $x = 1.96$ in., from the flat plate leading edge. The shock angle of 32.585 deg corresponds to the test conditions of Hakkinen et al.[19] for the separated flow case. The computations are performed at the same freestream conditions and shock strength, with bleed applied through a normal slot that is 0.011 in. wide and 0.033 in. deep. The slot width was equal to the boundary-layer displacement thickness before the interaction, and its depth-to-width ratio of 3 is selected based on the experimental results of the optimization study by Syberg and Koncsek.[2] The slot was positioned at three different locations, upstream, downstream, and across the shock impingement point. For across the shock bleed, the slot center was positioned directly at the shock impingement point with the flat plate surface ($X_{sh} = 1.96$ in.). The downstream bleed case was chosen such that the centerline of the bleed slot is at the location of the maximum computed surface shear stress in the separated flow case without bleed ($x = 2.167$ in.). The upstream bleed location was similarly selected at the opposite side relative to the shock impingement point with the centerline at $x = 1.753$ in. from the leading edge. The slot base pressure was maintained at the same value (0.42 of preshock pressure), which resulted in bleed mass rates of 3.42, 4.65, and 5.05% of the upstream boundary-layer mass flow for upstream, across, and downstream bleed cases, respectively. Some of the computed results for downstream bleed configuration were reported earlier.[18] Here, the results of the flowfield computations in the shock/boundary-layer/bleed interaction zone are presented for the upstream and across the shock bleed. The computed results are compared for the three bleed locations and for the case with no bleed.

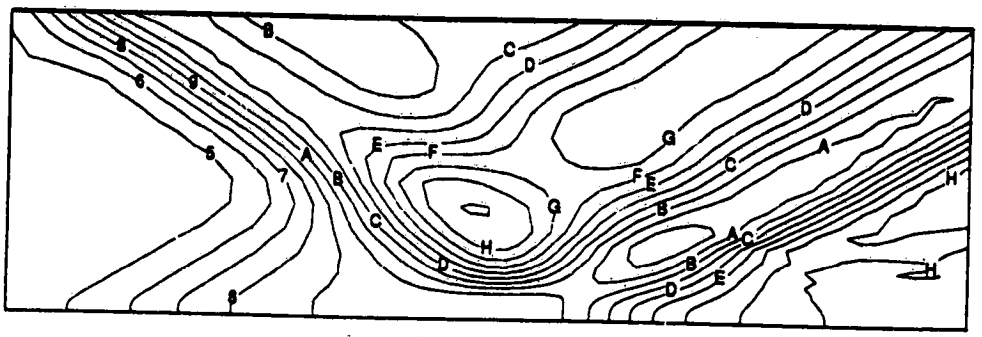

Fig. 2 Pressure contours for the no-bleed case.

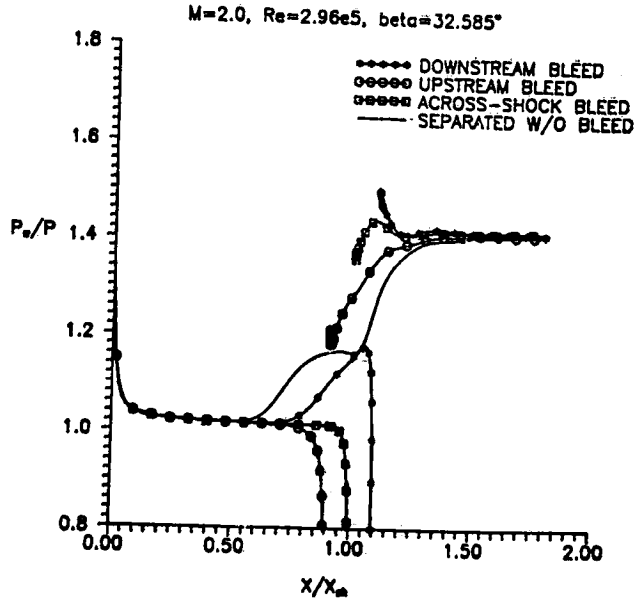

Fig. 3 Comparison of surface pressure distribution for the different bleed configurations.

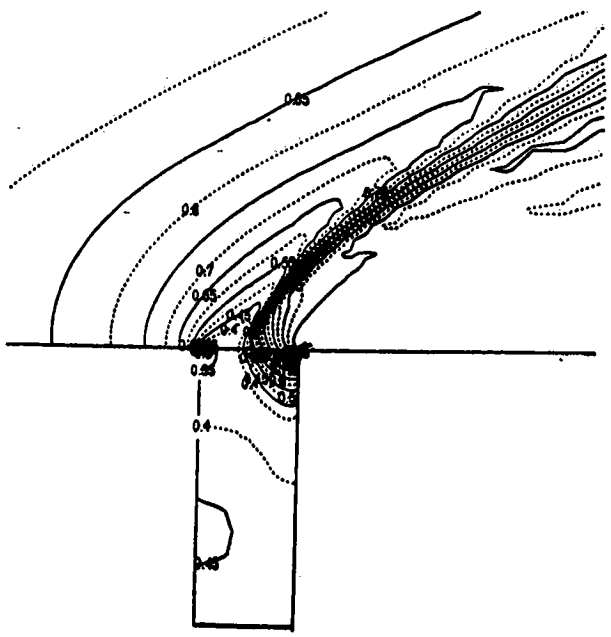

Fig. 4 Pressure contours for upstream bleed.

Figure 2 shows the pressure distribution near the interaction zone for the no bleed case. The incident shock and the separation and reattachment shocks are seen in this figure. Figure 3 shows the plate surface pressure distribution of the three bleed cases and for no bleed. The wall pressure distribution shows a significant reduction in the length of the interaction region compared to the nonbleed case, and an elimination of the pressure plateau in all three bleed configurations. Furthermore, the pressure ratio downstream is slightly increased over the nonbleed interaction case. These observations agree with previous reports on the effect of bleed, as discussed by Hamed and Shang.[1] Figure 3 clearly shows that there is a big difference in the static pressure, at the corner of the flat plate surface and the downstream slot wall for the three bleed cases. This pressure is lowest (p/p_∞ = 1.22) for the upstream bleed case, and highest (p/p_∞ = 1.5) for the downstream bleed case with the across the shock pressure value in between (p/p_∞ = 1.36). As for the static pressure distribution downstream of the bleed slot, there is an abrupt pressure drop for a short distance followed by a gradual pressure rise in the upstream bleed case. However, in the downstream bleed case, the static pressure over the plate surface drops downstream of the bleed slot, whereas in the across the shock bleed case the pressure rises first, then drops slightly.

One can see that in both the upstream and across the shock bleed cases, the pressure starts to drop before the slot opening and reaches a value of $p/p_\infty \sim 0.8$ at the intersection of the flat plate with the upstream slot wall. In the case of downstream bleed, the pressure initially builds up on the plate surface upstream of the slot opening, reaching a value slightly higher than that of the plateau pressure in the case of separated flow without bleed ($p/p_\infty \sim 1.2$), followed by a very sharp drop to 0.8 at the upstream slot wall corner. In all three cases, there is an initial moderate pressure drop over the first

part of the slot opening followed by a sharp rise across a shock emanating inside the slot as shown for the upstream bleed pressure contours of Fig. 4.

The Mach number contours are presented in Figs. 5–7. The contours indicate a choked flow in all three bleed cases. The subsonic boundary-layer flow entering the bleed slot initially accelerates due to the separation bubble at the upstream wall of the bleed slot that acts as a converging-type constriction. After passing through the convergent section of the constriction, the now choked flow goes through a brief expansion region where the flow is further accelerated. The flow then decelerates towards the slot exit as it reaches an effectively constant area downstream of the separation bubble.

The velocity distributions across the slot opening are shown in Figs. 8–10. Generally the normal velocity component increases gradually across the slot opening and reaches a plateau $v/U_\infty \sim -0.3$ somewhere in the downstream half of the bleed slot, with a slight increase further near the downstream slot wall in the two cases of across the shock and downstream

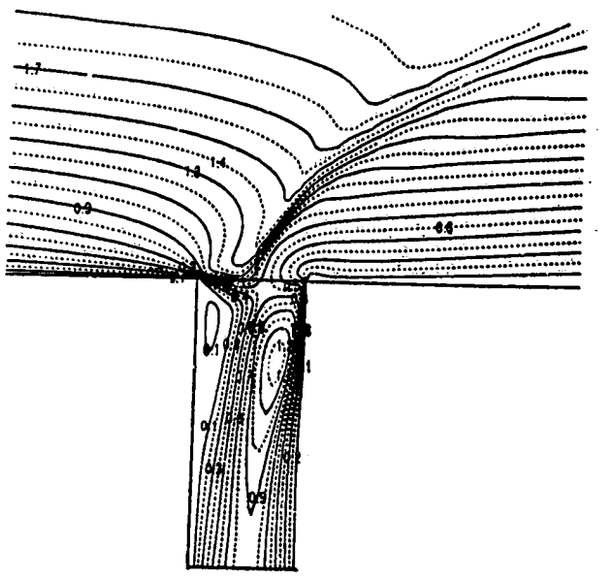

Fig. 5 Mach number contours for upstream bleed.

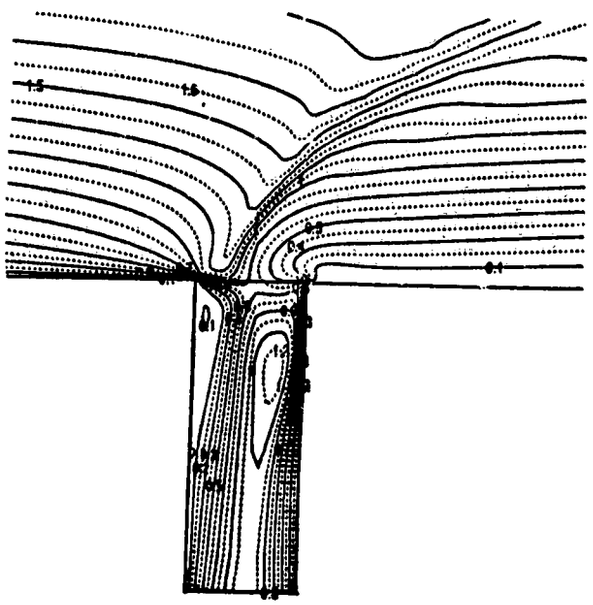

Fig. 6 Mach number contours for across the shock bleed.

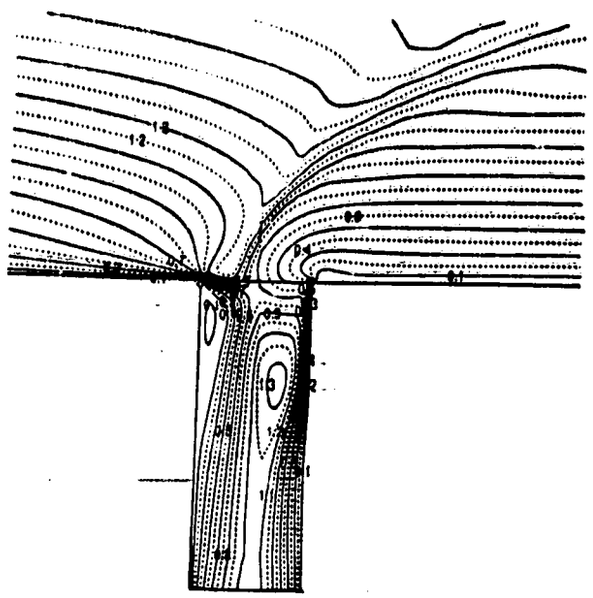

Fig. 7 Mach number contours for downstream bleed.

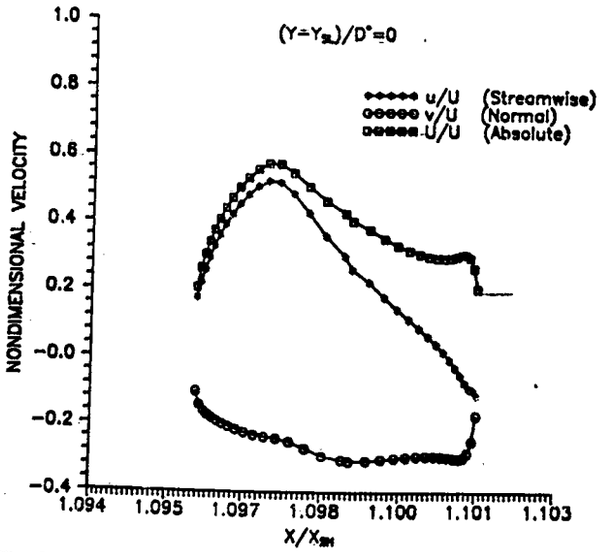

Fig. 8 Velocity distribution across slot opening for upstream bleed.

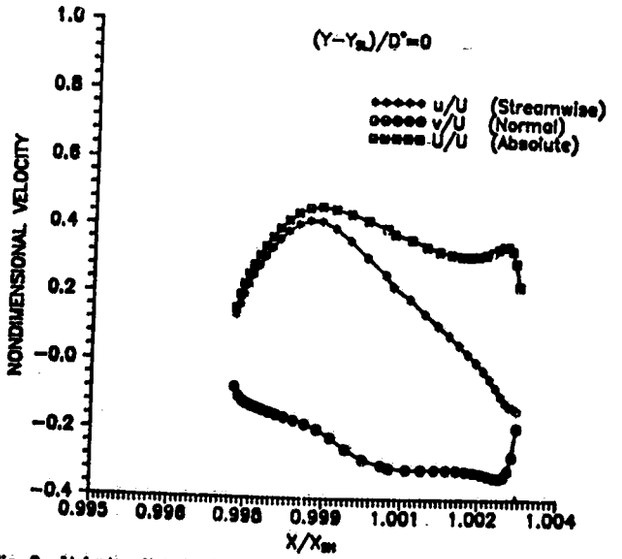

Fig. 9 Velocity distribution across slot opening for across the shock bleed.

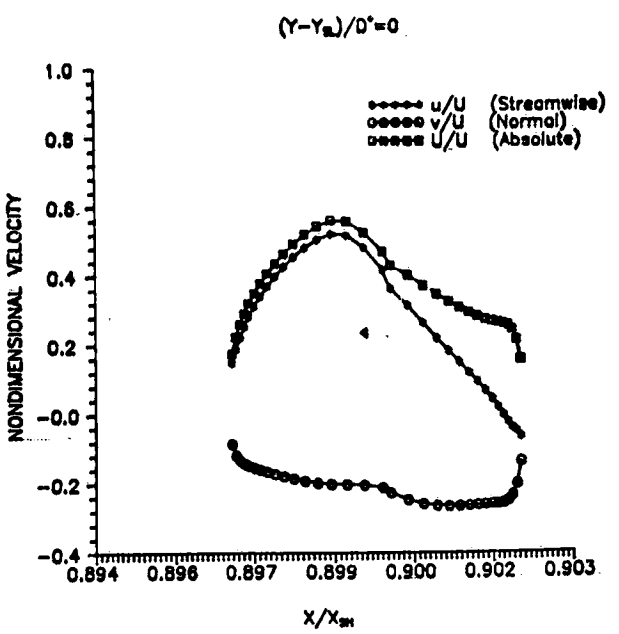

Fig. 10 Velocity distribution across slot opening for downstream bleed.

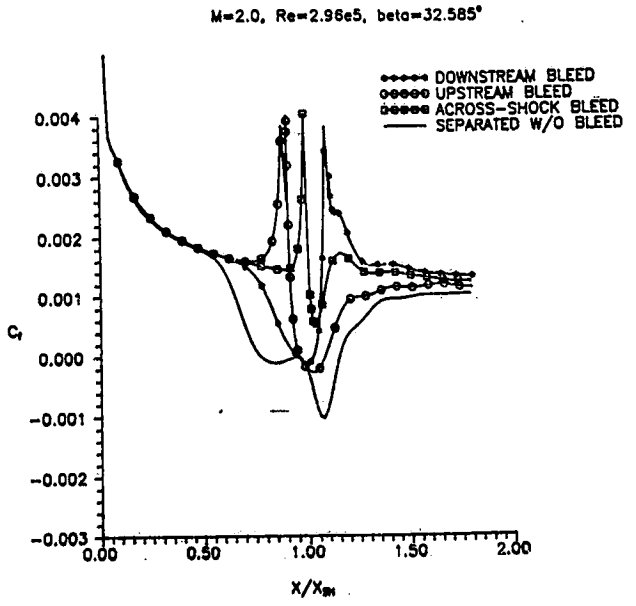

Fig. 11 Comparison of the skin friction coefficients for the different bleed configurations.

bleed. On the other hand, the streamwise velocity component reaches a local u/U_e of 0.5–0.6 upstream of the slot shock, then drops linearly reaching slightly negative values (−0.02 to −0.1) near the downstream slot corner. Typically, in the computations of flowfields involving bleed, the bleed mass flux is specified while the tangential velocity is set equal to zero across the bleed zone. The results of Figs. 8–10 suggest that the neglect of the streamwise velocity component in the bleed zone of shock wave/boundary-layer interaction can constitute a serious source of error in the computations. This might be a major cause of discrepancies between the computed and experimental results downstream of the interaction bleed zone in supersonic inlets.[5-7]

Figure 11 presents the computed skin friction distribution over the flat plate surface for the three bleed locations and for the no bleed separated flow case. The reduction in the length of the interaction zone due to bleed is clear in this

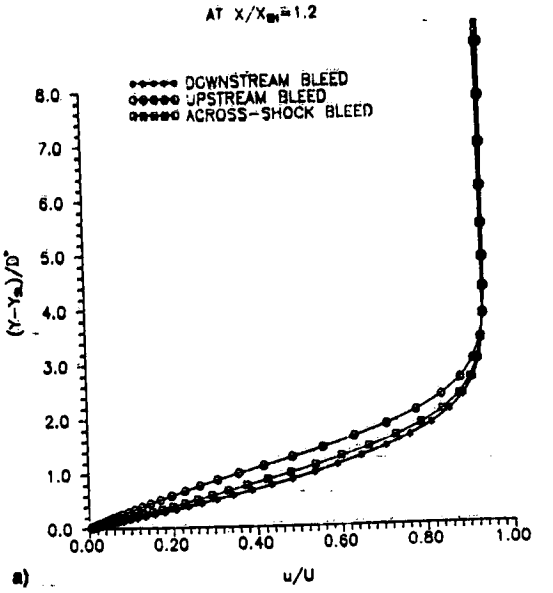

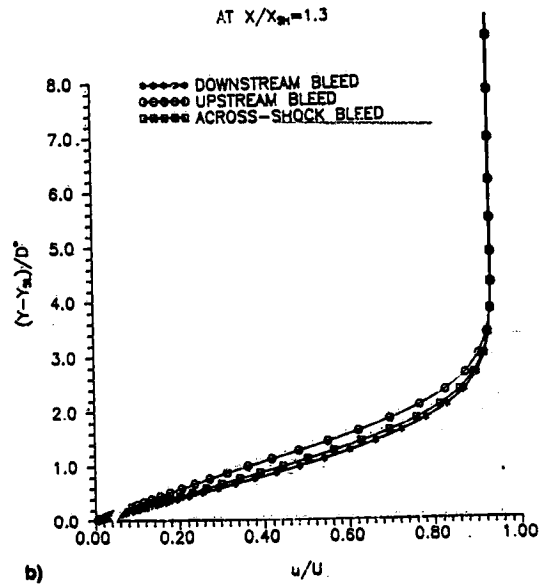

Fig. 12 Comparison of the velocity profiles downstream of the interaction zone for the different bleed configurations.

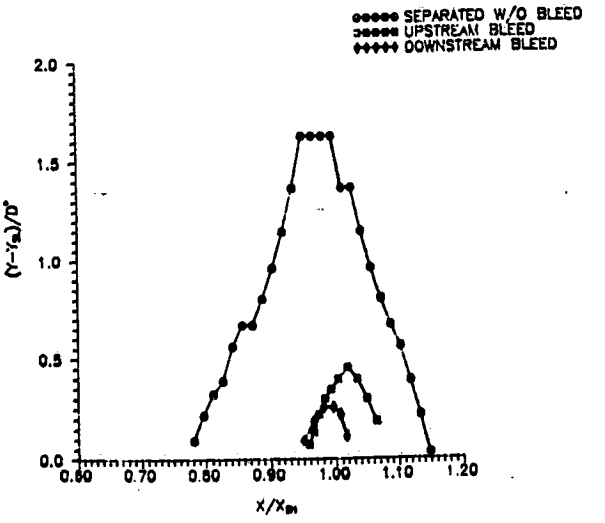

Fig. 13 Comparison of separation region for the different bleed configurations.

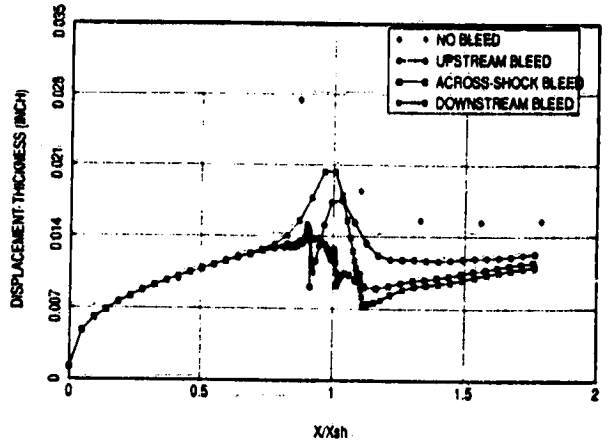

Fig. 14 Comparison of the boundary-layer displacement thickness for the different bleed configurations.

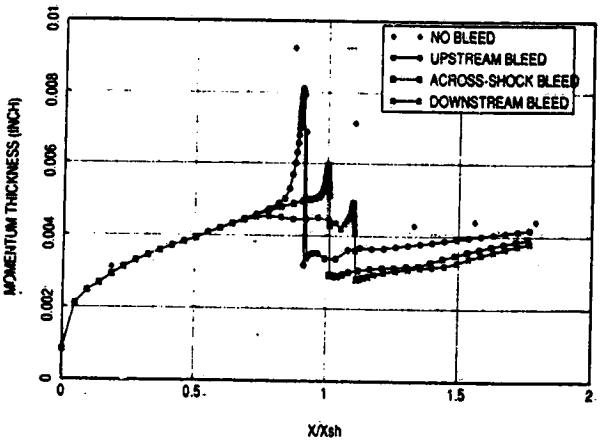

Fig. 15 Comparison of the boundary-layer momentum thickness for the different bleed configurations.

figure for all three cases. However, a small flow separation zone as indicated by the negative skin friction coefficient can be observed for the upstream and downstream bleed cases, but not for across the shock bleed. The friction coefficients are higher for all three bleed cases downstream of the interaction zone in comparison to the no bleed friction, indicating fuller velocity profiles. The highest friction coefficient value downstream of the interaction is for the downstream bleed, and the lowest for the upstream bleed. These differences in the velocity profiles appear to persist for a long distance downstream of the interaction as can be seen in the velocity profiles of Fig. 12.

Figure 13 compares the extent of the separation regions as determined from $u = 0$. One can observe that the separation bubble height is reduced to 32 and 25% of its value without bleed for the cases of upstream and downstream bleeds, respectively. Across the shock bleed completely eliminates separation as indicated by the skin friction results of Figs. 11 and 12. The boundary layer's displacement and momentum thickness are presented for the three bleed locations and for no bleed in Figs. 14 and 15. One can see that the largest reduction in δ^* and θ are realized in the downstream bleed case and the least reduction for upstream bleed.

Conclusions

A numerical investigation was conducted to determine the effect of bleed location on the flow in an oblique shock/boundary-layer interaction. The implicit factored scheme of Beam and Warming[15] was used to obtain numerical solutions of the two-dimensional compressible Navier-Stokes equations in strong conservation law form. The investigation was restricted to laminar flows to avoid the uncertainties associated with turbulence modeling. The solution domain extended inside the normal bleed slot, and computational grid was clustered near the surfaces. Three bleed locations upstream, across, and downstream of the shock impingement point were investigated for the same slot size and static pressure at the bottom of the bleed port. Results were presented for pressure and Mach number throughout the interaction region and inside the bleed port, and for the surface pressure and skin friction distribution. According to the computed results, the across-shock bleed proved to be the most effective in preventing separation and shortening the interaction length, whereas the upstream bleed slot proved to be the least effective. The results indicate that the downstream bleed slot location produced the most favorable velocity profiles and skin friction recovery downstream of the interaction region, as well as the maximum reduction in boundary-layer momentum and displacement thickness. The results suggest that a combination of across-shock and downstream bleed slots might provide the two advantages, namely no flow separation in the interaction region and fuller boundary-layer profiles downstream of the interaction zone.

Acknowledgments

This work was supported by NASA Lewis Research Center Contract NASA NAG3-1213. The computational work was performed on the Cray Y-MP128 of Ohio Supercomputer, Columbus, Ohio.

References

[1]Hamed, A., and Shang, J., "Survey and Assessment of the Validation Data Base for Shock Wave Boundary Layer Interactions in Supersonic Inlets," AIAA Paper 89-2939, July 1989.

[2]Syberg, J., and Koncsek, J. L., "Bleed System Design Technology for Supersonic Inlets," AIAA Paper 72-1138, Nov./Dec. 1972.

[3]Fukuda, M. K., Hingst, W. R., and Reshotko, E., "Bleed Effects on Shock/Boundary-Layer Interactions in Supersonic Mixed Compression Inlets," *Journal of Aircraft*, Vol. 14, No. 2, 1977, pp. 151–156.

[4]Hamed, A., "Flow Separation in Shock Wave-Bounday Layer Interactions at Hypersonic Speeds," NASA CR 4274, Feb. 1990.

[5]Martin, A. W., Koslin, L. C., and Sidney, D. M., "Dynamic Distortion at the Exit of a Subsonic Diffuser of a Mixed Compression Inlet," NASA CR-1644, Dec. 1970.

[6]Knight, D. D., "Improved Calculation of High Speed Inlet Flows. Part I: Numerical Algorithm," *AIAA Journal*, Vol. 19, No. 1, 1981, pp. 34–41; also see "Part II: Results," *AIAA Journal*, Vol. 19, No. 2, 1981, pp. 172–179.

[7]Weir, L. J., Reddy, D. R., and Rupp, G. D., "Mach 5 Inlet CFD and Experimental Results," AIAA Paper 89-2355, July 1989.

[8]Carter, T. D., and Spong, E. D., "High Speed Inlet Investigation. Vol. I Description of Program and Results; Vol. II Data Summary," Air Force Flight Dynamics Lab., AFFDL-TR-77-105, Wright-Patterson AFB, OH, Nov. 1977.

[9]Strike, W. T., and Rippy, J., "Influence of Suction on the Interaction of an Oblique Shock with a Turbulent Boundary Layer at Mach 3," Arnold Engineering Development Center, AEDC-TN-61-129, Tullahoma, TN, Oct. 1961.

[10]Seebaugh, W., and Childs, M., "Conical Shock Wave Boundary-Layer Interaction Including Suction Effects," *Journal of Aircraft*, Vol. 7, No. 4, 1970, pp. 334–340.

[11]Benhachmi, D., Greber, I., and Hingst, W., "Experimental and Numerical Investigation of an Oblique Shock-Wave/Turbulent Boundary Layer Interaction with Continuous Suction," AIAA Paper 89-0357, Jan. 1989.

[12]Gubbison, R. W., Meleason, E. T., and Johnson, D. F., "Performance Characteristics from Mach 2.58 to 1.98 of an Axisymmetric Mixed Compression Inlet System with 60 Percent Internal Contraction," NASA TM X-1739, Feb. 1969.

[13]Fukuda, M. K., Hingst, W. G., and Reshotko, E., "Control of

Shock Boundary Layer Interactions by Bleed in Mixed Compression Inlets," NASA CR 2595, 1975.

[14]Wong, W. F., "The Application of Boundary Layer Suction to Suppress Strong Shock-Induced Separation in Supersonic Inlets," AIAA Paper 74-1063, Oct. 1974.

[15]Beam, R., and Warming, R., "An Implicit Factored Scheme for the Compressible Navier-Stokes Equations," *AIAA Journal*, Vol. 16, No. 4, 1978, pp. 393–402.

[16]Visbal, M., and Shang, J., "Comparative Study Between Two Navier-Stokes Algorithms for Transonic Airfoils," *AIAA Journal*, Vol. 24, No. 4, 1986, pp. 599–606.

[17]Visbal, M. R., "Calculation of Viscous Transonic Flows About a Supercritical Airfoil," Air Force Wright Aeronautical Labs., AFWAL-TR-86-3013, Wright-Patterson AFB, OH, July 1986.

[18]Hamed, A., and Lehnig, T., "An Investigation of Oblique Shock/Boundary Layer Interaction," *Journal of Propulsion and Power*, Vol. 8, No. 2, 1992, pp. 418–424.

[19]Hakkinen, R. J., Greber, I., Trilling, L., and Aberbanel, S. S., "The Interaction of an Oblique Shock Wave with a Laminar Boundary Layer," NASA Memo 2-18-58W, March 1959.

APPENDIX B

JOURNAL OF PROPULSION AND POWER
Vol. 10, No. 1, Jan.-Feb. 1994

Investigation of Shock/Turbulent Boundary-Layer Bleed Interactions

A. Hamed,* S. Shih,† and J. J. Yeuan†
University of Cincinnati, Cincinnati, Ohio 45221

A numerical investigation was conducted to determine the effect of bleed on oblique shock wave/turbulent boundary-layer interactions (SWBLI). The numerical solutions to the compressible Navier-Stokes equations reveal the flow details throughout the interaction zone and inside the normal bleed slot. Results are presented for an incident oblique shock of sufficient strength to cause boundary-layer separation on a flat plate in the absence of bleed at a freestream Mach number of 2.96 and Reynolds number of 1.2×10^7/ft, with bleed applied across the shock impingement location over a range of bleed mass flow rates corresponding to different values of plenum pressures. The results indicate a complex flow structure with large variations in both the normal and tangential flow velocities across the bleed slot. The flow entrainment into the slot is accompanied by an expansion-compression wave system with a bow shock originating inside the bleed slot. Increasing the bleed mass flow by decreasing the plenum pressure caused an initial decrease, then a later increase in boundary-layer momentum and displacement thickness downstream of the interaction.

Introduction

THE control of flow separation in shock boundary-layer interactions can be accomplished through flow suction (bleed) in the interaction zone. In the case of mixed compression supersonic inlets, the bleed system design is critical to the efficient and stable operation of the system. Hamed and Shang[1] reviewed the existing experimental data for shock wave boundary-layer interactions in supersonic inlets and other related configurations. According to this survey, there is enough experimental evidence[2-7] to indicate that local bleed can control flow separation in shock wave/boundary-layer interactions. There are disagreements,[1] however, among the different experimental results regarding the effects of bleed location relative to the shock[2-4,7] and of bleed hole size.[7,8]

Strike and Rippy[2] obtained surface pressure measurements with porous bleed applied across and upstream of the shock impingement. Based on the minimum mass flow required for the static pressure downstream of the interaction to reach the theoretical pressure ratio, they determined that less suction is required when applied upstream. Seebough and Childs[3] who conducted their oblique shock wave boundary-layer bleed study over the inner surface of a cylinder, with a cone as a shock generator, concluded that across the shock bleed was more effective in controlling boundary-layer separation. Hingst and Tanji[4] and Benhachmi et al.[5] used pressure taps to measure the surface pressure, and hot wire to measure the bleed mass flow distribution through normal holes in SWBLI. Their results indicated that the bleed mass flow distribution followed the surface pressure distribution. In addition, Hingst and Tangi[4] used pitot probe surveys and surface flow visualization to compare the performance of bleed locations upstream, across, and downstream the shock. According to this study, across the shock and downstream bleed produced similar results in terms of removing flow separation, shortening the interaction length, increasing the pressure gradient, and producing fuller velocity profiles downstream of the interaction. Lee and Leblanc[6] presented their experimental results from taps, schlieren, pitot, and static probes for two levels of suction applied through porous wall sections across the shock impingement point. The poor performance of the weak suction was attributed to the effects of surface roughness.

Fukuda et al.[7] determined experimentally the change in boundary-layer characteristics across oblique shock wave interactions with bleed over the centerbody and cowl of a supersonic inlet. This study was conducted at different bleed mass flow rates, bleed hole sizes, bleed locations relative to the shock, and bleed hole inclination relative to the surface. Based on the change in boundary-layer displacement and momentum thicknesses, and in the transformed form factor for the different bleed configurations, they concluded that bleeding upstream and downstream of the interaction was preferable to bleeding across the shock. These results were unchanged by the normal bleed hole size which was found to have a negligible effect on the results.

Most viscous flow computations in supersonic inlets[9-15] require some knowledge of bleed flow rates and/or pressure distribution in the bleed regions. Comparisons of internal flow computational results with the experimental measurements in supersonic inlets revealed reasonable agreement between the computed and measured surface pressures upstream of the ramp bleed. However, discrepancies in the predicted shock locations and velocity profiles downstream of shock boundary-layer interactions with bleed suggest deficiencies in the bleed modeling. Other investigators actually solved the flow through the boundary layer and into the bleed slot, providing insight into the bleed flow region.[16,17] This approach eliminates the need for experimentally derived bleed models for supersonic inlet flow simulations, but can be very costly computationally.

Recently, some research efforts have been directed at improving bleed models. Paynter et al.[18] used the rough wall algebraic turbulence model of Cebeci and Chang[19] to simulate the overall effect of bleed on the growth of the boundary layer. The proper values of the roughness parameters were determined through matching the computational and test results for near wall velocity distributions downstream of the bleed band for seven bleed configurations, with shock boundary-layer interactions in some cases. The results of this in-

Presented as Paper 92-3085 at the AIAA/SAE/ASME/ASEE 28th Joint Propulsion Conference, Nashville, TN, July 6-8, 1992; received Aug. 20, 1992; revision received April 5, 1993; accepted for publication April 29, 1993.

*Professor, Department of Aerospace Engineering and Engineering Mechanics. Fellow AIAA.
†Department of Aerospace Engineering and Engineering Mechanics. Student Member AIAA.

vestigation demonstrate a strong dependence of the surface roughness on the fraction of the upstream boundary-layer mass flux removed. High roughness values were found for bleed rates between 3–15% of the upstream boundary-layer mass flux, but were insignificant for lower and higher bleed rates. Choked bleed flow through slanted holes gave the best boundary-layer profile in terms of flow separation control.

Hamed and Lehnig[20,21] conducted a numerical study in an incident oblique shock/laminar boundary-layer interaction, with bleed through a normal slot. By obtaining the flow solution in a domain that included the shock boundary-layer and extended inside the bleed slot, they were able to reveal the various regimes in this complex flowfield. Their results demonstrated a large variation in both the normal and tangential flow velocity distribution across the bleed slot opening at the plate surface. A separated flow region inside the bleed slot in the computed results suggests a reduction in the flow coefficient and total pressure. Hamed and Lehnig[21] presented the flowfields for three locations of the normal bleed slot, upstream, across, and downstream of the shock impingement point. The results demonstrated that for a given plenum pressure at the slot exit, the shock-induced flow separation on the plate was eliminated in the across the shock bleed configuration and reduced in the upstream and downstream bleed cases. Edwards and McRae[22] also computed the flowfield for an oblique incident shock, on a laminar boundary layer, with bleed through a normal slot across the shock impingement point. They compared the computed surface pressure distributions for a specified uniform normal bleed velocity across the slot to the plenum case, and demonstrated that the first case underpredicts the initial flow expansion into the slot. The solution domain for the plenum case was similar to that of Hamed and Lehnig,[20,21] but a uniform suction velocity was specified at the slot exit.

The discrepancies among the different experimental studies is an indication of the complexity of the flow in these configurations. Based on the comparison of their computational results with the experimental data of supersonic inlet flowfields, Reddy et al.[13] stressed the need for a detailed study of the effect of the individual bleed ports. Bleed optimization can only be accomplished through a parametric investigation in which the bleed conditions are changed systematically. The large number of parameters and the difficulties in obtaining accurate flow measurements in the interaction zone precludes a complete experimental investigation.

The purpose of the present study is to conduct a numerical investigation to characterize the flowfield in oblique shock wave/turbulent boundary-layer interactions with bleed, and to provide a basic understanding of the bleed flow controlling mechanisms. In the investigated configuration, flow suction (bleed) is applied through a normal slot located across the incident oblique shock on a flat plate turbulent boundary layer. The region inside the slot from the bleed surface to the plenum exit was included in the solution domain in order to realistically model the bleed flow and its variation with the plenum pressure. The results of the flow computations with different bleed mass flow rates reveal in detail the various flow regimes in the interaction region and within the bleed slot.

Computational Details

The PARC code[23] was used in the present investigation after conducting validation studies for shock wave/turbulent boundary-layer interactions,[24] with and without flow separation. The performance of four different codes with different turbulence models was assessed in terms of the agreement of their computed results with the experimental data of Refs. 25 and 26. The required grid refinement and computer time to reach this agreement were compared for incident shock on a flat plate boundary layer, and for flow over a compression corner. The prediction of the separation length, the surface pressure propagation upstream of the interaction, and the recovery of the skin friction downstream of the interaction received special attention. From the four assessed codes, the two[23,27] that use the implicit approximate factorization technique of Beam and Warming[28] to advance the solution, performed best both in terms of computer time and grid independence. Visbal's code[27] was the most robust, required the least number of time steps to reach convergence, and its computed results were consistently better than those obtained from the other codes with algebraic turbulence model. However, Avva et al.[29] proved the two equation k-ε model to be superior to the algebraic models for applications with separated flows. Consequently, the PARC code[23] was used in the present study because among the codes with the two equation turbulence models, it performed best, in terms of agreement with the experimental results and required the least grid refinement to achieve this agreement.[24] In addition, the PARC code was validated[30] through comparisons with experimental data for several flow configurations including supersonic flow over compression with separation, and has been used in several supersonic and hypersonic inlet flow simulations.[12–14,31]

Central differencing explicit and implicit dissipation schemes[32] are used in the PARC code for the solution of the Reynolds-averaged Navier-Stokes equations in strong conservation form. The Beam and Warming factorization algorithm coupled with Pulliam's pentadiagonal formulation form the basis of its implicit LU-ADI style solution scheme. The turbulence model used in the PARC code is based on Chien's low Reynolds number k-ε model[33] with Nichols[30] modifications to add com-

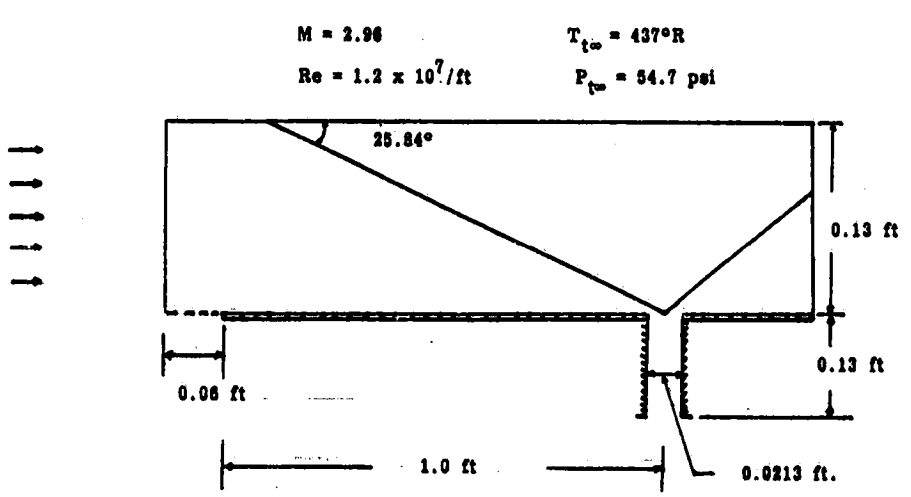

Fig. 1 Schematic of the solution domain.

pressibility effects. For the simulation, flow was considered to be turbulent throughout the calculation domain; no attempt was made to model transition and/or relaminarization.

Referring to Fig. 1, the solution domain used in the two-dimensional flow simulations extends upstream of the flat plate leading edge, downstream of the shock wave/turbulent boundary-layer interaction region, and inside the bleed slot, where the specified plenum pressure at the bottom controlled the amount of bleed mass flow. The incident oblique shock crosses the upper boundary, all other wave systems including the reflected, and any separation and reattachment shocks, cross the outflow boundary. Uniform freestream flow conditions are applied at the inflow boundary and all variables were extrapolated at the outflow boundary. No slip adiabatic flow conditions are applied at the plate and bleed walls. The static pressure is specified and first order extrapolation is applied for the rest of the flow variables at the bottom of the bleed slot. The location of the incident shock is fixed at the upper boundary with freestream and postshock conditions specified upstream and downstream. The slot was centered around the shock impingement location 1 ft from the flat plate leading edge. The grid spacing was varied in both x and y directions with clustering around both bleed walls and at the plate surface as shown in Fig. 2. The computational results were obtained with $\Delta y_{min} = \Delta x_{min} = 0.25794 \times 10^{-4}$ ft, corresponding to $y^+ = 2.0$ at $x = 0.9$ ft, using a 308/68 grid over the plate surface and a 75/68 grid inside the bleed slot, based on the grid refinement study results of Ref. 24. The computations for a typical bleed case required 5000 local time steps at 0.3 Courant-Friedrichs-Lewy (CFL) number to reach steady-state solution based on six orders of magnitude reductions in the averaged rms error in the flux.

Results and Discussion

The computations were performed at the incoming flow conditions of $M_\infty = 2.96$, $Re_\infty = 1.2 \times 10^7$/ft, $T_{t\infty} = 437°R$ and $P_{t\infty} = 54.7$ psi, and an impinging oblique shock angle of 25.84 deg. These are the same as the experimental test conditions of Law[25] for the separated flow case at a deflection angle δ of 7.93 deg. In his experimental study, Law used oil

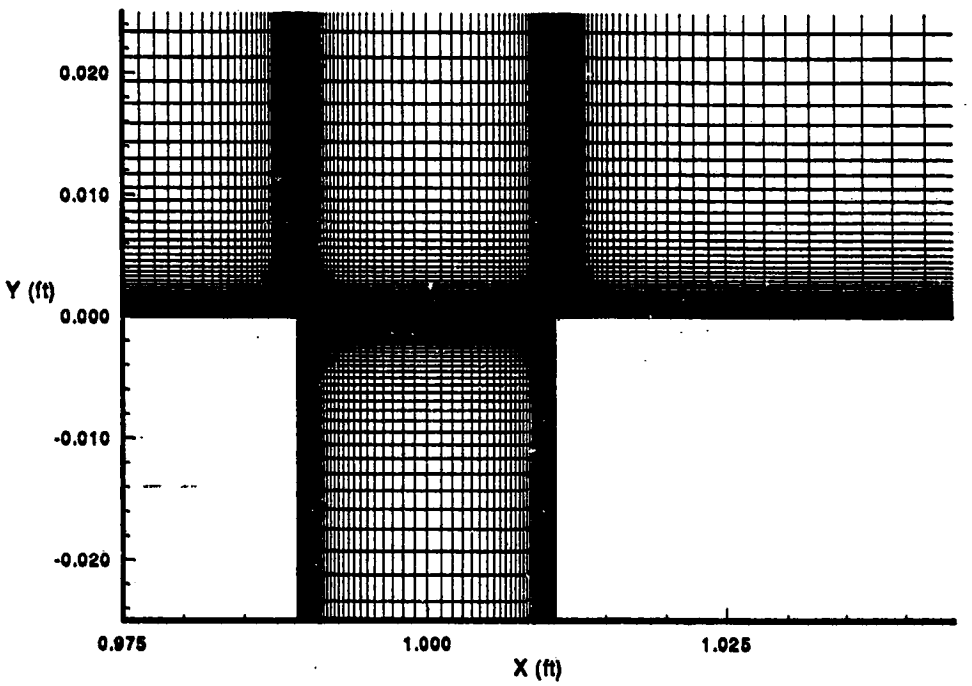

Fig. 2 Computational grid in the interaction region, bleed width = 0.0213 ft.

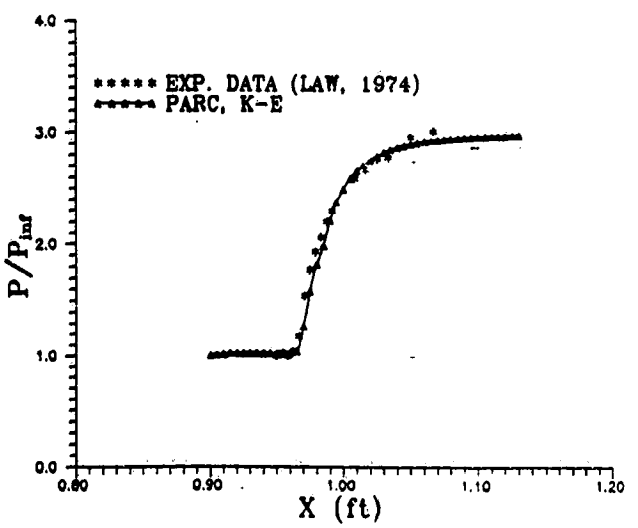

Fig. 3 Surface pressure distribution in the interaction region without bleed.

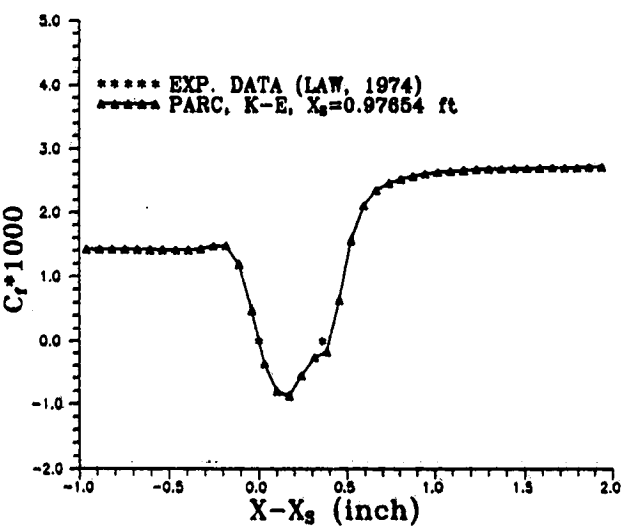

Fig. 4 Friction coefficient distribution in the interaction region without bleed. X_s = location of separation point.

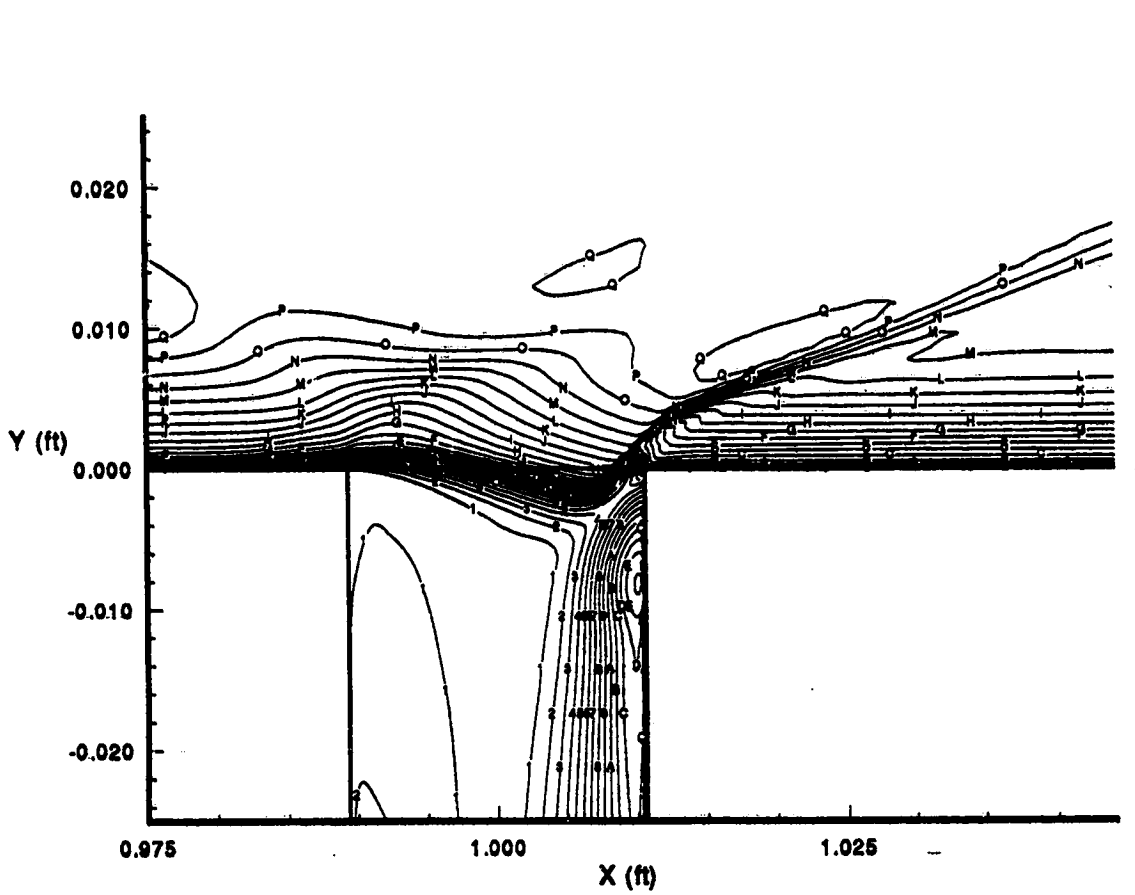

Fig. 5 Mach number contours, bleed width = 0.0213 ft, $P_b/P_{inf} = 1.5$.

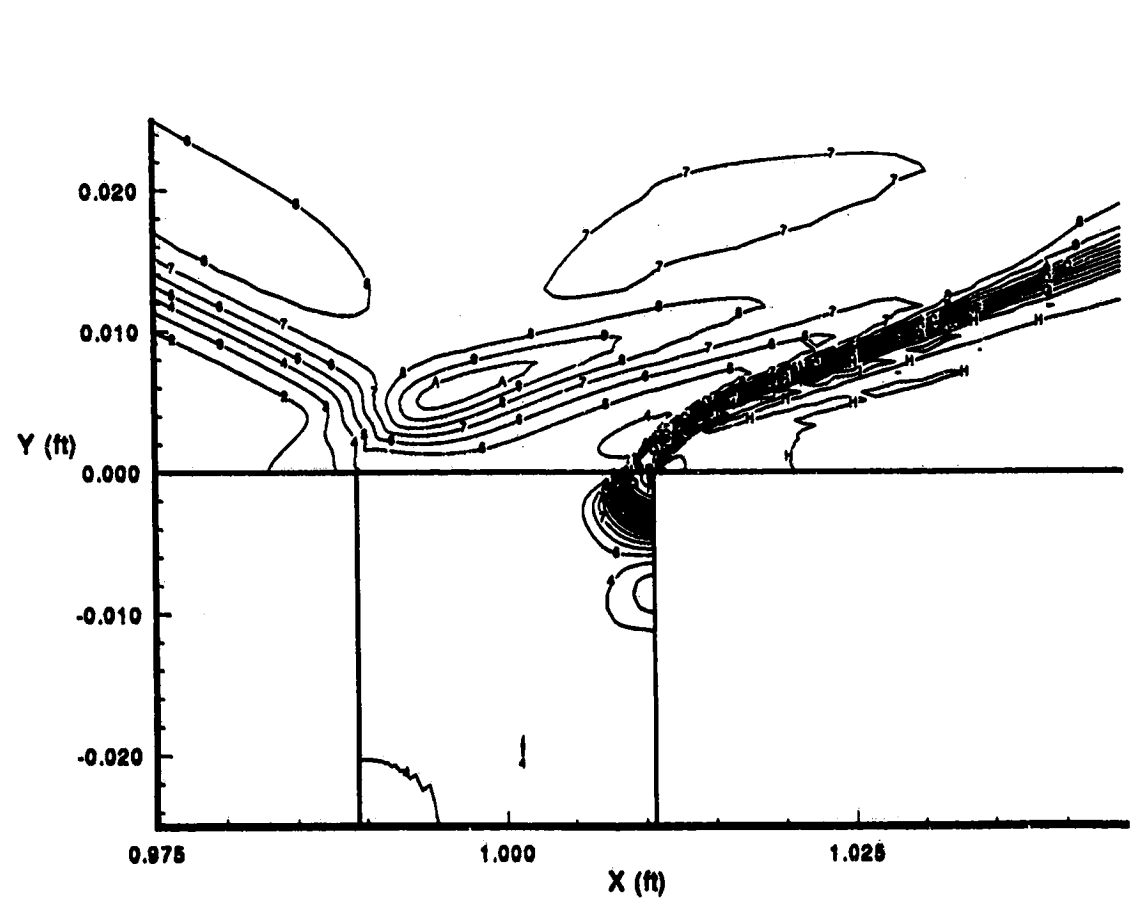

Fig. 6 Pressure contours, bleed width = 0.0213 ft, $P_b/P_{inf} = 1.5$.

flow visualization to reveal non-two-dimensional effects of the corner on the flat plate interior region. He measured the separation length for different shock generation spans and used these results to determine the proper reduced span to minimize the influence of the side wall interactions on the flat plate centerline. Figures 3 and 4 compare the computed surface pressure and skin friction without bleed to Law's centerline experimental data. One can see that the predicted separation length and surface pressure distribution are in very good agreement with the experimental results. The computations accurately predict the extent of the upstream influence of the shock boundary-layer interactions on the surface pressure and slightly overpredict the separation length.

The computations were performed under the same flow conditions with a bleed slot normal to the plate at different plenum pressure ratios ($0.95 \leq p_b/p_\infty \leq 1.95$). For an inviscid pressure ratio across the reflected shock p_2/p_∞ equals 2.962, and based on the downstream pressure p_2 the bleed plenum pressures are set to vary from choked to unchoked slot conditions ($0.321 < p_b/p_2 < 0.658$). The bleed slot width was 0.0213 ft, which is equal to 1.617 times the boundary-layer thickness upstream of the interaction at $x = 0.9$ ft. The details of the flowfield computational results near the bleed slot entrance are presented in Figs. 5–7 for a plenum pressure ratio of 1.5. They indicate a complex flow structure in which an expansion-compression system is associated with the flow entrainment into the slot opening. The initial flow turning is weak, then the flow is turned more strongly in the second

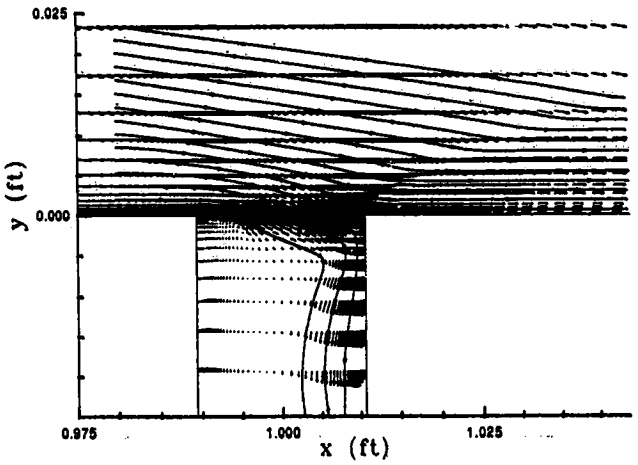

Fig. 7 Velocity fields and streamlines in the interaction region for bleed width = 0.0213 ft, $P_b/P_{inf} = 1.5$.

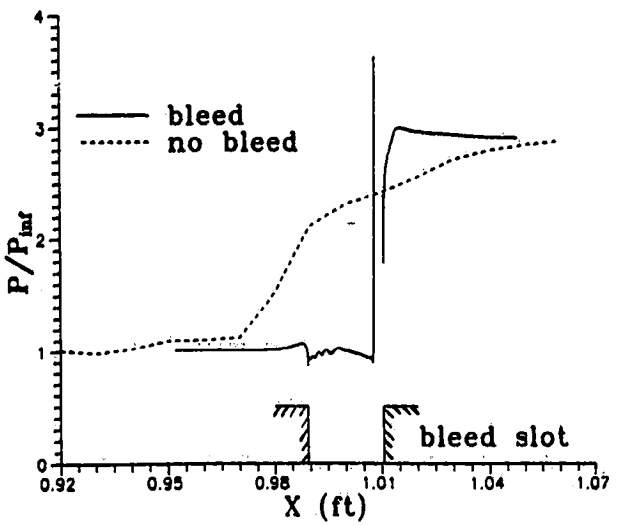

Fig. 8 Pressure distribution across the bleed opening for $P_b/P_{inf} = 1.5$.

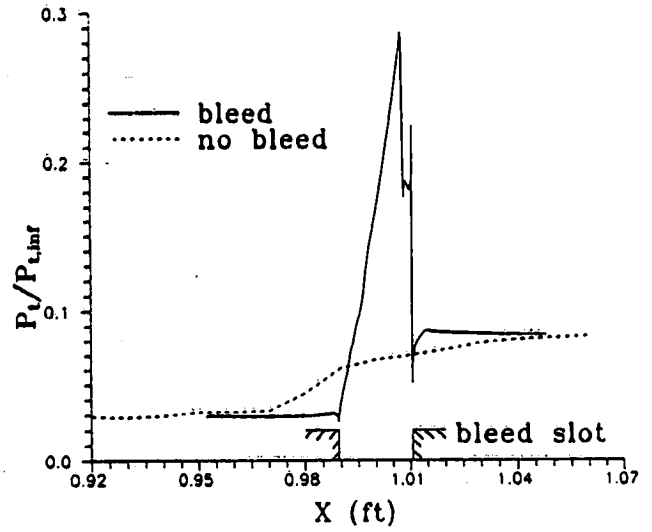

Fig. 9 Total pressure distribution across the bleed opening for $P_b/P_{inf} = 1.5$.

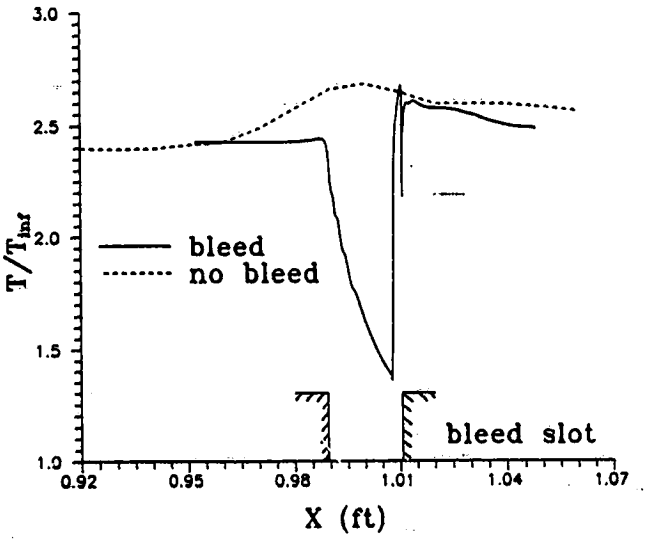

Fig. 10 Temperature distribution across the bleed opening for $P_b/P_{inf} = 1.5$.

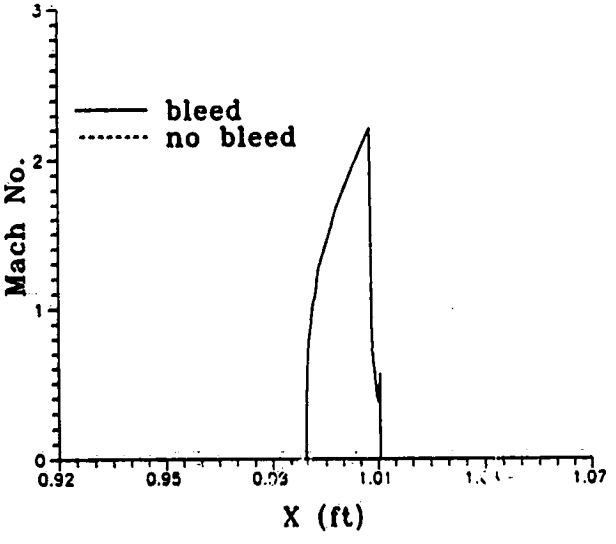

Fig. 11 Mach number distribution across the bleed opening for $P_b/P_{inf} = 1.5$.

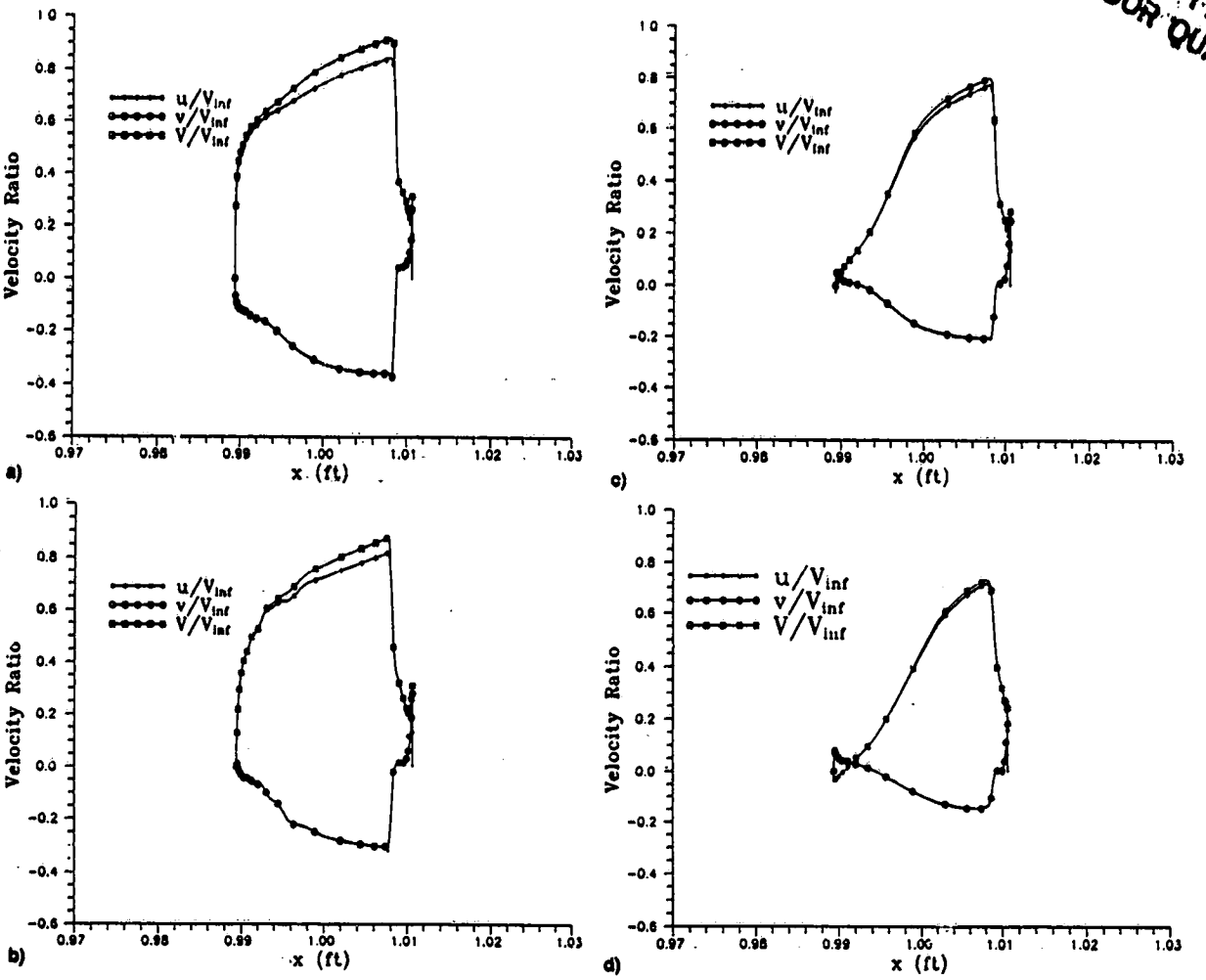

Fig. 12 Velocity distributions across the bleed opening for P_b/P_{inf} = a) 1.2, b) 1.5, c) 1.75, and d) 1.95.

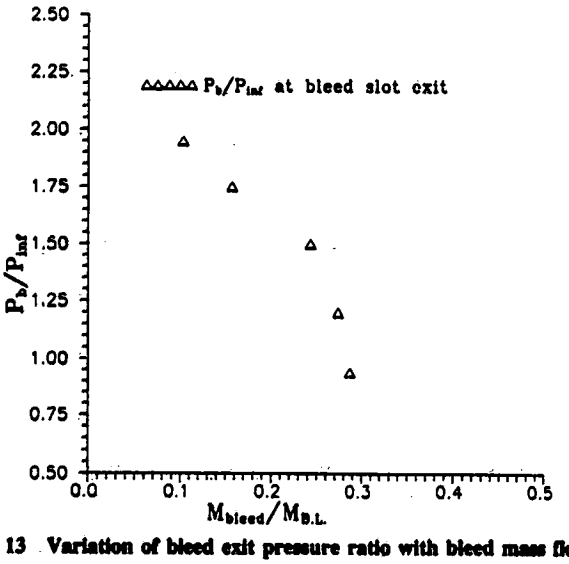

Fig. 13 Variation of bleed exit pressure ratio with bleed mass flow rate.

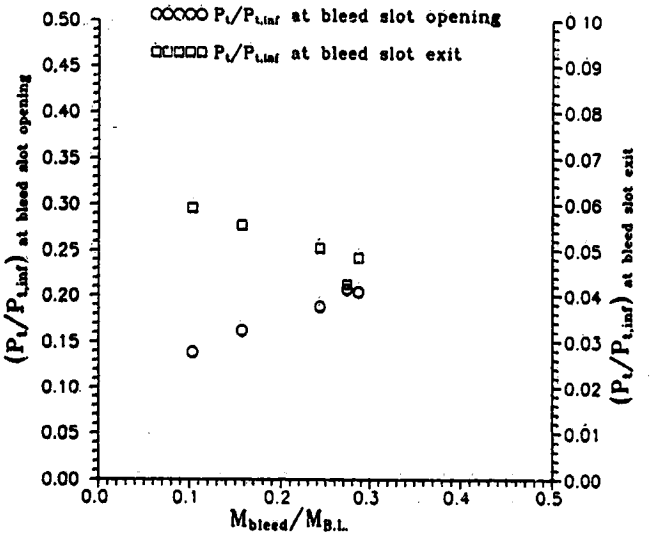

Fig. 14 Variation of bleed total pressure ratios at bleed slot opening and exit with bleed mass flow ratio.

half before crossing the bow shock that originates inside the slot. The Mach number contours show a stagnation point behind the bow shock near the plate corner, followed by an expansion fan. The flow inside the bleed slot is mostly confined to a strip adjacent to the back wall of the bleed slot, where the flow velocities reach supersonic values. A flow recirculation zone much larger than the laminar case[21] occupies most of the bleed slot. The computational results at different plenum pressure settings show that the dual separation and reattachment shock system is replaced by a single reflected shock structure, indicating no flow separation, for plenum pressure ratios ≤1.5. The corresponding variations in static and total pressures, static temperature, and Mach number across the bleed slot are presented in Figs. 8–11. These figures show the sudden change in the flow properties across the bow shock. One can observe a reduction in both the static and total pressure over the plate surface upstream

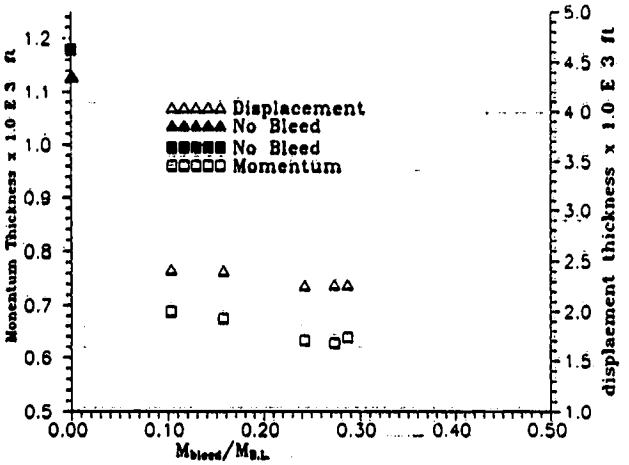

Fig. 15 Variation of displacement and momentum thickness downstream of the interaction at x = 1.13 ft with bleed mass flow rate.

of the slot opening due to the flow entrainment into the slot. Downstream of the slot opening, both the static and total pressure increase more sharply compared to the no bleed case.

Figure 12 presents the velocity distribution across of the bleed slot opening for different bleed flow rates. Large variations in both the normal and tangential velocity components can be seen across the slot opening with some mass injection near the upstream corner at the high-pressure plenum settings. The tangential velocity reaches values as high as 90% of the freestream velocity before dropping sharply behind the bow shock near the back wall.

The variations in the static pressure at the bleed slot exit with the calculated bleed mass flow are presented in Fig. 13. The corresponding changes in the mass averaged total pressure at the bleed slot inlet and exit are presented in Fig. 14. In these figures, the bleed mass flow is normalized with respect to the mass flow in the incoming boundary layer at x = 0.9, and the static and total pressures are normalized with respect to the freestream values. With the static pressure nearly constant across the bleed slot opening, except for the

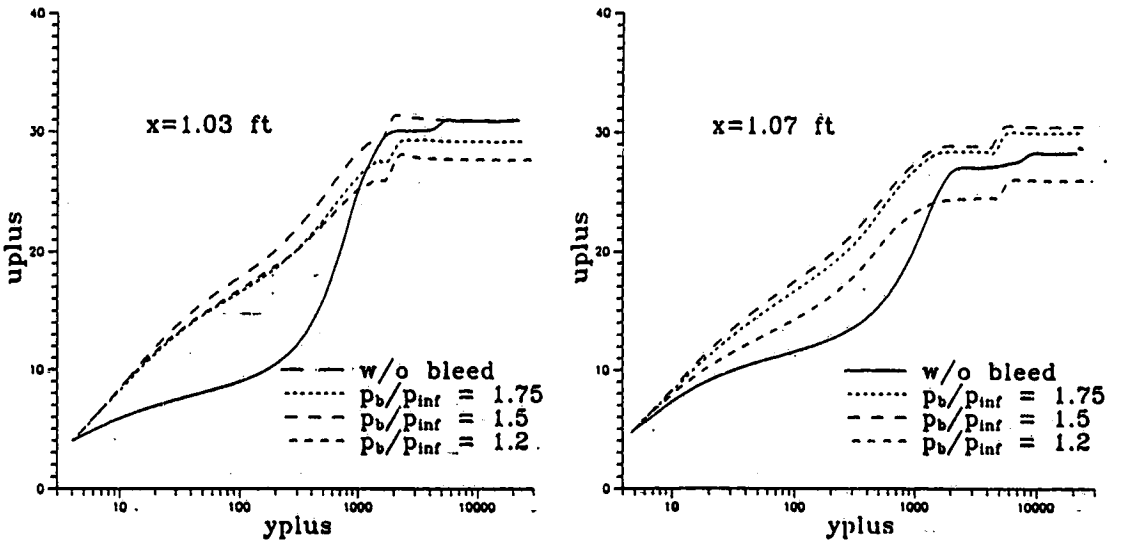

Fig. 16 Near wall velocity profiles downstream of the interaction at different bleed pressure ratios.

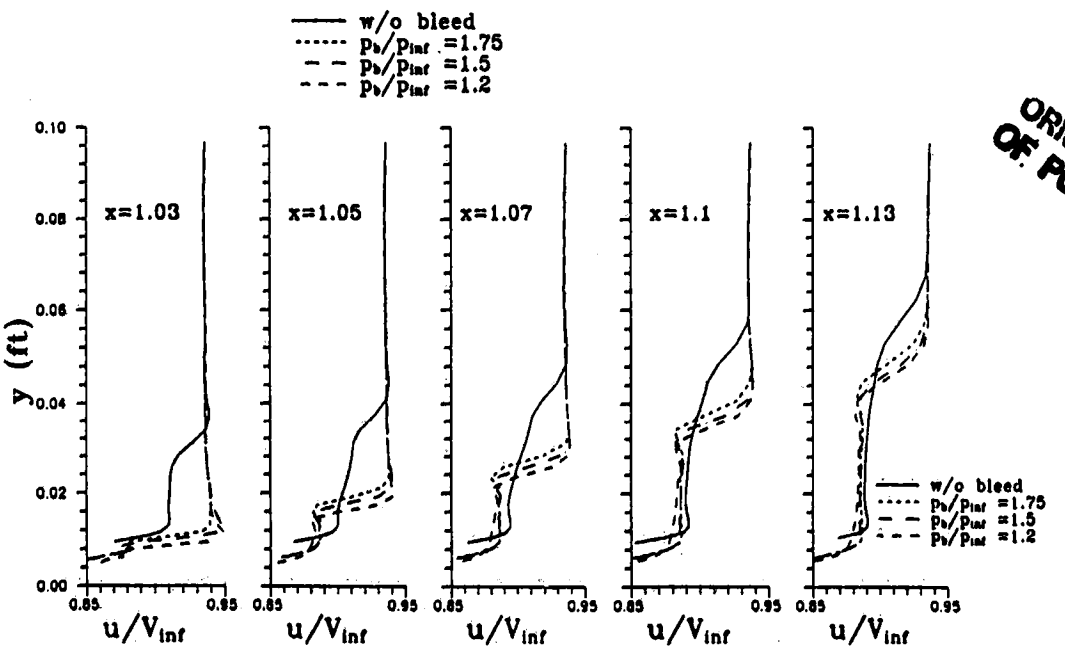

Fig. 17 Velocity profiles downstream of the interaction at different bleed pressure ratios.

sudden rise across the bow shock, the total pressure increase across the bleed slot opening is mainly associated with the increased flow velocities as the bleed mass flow increases. However, at the slot exit, the mass averaged total pressure is mostly influenced by the value of the static pressure due to the greater effects of the flow recirculation before choking. The corresponding variation in the boundary-layer displacement and momentum thickness are presented in Fig. 15. The results indicate that the boundary-layer displacement and momentum thicknesses downstream of the interaction initially decrease, then slightly increase with the increase in the bleed mass flow. According to Fig. 15, the maximum reduction in the boundary-layer displacement and momentum thickness downstream of the interaction are achieved at plenum pressure ratios of 1.2 and 1.5, respectively. The corresponding bleed mass flows are 27.38 and 24.51% of the incoming boundary-layer mass flow upstream of the interaction.

The near wall velocity profiles downstream of the interaction are presented in Fig. 16 for three cases with plenum pressure ratios of 1.2, 1.5, and 1.75. This figure shows that the velocities near the wall are higher for the case $p/p_\infty = 1.5$ than for both higher and lower bleed mass flow cases, $p/p_\infty = 1.2$ and $p/p_\infty = 1.75$. This can be attributed to the balance between the increases in the flow velocities and bow shock strength with the increased bleed mass flow. Figure 17 shows the variation in the flow velocity profiles downstream of the interaction outside the boundary layer for the three bleed cases corresponding to plenum pressure ratios of 1.2, 1.5, and 1.75 and for the no bleed case. This figure illustrates the reflected shock structure, with the strong bow shock closest to the wall, followed by the expansion fan, then the weaker separation shock further out. Figure 17 shows that as the bleed mass flow increases, the reflected shock system moves closer to the wall.

Conclusions

The objective of this work was to provide a basic understanding of the flow in the shock boundary-layer interactions and of the mechanisms for its control. Numerical computations were conducted in oblique shock wave/turbulent boundary-layer interaction to reveal in details the flow characteristics, and how they are altered by bleed. Flow suction (bleed) was accomplished through a normal slot across the shock incident point. The bleed results reveal a complex flow structure in the interaction zone and inside the bleed slot. The flow accelerates across the top of the bleed port, crosses a bow shock formed near the downstream corner, then goes through an expansion fan at the corner. A large recirculation region dominates the flow inside the bleed slot, and the bleed mass flow is limited to a narrow region adjacent to the downstream bleed wall, where the velocity reaches supersonic values. The effect of the bleed mass flow rate was investigated by changing the specified plenum pressure at the bottom of the slot and comparing the boundary-layer characteristics downstream of the interaction. As the bleed mass flow increased, the boundary-layer momentum and displacement thickness initially decreased, then slightly increased downstream of the interaction. In terms of the boundary-layer characteristics downstream of the interaction, the best performance was obtained when 24–27% of the boundary-layer mass flow upstream of the interaction was removed.

Acknowledgments

This work was sponsored by Air Force Office of Scientific Research Contract 91-0101, L. Sakell, Project Monitor; and by NASA Grant NAG3-1213, Dave Saunders, Project Monitor. The authors would like to acknowledge the invaluable discussions of Bob Coltrin of NASA Lewis Research Center. The computational work was performed on the CRAY YMP of the Ohio Supercomputer.

References

[1]Hamed, A., and Shang, J., "Survey of Validation Data Base for Shock Wave Boundary-Layer Interactions in Supersonic Inlets," *Journal of Propulsion and Power*, Vol. 7, No. 4, 1991, pp. 617–625.

[2]Strike, W. T., and Rippy, J., "Influence of Suction on the Interaction of an Oblique Shock with a Turbulent Boundary Layer at Mach 3," Arnold Engineering Development Center TN-61-129, Oct. 1961.

[3]Seebaugh, W., and Childs, M., "Conical Shock Wave Boundary-Layer Interaction Including Suction Effects," *Journal of Aircraft*, Vol. 7, No. 4, 1970, pp. 334–340.

[4]Hingst, W. R., and Tanji, F. T., "Experimental Investigation of Two-Dimensional Shock-Boundary Layer Interaction with Bleed," AIAA Paper 83-0135, Jan. 1983; see also NASA TM-83057, Jan. 1983.

[5]Benhachmi, D., Greber, I., and Hingst, W., "Experimental and Numerical Investigation of an Oblique Shock-Wave/Turbulent Boundary Layer Interaction with Continuous Suction," AIAA Paper 89-0357, Jan. 1989.

[6]Lee, D. B., and Leblanc, R., "Interaction onde de Choc Oblique-Couche Limite sur Paroi Poreuse avec Aspiration," Improvement of Aerodynamic Performance Through Boundary Layer Control and High Lift Systems, Paper 23, AGARD CP-365, Aug. 1984.

[7]Fukuda, M. K., Hingst, W. R., and Reshotko, E., "Bleed Effects on Shock/Boundary-Layer Interactions in Supersonic Mixed Compression Inlets," *Journal of Aircraft*, Vol. 14, No. 2, 1977, pp. 151–156.

[8]Wong, W. F., "The Application of Boundary Layer Suction to Suppress Strong Shock-Induced Separation in Supersonic Inlets," AIAA Paper 74-1063, Oct. 1974.

[9]Hunter, L. G., Tripp, J. M., and Howlett, D. G., "A Mach 2.0 Plus Supersonic Inlet Study Using the Navier-Stokes Equations," AIAA Paper 85-1211, July 1985.

[10]Chyu, W. J., Kawamara, T., and Bencz, D. P., "Navier-Stokes Solutions for Mixed Compression Axisymmetric Inlet Flow with Terminal Shock," *Journal of Propulsion and Power*, Vol. 5, No. 1, 1989, pp. 4, 5.

[11]Shigematsu, J., Yamamoto, K., and Shiraishi, K., "Numerical Investigation of Supersonic Inlet Using Implicit TVD Scheme," AIAA Paper 90-2155, July 1990.

[12]Weir, L. J., Reddy, D. R., and Rupp, G. D., "Mach 5 Inlet CFD and Experimental Results," AIAA Paper 89-2355, July 1989.

[13]Reddy, D. R., Benson, T. J., and Weir, L. J., "Comparison of 3-D Viscous Flow Computations of Mach 5 Inlet with Experimental Data," AIAA Paper 90-0600, Jan. 1990.

[14]Saunders, J. D., and Keith, T. G., Jr., "Results from Computational Analysis of a Mixed Compression Supersonic Inlet," AIAA Paper 91-2581, June 1991.

[15]Rizzetta, D. P., "Numerical Simulation of a Supersonic Inlet," AIAA Paper 91-0128, Jan. 1991.

[16]Forester, C. K., and Tjonneland, E., "New Guide for Accurate Navier-Stokes Solution of Two-Dimensional External Compression Inlet with Bleed," International Council of the Aeronautical Sciences 88-2.5.1, 1988.

[17]Fujimoto, A., Niwa, N., and Sawada, K., "Numerical Investigation on Supersonic Inlet with Realistic Bleed and Bypass Systems," AIAA Paper 91-0127, Jan. 1991.

[18]Paynter, G. C., Treiber, D. A., and Knelling, W. D., "Modeling Supersonic Inlet Boundary Layer Bleed Roughness," AIAA Paper 92-0269, Jan. 1992.

[19]Cebeci, T., and Chang, K. C., "Calculation of Incompressible Rough-Wall Boundary Layer Flows," *AIAA Journal*, Vol. 16, No. 7, 1978, pp. 730, 731.

[20]Hamed, A., and Lehnig, T., "An Investigation of Oblique Shock/Boundary Layer/Bleed Interaction," *Journal of Propulsion and Power*, Vol. 8, No. 2, 1992, pp. 418–424.

[21]Hamed, A., and Lehnig, T., "The Effect of Bleed Configuration on Shock/Boundary Layer Interactions," AIAA Paper 91-2014, June 1991.

[22]Edwards, J., and McRae, D., "Solution Technique for Shock-wave-Boundary Layer Interactions with Flow Separation and Slot Suction Effects," AIAA Paper 91-0652, Jan. 1991.

[23]Cooper, G. K., and Sirbaugh, J. R., "PARC Code: Theory and Usage," Arnold Engineering Development Center TR-89-15, Dec. 1989.

[24]Hamed, A., "An Investigation of Oblique Shock/Boundary Layer Interaction Control," Univ. of Cincinnati, Dept. of Aerospace Engineering and Engineering Mechanics, Air Force Office of Scientific Research Annual Rept. 101, Cincinnati, OH, Jan. 24, 1992.

[25]Law, C. H., "Supersonic Turbulent Boundary-Layer Separation," *AIAA Journal*, Vol. 12, No. 6, 1974, pp. 794–797.

[26]Settles, G. S., Fitzpatrick, P. J., and Bogdonoff, S. M., "Detailed Study of Attached and Separated Compression Corner Flowfields in High Reynolds Number Supersonic Flow," *AIAA Journal*, Vol. 17, No. 6, 1979, pp. 579–585.

[27]Visbal, M., "Calculation of Viscous Transonic Flows About a Supercritical Airfoils," Air Force Wright Aeronautical Labs. TR-86-3, July 1986.

[28]Beam, R., and Warming, R. F., "An Implicit Factored Scheme for the Compressible Navier-Stokes Equations," *AIAA Journal*, Vol. 16, No. 4, 1978, pp. 393–402.

[29]Avva, R., Smith, C., and Singal, A., "Comparative Study of High and Low Reynolds Number Versions of k-ε Models," AIAA Paper 90-0246, Jan. 1990.

[30]Nichols, R. H., "A Two-Equation Model for Compressible Flows," AIAA Paper 90-0494, Jan. 1990.

[31]Reddy, D. R., Smith, G. E., and Liou, M. F., "Three-Dimensional Viscous Analysis of a Hypersonic Inlet," AIAA Paper 89-0004, Jan. 1989.

[32]Jameson, A., Schmidt, W., and Turkel, E., "Numerical Solutions of the Euler Equations by Finite Volume Methods Using Runge-Kutta Time-Stepping Schemes," AIAA Paper 81-1259, 1981.

[33]Chien, K.-Y., "Prediction of Channel and Boundary-Layer Flows with a Low Reynolds Number Turbulence Model," *AIAA Journal*, Vol. 20, No. 1, 1982, pp. 33–38.

APPENDIX C

AIAA 93-0294

A Parametric Study of Bleed in Shock Boundary Layer Interactions

A. Hamed, S.H. Shih, and J.J. Yeuan
University of Cincinnati
Cincinnati, Ohio

31st Aerospace Sciences Meeting & Exhibit
January 11-14, 1993 / Reno, NV

AIAA 93-0294

A PARAMETRIC STUDY OF BLEED IN SHOCK BOUNDARY LAYER INTERACTIONS

A. Hamed, S.H. Shih and J.J. Yeuan
Department of Aerospace Engineering and Engineering Mechanics
University of Cincinnati
Cincinnati, OH 45221

Abstract

A numerical investigation was conducted to study the effect of bleed configuration on oblique-shock wave/turbulent boundary-layer interactions. Bleed is applied through a normal slot across the shock impingement location. The numerical solution to the compressible Navier-Stokes equations is obtained for the turbulent flow throughout the interaction zone and inside the bleed slot for bleed mass flow rates up to 57% of the boundary layer mass flow upstream of the interaction. The results indicate that the bleed slot performance improves as the slot width decreases and the length to width ratio increases. This is reflected as an increase in the bleed discharge coefficient and total pressure, and a reduction in the boundary layer momentum and displacement thickness downstream.

Introduction

The control of shock wave boundary layer interaction through bleed (suction) is essential for the efficient and stable operation of supersonic inlets. Bleed reduces the unfavorable effects associated with these interactions such as boundary layer thickening and flow distortion, and is especially critical for interactions with shock strong enough to cause separation. Hamed and Shang [1] reviewed the existing data base on shock wave boundary layer interactions in supersonic inlets. In spite of the very limited number of investigations with local flow measurements in the interaction region, their conclusions regarding the effect of bleed configuration were not in agreement. Fukuda et al. [2] reported no significant change in the bleed system performance with the change in bleed hole size. Wong [3] on the other hand reported significant hole size effects and recommended hole sizes below the boundary layer thickness for better bleed performance. Similarly, contradictions can be found regarding the effect of bleed location relative to the shock [4, 5].

Different approaches have been tried to model bleed without resolving the flow through the individual bleed holes. Cebeci's algebraic turbulence models [6, 7] for rough wall boundary layers, have been used by Abrahmson et al. [8], Benhachmi et al. [9] and Paynter et al. [10] to simulate the bleed hole roughness effects in the numerical solutions to the Navier-Stokes equations. Empirical boundary conditions for the mass flux distribution across the bleed zone in the shock boundary layer interactions were used with this turbulence model to simulate the bleed influence in the numerical computations of references [8] and [9]. Paynter et al. [10] used the experimental data for different bleed configurations to determine the appropriate value of roughness [7] that models the overall effect of bleed on the boundary layer growth rate. They determined that the roughness parameter depends on the fraction of the upstream boundary layer mass flow removed.

Hamed et al. [11-13] and Rimlinger et al. [14] conducted numerical studies of shock wave/boundary layer/bleed interactions which simulated the flow field throughout the interaction zone and inside the bleed port. These studies revealed a complex pattern of expansion and compression waves across the bleed opening for selected slot [11-13] and hole [14] configurations. Both Hamed et al. [12] and Rimlinger et al. [14] studied the effect of bleed location relative to the shock on the resulting flow field. In addition, Hamed et al. [13] predicted the variations in the boundary layer characteristics downstream with the bleed mass flow.

A complete bleed data base is critical to achieving inlet bleed system design objectives of eliminating or reducing the effects of flow separation in SWBLI, while minimizing bleed drag and bleed mass flow. A large number of parameters such as the local Mach number and shock strength, the bleed hole size, slant angle and the bleed location relative to the shock can influence the performance. The various bleed studies addressed different aspects of this complex phenomena and presented results for one or more of the bleed performance parameters. The test results of Syberg and Koncsek [15] consisted of the measured bleed mass flow variation with plenum pressures and the bleed drag for choked holes. The results were presented for different bleed hole diameters, aspect ratios and slanting angles at free stream Mach numbers ranging between 0.8 and 2.19. The test cases did not include shock interactions or pressure gradient. Fukuda et al. [2] obtained boundary layer

measurements downstream of boundary layer interactions on the center body and cowl of a supersonic inlet. Over the range of the tested bleed mass flows, the transformed form factor downstream of the interaction initially decreased then reached a plateau or slightly increased as the bleed mass flow increased. As expected, the slanted holes produced the lowest form factor but the hole size effect was insignificant. Hingst and Tangi [16] studied bleed configurations consisting of normal bleed hole rows in regions upstream, across and downstream of the impinging shock. Their results indicated that fuller boundary layer profiles, shorter interaction length and higher pressure gradients were obtained with the bleed region across the shock. They also used hot wire to measure the bleed mass flux distribution through the porous wall which was found to change in a pattern similar to the surface pressure.

Based on the previous discussion, the data base required to optimize bleed system design is not complete and does not provide sufficiently detailed information. The purpose of the present numerical study is to investigate the effect of bleed configuration on the flow throughout the shock boundary layer interaction and inside the bleed port. A parametric study was conducted in which bleed configuration parameters such as the bleed slot width and bleed aspect ratio were changed systematically to determine their effects over a wide range of bleed plenum pressures. The results are presented for the flow field and also for the bleed performance parameters in terms of the discharge coefficient, total pressure recovery and boundary layer characteristics downstream.

Computational Details

The PARC code [17] with a two-equation k-ε turbulence model was used in this bleed study. The turbulence model is based on Chien's low Reynolds number k-ε model [18] with Nichols [19] modifications to add compressibility effects. This code has been used in several supersonic and hypersonic inlet flow computations [20-21].

Numerical flow simulations were conducted for bleed applied through a slot normal to the wall in the interaction region of an externally generated incident oblique shock and a turbulent boundary layer. The flow was considered to be turbulent throughout the calculation domain; no attempt was made to model transition and/or relaminarization. As in our previous studies [11-13], the solution domain used in the two dimensional flow simulations extends upstream of the flat plate leading edge, downstream of the interaction region and inside the bleed slot, where the specified plenum pressure at the bottom controlled the amount of bleed mass flow. The incident oblique shock crosses the upper boundary, and all other wave systems including the reflected, and any separation and reattachment shocks, cross the outflow boundary. Uniform freestream flow conditions are applied at the inflow boundary and all variables are extrapolated at the outflow boundary. No slip adiabatic flow conditions are applied at the plate and bleed walls. The static pressure is specified and first order extrapolation is applied for the rest of the flow variables at the bottom of the bleed slot. The location of the incident shock is fixed at the upper boundary with free stream and post shock conditions specified upstream and downstream.

A 308×68 grid was used over the plate surface with $\Delta y_{min} = 0.25794 \times 10^{-4}$ ft. corresponding to $y^+=2.0$ upstream of the interaction at x = 0.9 ft. An 89×68 grid was used inside the slot which was centered around the shock impingement location at 1 ft from the flat plate leading edge. The grid spacing was varied in both x and y directions with clustering around both bleed walls and at the plate surface [13]. The computations for a typical bleed case required 5000 local time steps at 0.3 CFL number to reach steady state solution based on six orders of magnitude reductions in the averaged root mean square error in the flux.

Results and Discussion

The computations were conducted at the incoming flow conditions of $M_\infty = 2.96$, $Re_\infty = 1.2 \times 10^7$/ft, and impinging oblique shock angle of 25.84° (wedge angle of 7.93°) corresponding to the test conditions of reference [22] for the separated flow case with no bleed. The flow characteristics inside the normal bleed slot, and throughout the interaction were determined for different values of bleed mass flow, slot width, D, and length L. The pressure at the bottom of the bleed slot, p_b, was varied between 1.95 and 0.42 times the free stream values to obtain normalized bleed mass flows ranging from zero up to 0.5679 of the incoming boundary layer mass flow rate. The results are presented and compared for three different bleed slot width values of 0.0106, 0.0213 and 0.0426 ft. which represent 0.8085, 1.617 and 3.234 times the boundary layer thickness upstream of the interaction, and for bleed slot length to width ratios of 3.05 and 6.10.

Typical results of the flow field computations are presented in Fig. 1 for two bleed cases with slot widths of D/δ = 0.8085 and 1.617 at p_b/p_{loc}=0.845. Inside the slot, a significant part of the width is occupied by a large recirculaton zone while the bleed flow near the back wall reaches supersonic velocities. The pressure contours indicate a complex wave system across the bleed slot opening, starting with an expansion fan at the upstream slot corner, then a bow shock originating inside the slot. A separated flow region over the plate surface upstream of the narrow slot is indicated by the Mach number contours and the island of high pressure contours above the slot at this pressure level. This effect is greatly reduced in the wider slot with the higher bleed mass flow, where the flow reaches higher Mach numbers upstream of the outgoing slot shock. Figure 2 presents the Mach number contours for the narrow slot at different bleed plenum

pressures while Fig. 3 presents the corresponding variation in the flow properties across the slot opening. One can see that as the plenum pressure is reduced and the flow expands to higher Mach numbers at the slot opening, the shock originating in the slot becomes stronger. Eventually, the flow conditions across the slot opening remain unchanged with further plenum pressure reductions below p_b/p_{loc}=0.3831. Figure 2 indicates that at these low plenum pressures, the flow separates along the slots downstream wall, effectively producing a converging flow path leading to supersonic flow diffusion inside the slot from M ≅ 2.5 to 1.5. On the other hand, at the highest plenum pressure, p_b/p_{loc}=1.098, Fig. 3 indicates that no shock originates inside the slot, but that the mass flux out of the slot opening behind the upstream corner causes a weak oblique shock to form there.

The detailed flow field results for the different bleed configurations were further processed to characterize the bleed system performance in terms of integrated parameters such as the discharge coefficient, total pressure recovery and the boundary layer displacement and momentum thicknesses downstream of the interaction. The bleed mass flow for the individual slot is characterized in terms of the discharge coefficient, which is defined as follows:

$$C_d = m_b / AP_s \sqrt{\frac{\gamma}{RT_{t_\infty}} \left(\frac{2}{\gamma+1} \right)^{\frac{\gamma+1}{\gamma-1}}}$$

In the above definition, the bleed mass flow is normalized with respect to the ideal mass flow if isentropic flow was to expand to sonic conditions from a total temperature equal to that of the free stream and a total pressure equal to the local static pressure. With the bleed slot centered at the shock incident point at the surface, the post shock static pressure, p_{loc}, was used in the bleed discharge coefficient calculations. At the incident shock wedge angle of 7.93° and an incoming free stream Mach number of 2.96, the post shock static and total pressure ratios are p_{loc}/p_{inf} = 1.7752 and $p_{t,loc}/p_{t,inf}$ = 0.981 respectively, while the corresponding values after the reflected shock are p_2/p_{inf} = 2.96 and $p_{t2}/p_{t,inf}$ = 0.964.

Effect of Slot Width

Figures 4a and 4b present the variation in the bleed discharge coefficient and the normalized bleed mass flow with the bleed plenum pressure for different slot widths. According to this figure, the discharge coefficient is higher for the narrower slots, and the bleed mass flow continues to increase for p_b/p_{loc} < 0.528, reaching a maximum in the narrow and intermediate slot at p_b/p_{loc}≅0.2. Figure 5 presents the variation of the mass averaged total pressure at the bleed slot inlet and exit with the bleed mass flow for the different bleed widths. According to Fig. 5, the mass averaged total pressure at the slot opening changes only with the bleed mass flow and is independent of the bleed geometry. It increases with the bleed mass flow for values above 12% of the incoming boundary layer. The decrease in the slot inlet total pressure with the bleed mass flow below this value is associated with the formation of the slot bow shock at p_b/p_{loc} < 1.09 and its location relative to the slot back corner as was seen in Fig. 3. The behavior of the mass averaged total pressure at the slot exit is more complex (Fig. 5). Initially it decreases with the bleed mass flow for the narrow and intermediate slot, while it remains unchanged for the wide slot. Then the total pressure at the slot exit increases for all slot sizes and peaks at a different bleed mass flow in each case corresponding to p_b/p_{loc}≅ 0.528 (see Fig. 4). The subsequent drop in the exit total pressure in Fig. 5 was found to be associated with flow separation over slot back wall at the lower plenum pressures (see Fig. 2).

The results for the separated flow length over the plate surface, and the boundary layer displacement, and momentum thickness downstream of the interaction are presented in Figs. 6a through 6c. According to these results, both the displacement and momentum thicknesses initially decrease then start to increase with increased bleed mass flow even while the flow separation is reduced or eliminated. The narrow slot is found to perform best in terms of the maximum reduction in θ and δ* with minimum bleed mass flow, $m_b / m_{bl} < 0.10$. To explain this phenomena, Figs. 7a and 7b present the total pressure distribution across the opening and the skin friction variation over the plate surface for the three slot widths at approximately the same bleed mass flow, $m_b / m_{bl} \cong 0.12$. According to this figure, the large reductions in θ, δ* are closely associated with the weaker shock inside the narrow slot, and not with the elimination of flow separation over the plate surface.

Effect of Slot Aspect Ratio

The pressure, and Mach number distribution, across the slot opening for aspect ratios of 3.05 and 6.10 are presented in Fig. 8. According to these figures, lower static pressures, and higher flow velocities are associated with higher aspect ratio. The effect of the slot length to width ratio on bleed performance is presented in Fig. 9. The increase in L/D increases the discharge coefficient for both the narrow and intermediate slots (Fig. 9a) On the other hand, the bleed exit total pressure decreases with the increased aspect ratio as shown in Fig. 9b. The boundary layer momentum thickness downstream of the interaction decreases with L/D in the case of the intermediate slot and slightly increases for the narrow slot, but is generally not very sensitive to changes in L/D.

Conclusions

A numerical investigation was conducted to reveal the flow characteristics, and how they are affected by the bleed

configuration in an oblique shock wave/turbulent boundary layer interaction. Flow suction (bleed) was accomplished through a normal slot across the shock incident point. The bleed results reveal a complex wave pattern across the slot opening consisting of an expansion wave at the upstream slot corner, a bow shock wave originating inside the slot. The bleed flow reaches supersonic velocities inside the slot with one or two large recirculation regions at the walls depending on the plenum pressure. The effect of bleed geometry was investigated by changing the slot width and length systematically and determining the corresponding flow field at different plenum pressures. The narrow slot ($D/\delta = 0.808$) gives the best bleed performance with the highest discharge coefficient and the lowest momentum thickness downstream for the least bleed mass flow. Most importantly, eliminating separation on the plate surface was not required to optimize the boundary layer characteristics downstream, which was achieved at narrow slot bleed mass flow of $m_b/m_{bL} \leq 0.1$. As the slot aspect ratio increases, the bleed discharge coefficient increases, but the bleed flow total pressure decreases. The boundary layer momentum thickness downstream of the interaction was not very sensitive to changes in L/D.

Acknowledgements

This work was sponsored by AFOSR Contract No. 91-0101, Dr. L. Sakell, Project Monitor, and NASA Grant NAG3-1213, Mr. Dave Saunders, Project Monitor whom the authors whish to thank for his valuable suggestions. The computational work was performed on the CRAY YMP of the Ohio Supercomputer.

References

1. Hamed, A. and Shang, J., "Survey of Validation Data Base for Shock Wave Boundary Layer Interactions in Supersonic Inlets," Journal of Propulsion and Power, Vol. 7, No. 4, July 1991, pp. 617-625.

2. Fukuda, M.K., Hingst, W.R. and Reshotko, E., "Bleed Effects on Shock/Boundary-Layer Interactions in Supersonic Mixed Compression Inlets," Journal of Aircraft, Vol. 14, No. 2, 1977, pp. 151-156.

3. Wong, W.F., "The Application of Boundary Layer Suction to Suppress Strong Shock-Induced Separation in Supersonic Inlets," AIAA Paper No. 74-1063, Oct. 1974.

4. Strike, W.T. and Rippy, J., "Influence of Suction on the Interaction of an Oblique Shock with a Turbulent Boundary Layer at Mach 3," AEDC-TN-61-129, October 1961.

5. Seebaugh, W. and Childs, M., "Conical Shock Wave Boundary Layer Interaction Including Suction Effects," Journal of Aircraft, Vol. 7, No. 4, 1970, pp. 334-340.

6. Cebeci, T., "Behavior of Turbulent Flow Near a Porous Wall with Pressure Gradient," AIAA Journal, Vol. 8, December 1970, pp. 2152-2156.

7. Cebeci, T. and Shang, K.C., "Calculation of Incompressible Rough-Wall Boundary-Layer Flows," AIAA J., Vol. 16, No. 7, July 1978, pp. 730-731.

8. Abrahamson, K.W. and Bower, D.L., "An Empirical Boundary Condition for Numerical Simulation of Porous Plate Bleed Flows," AIAA Paper 88-0306, January 1988.

9. Benhachmi, D., Greber, I. and Hingst, W., "Experimental and Numerical Investigation of an Oblique Shock Wave/Turbulent Boundary Layer Interaction with Continuous Suction," AIAA Paper 89-0357, January 1989.

10. Paynter, G.C., Treiber, D.A. and Kneeling, W.D., "Modeling Supersonic Inlet Boundary Layer Bleed Roughness," AIAA Paper 92-0269, January 1992.

11. Hamed, A. and Lehnig, T., "An Investigation of Oblique Shock/Boundary Layer/Bleed Interaction," Journal of Propulsion and Power, Vol. 8, No. 2, 1992, pp. 418-424.

12. Hamed, A. and Lehnig, T., "The Effect of Bleed Configuration on Shock/Boundary Layer Interactions," AIAA Paper 91-2014, Sacramento CA, June 1991.

13. Hamed, A., Shih, S.H. and Yeuan, J.J., "An Investigation of Shock/Turbulent Boundary Layer/Bleed Interaction," AIAA Paper 92-3085, January 1992.

14. Rimlinger, M.J., Shih, T.I-P and Chyu, W.J., "Three-Dimensional Shock-Wave/Boundary-Layer Interactions with Bleed Through a Circular Hole," AIAA Paper 92-3084, January 1992.

15. Syberg, J. and Koncsek, J.L., "Bleed System Design Technology for Supersonic Inlets," AIAA Paper 72-1138, December 1972.

16. Hingst, W.R. and Tanji, F.T., "Experimental Investigation of Two-Dimensional Shock-Boundary Layer Interaction with Bleed," AIAA Paper 83-0135, 1983; also NASA TM-83057, 1983.

17. Cooper, G.K., and Sirbaugh, J.R., "PARC Code: Theory and Usage," AEDC-TR-89-15, 1989.

18. Chien, K-Y, "Prediction of Channel and Boundary-Layer Flows with a Low Reynolds Number Turbulence Model," AIAA Journal, Vol. 20, January 1982, pp 33-38.

19. Nichols, R. H., "A Two-Equation Model for Compressible Flows," AIAA Paper 90-0494, AIAA 28th Aerospace Sciences Meeting, Reno, NV, January 1990.

20. Reddy, D.R., Smith, G.E. and Liou, M.F., "Three-Dimensional Viscous Analysis of a Hypersonic Inlet," AIAA Paper 89-0004, January 1989.

21. Weir, L.J., Reddy, D.R. and Rupp, G.D., "Mach 5 Inlet CFD and Experimental Results," AIAA Paper 89-2355, July 1989.

22. Law, C.H., "Supersonic Turbulent Boundary Layer Separation," AIAA Journal, Vol. 12, June 1974, pp. 794-797.

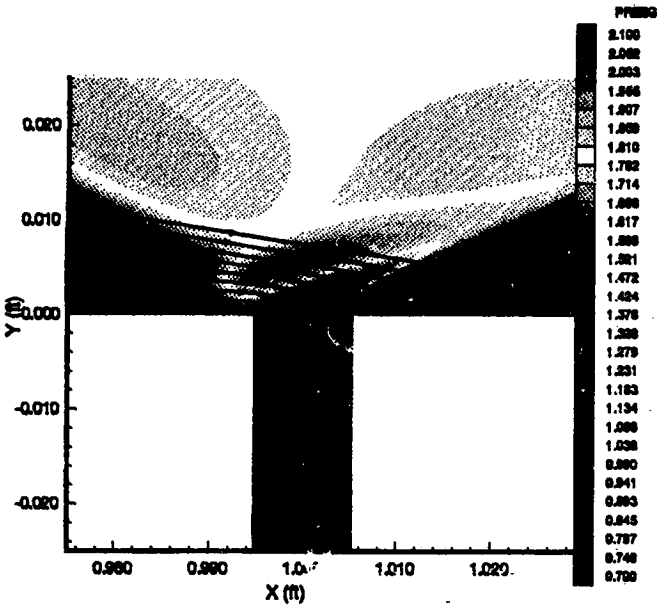

Fig. 1a. Pressure Contours and Streamlines, $D/\delta = 0.8085$, $L/D = 3.05$ and $p_b/p_{loc} = 0.676$.

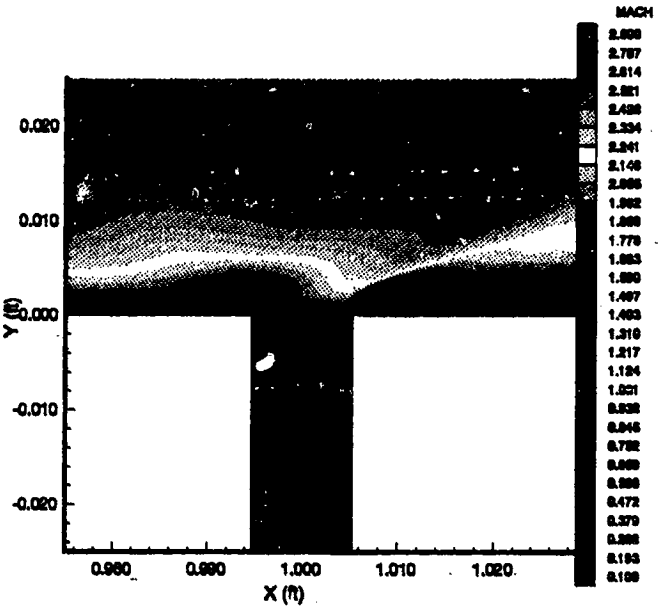

Fig. 1b. Mach Number Contours, $D/\delta=0.8085$ $L/D = 3.05$ and $p_b/p_{loc} = 0.676$.

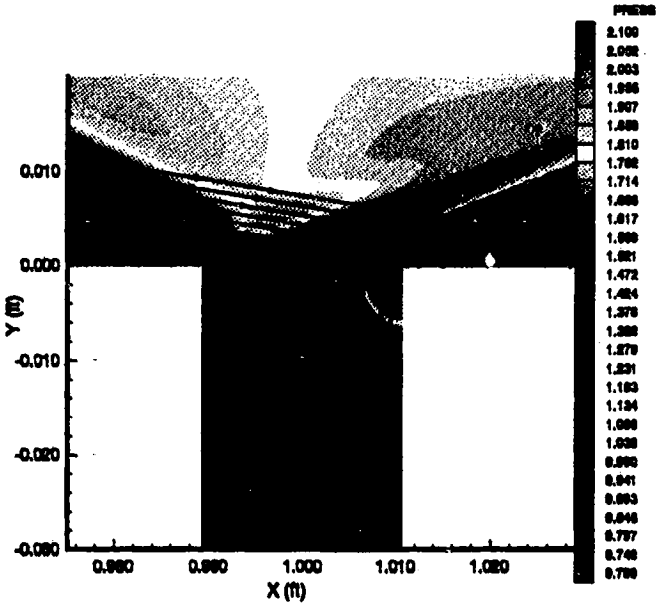

Fig. 1c. Pressure Contours and Streamlines, $D/\delta = 1.617$, $L/D = 3.05$ and $p_b/p_{loc} = 0.676$.

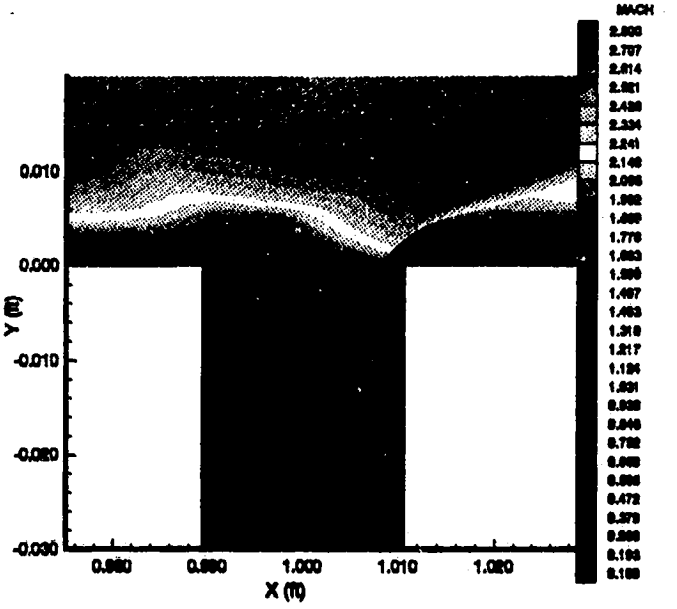

Fig. 1d. Mach Number Contours, $D/\delta=1.617$ $L/D = 3.05$ and $p_b/p_{loc} = 0.676$.

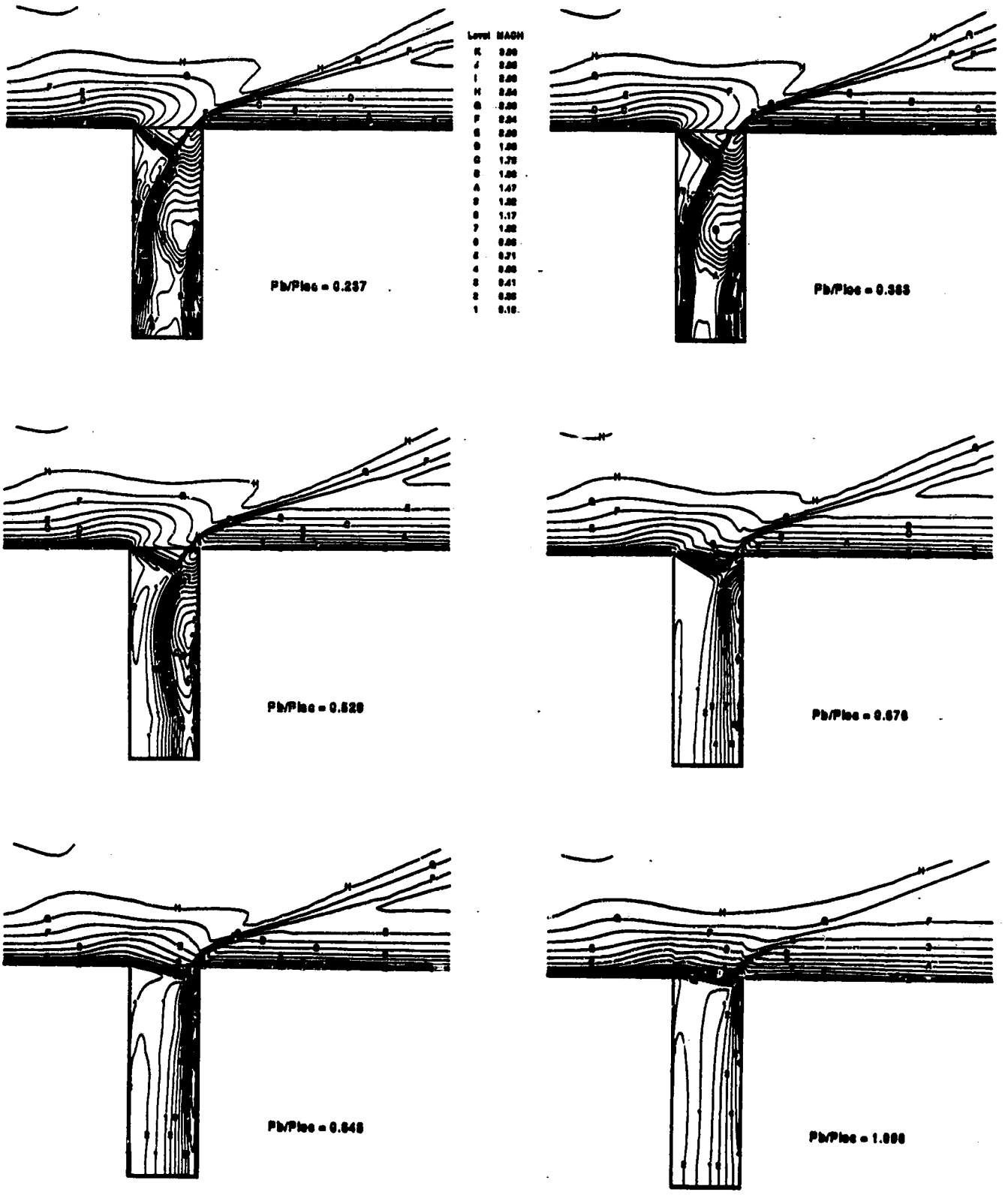

Fig. 2. Mach Number Contours at Different Plenum Pressures ($D/\delta = 0.808$, $L/D = 3.05$)

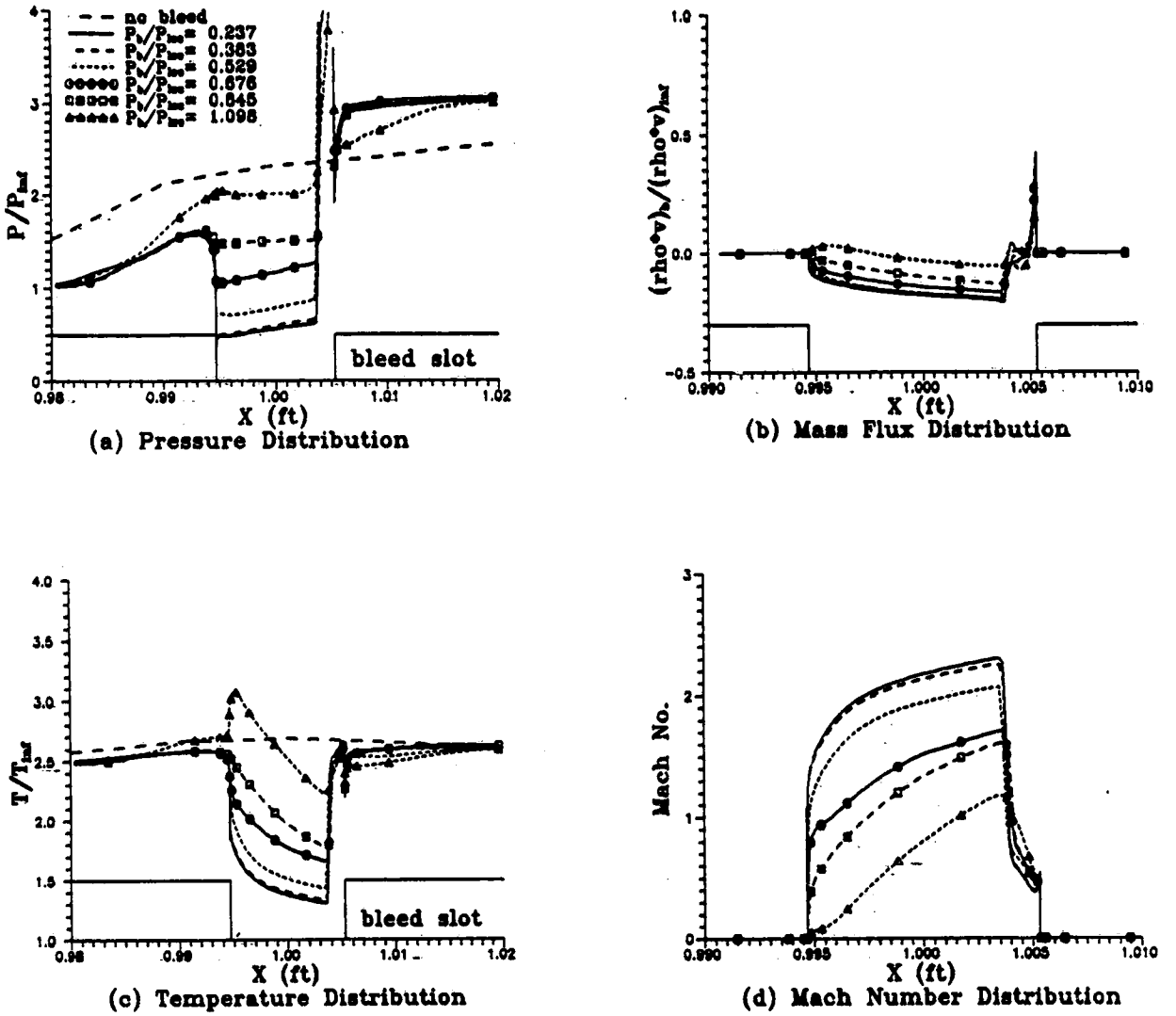

Fig. 3. Effect of Bleed Pressure on Flow Properties at the Slot Opening, D/δ = 0.808 and L/D = 3.05.

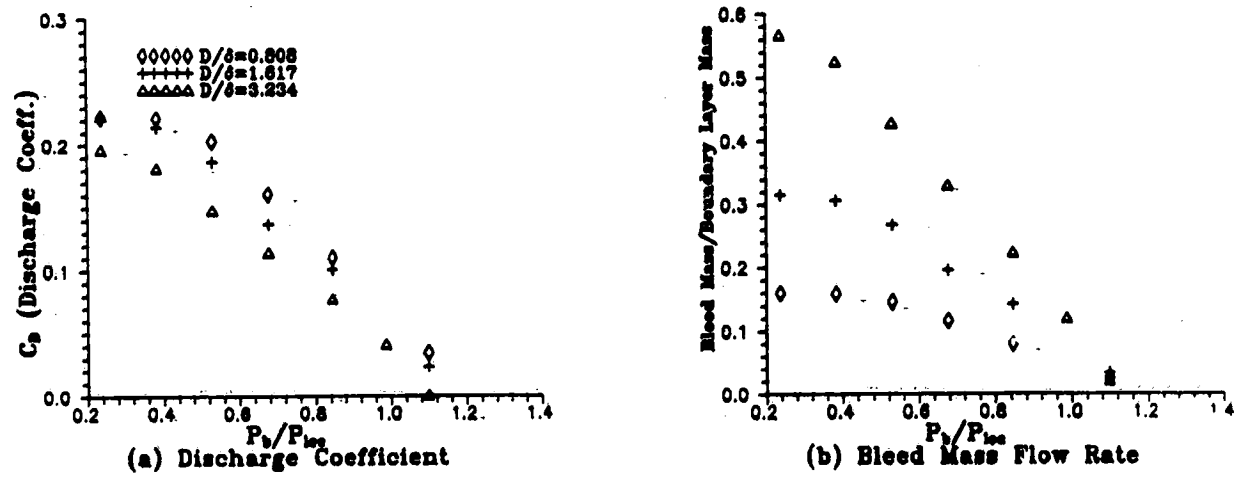

Fig. 4. Effect of Slot Width on Bleed Discharge Coefficient and Mass Flow Rate, L/D = 3.05.

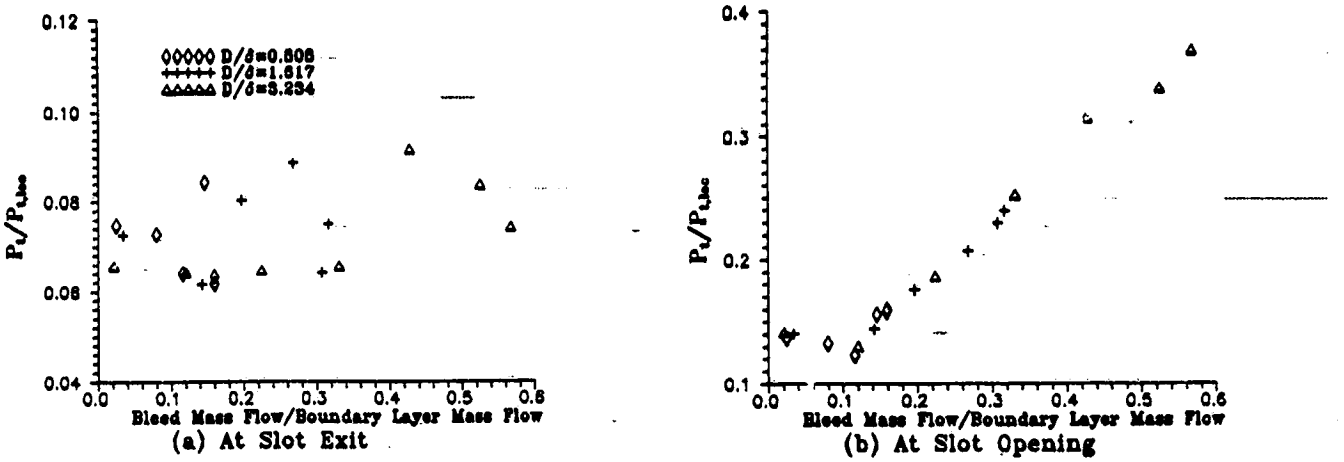

Fig. 5. Effect of Slot Width on Bleed Mass Averaged Total Pressure, L/D = 3.05

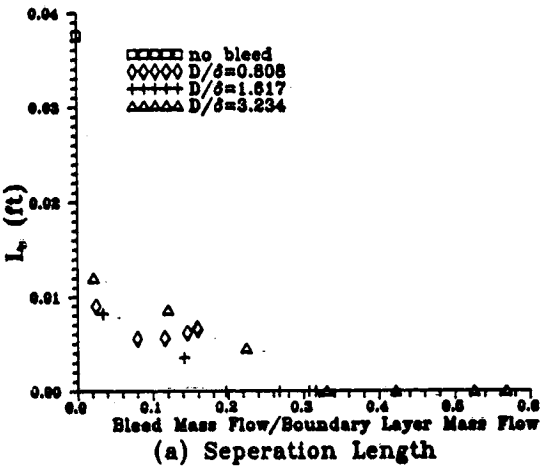

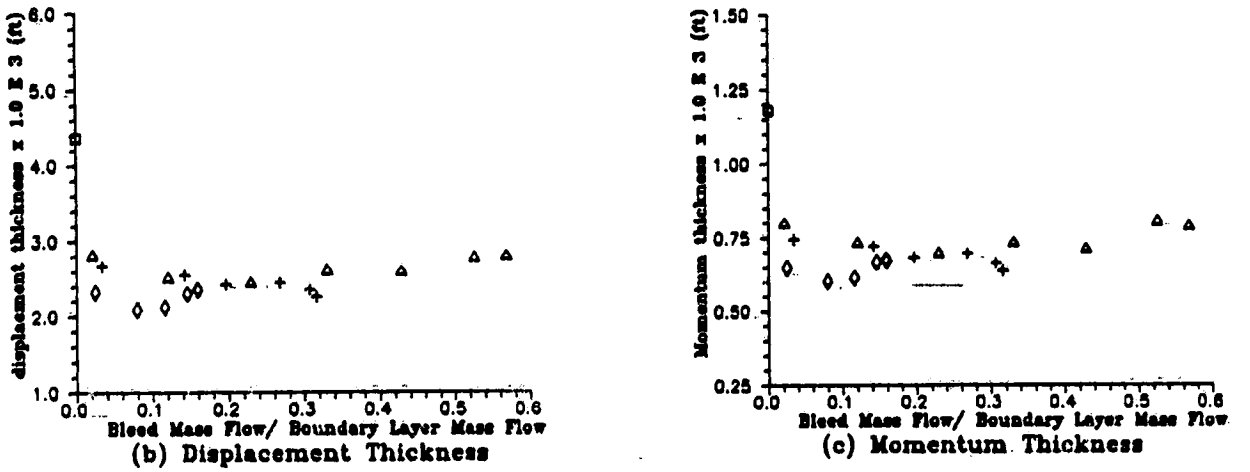

Fig. 6. Effect of Slot Width on Seperation Length, Displacement and Momentum Thickness Downstream of Interaction at x = 1.13 ft, L/D = 3.05

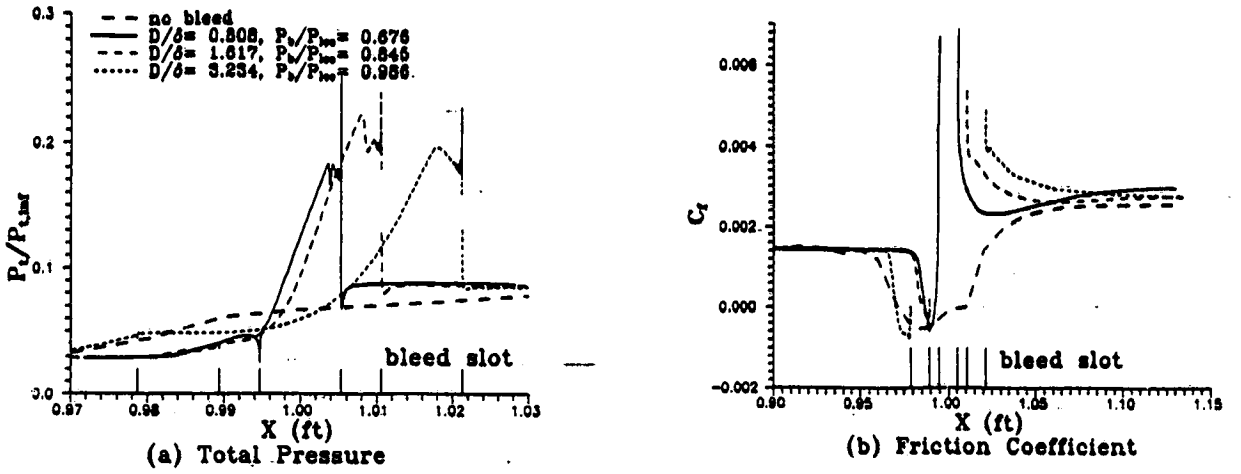

Fig. 7. Effect of Slot Width on Total Pressure and Friction Coefficient in the Interaction Region.

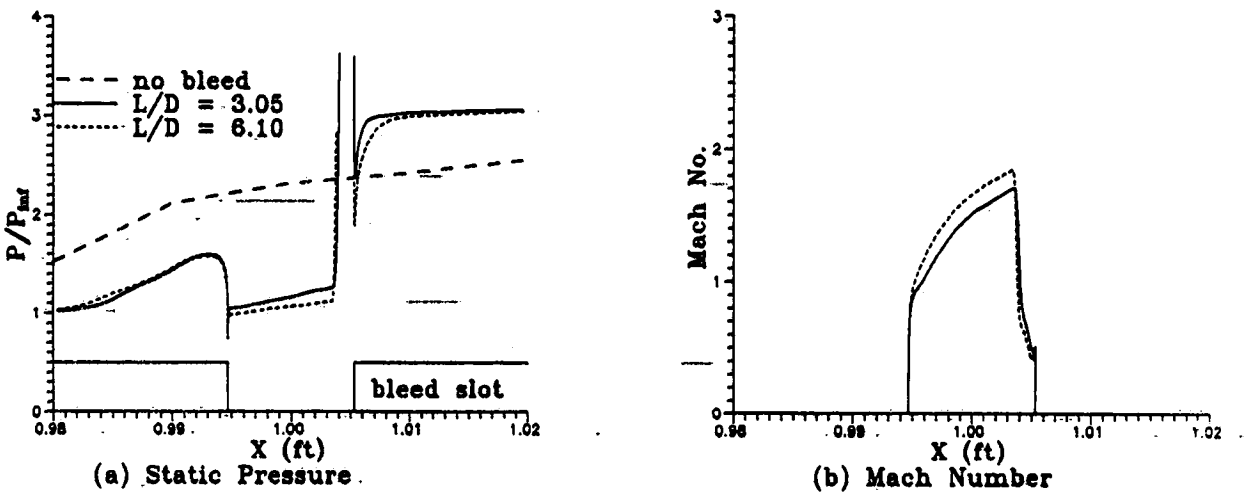

Fig. 8. Effect of Slot Aspect Ratio on Flow Properties Across the Slot Opening.

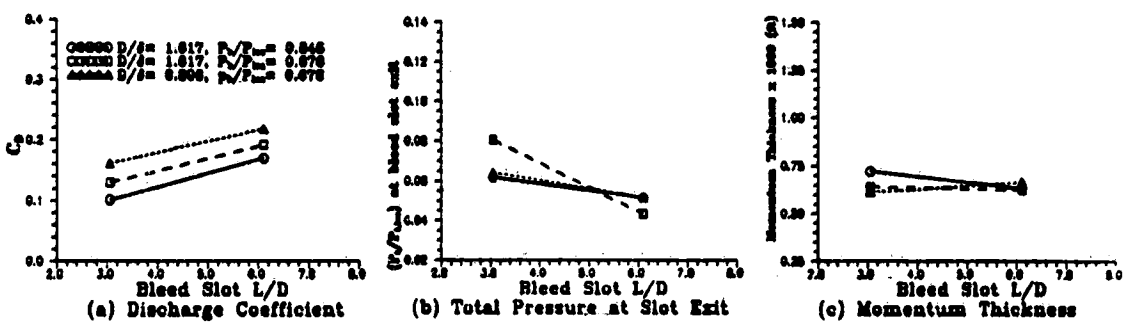

Fig. 9. Effect of Slot Aspect Ratio on Bleed Performance.

APPENDIX D

AIAA 93-2992

An Investigation of Shock Wave Turbulent Boundary Layer Interaction with Bleed Through Slanted Slots

A. Hamed, J.J. Yeuan and S.H. Shih
University of Cincinnati
Cincinnati, Ohio

AIAA 24th
Fluid Dynamics Conference
July 6-9, 1993 / Orlando, FL

AIAA 93-2992

AN INVESTIGATION OF SHOCK WAVE TURBULENT BOUNDARY LAYER INTERACTION WITH BLEED THROUGH SLANTED SLOTS

A. Hamed*, J.J. Yeuan**, and S.H. Shih***
Department of Aerospace Engineering and Engineering Mechanics
University of Cincinnati
Cincinnati, OH 45221

ABSTRACT

The flow field characteristics are simulated numerically in an oblique shock wave/turbulent boundary layer interactions with six different bleed slot configurations. The strong conservation-law form of the two-dimensional compressible Navier-Stokes equations and the k-ε equations are solved throughout the interaction region and inside the bleed slot. The computed results are presented for a normal and 20° slanted bleed slots at three different locations, upstream, across and downstream of the impingement point of an oblique shock of sufficient strength to cause boundary layer separation without bleed. The detailed flow characteristics in the interaction zone and inside the bleed slot are compared for the different bleed slot configurations. The resulting surface pressure and shear stress distributions as well as the boundary layer characteristics downstream of the interaction region are also presented for the six bleed configurations at different bleed mass flows up to choking.

INTRODUCTION

Air bleed systems are used for controlling the shock wave boundary layer interactions when operating at supersonic speeds. Proper bleed system design is particularly important for the efficient and stable operation of mixed compression supersonic inlets [1]. The fundamental objectives of supersonic inlet bleed system design are to provide good aerodynamic flow characteristics with minimum boundary layer bleed [2, 3].

Comparisons of internal flow computational results [5, 6, 7] with the experimental measurements in supersonic inlets [7, 8] revealed reasonable agreement between the computed and measured surface pressures upstream of the ramp bleed. However, discrepancies in the predicted shock locations and velocity profiles were observed downstream of shock boundary layer interactions with bleed.

Hamed and Shang [1] reviewed the existing experimental data base for shock wave/boundary layer interactions in supersonic inlets and other related configurations. According to this survey, there is enough experimental evidence [9-14] to indicate that local bleed can control flow separation in shock wave/boundary layer interactions. There are disagreements [1] however among the different experimental results regarding the effects of bleed location relative to the shock [9-12]. Strike and Rippy [9] measured the surface pressure in the interaction zone of an oblique shock wave impinging a turbulent boundary layer over a flat plate with suction. They determined that less suction is required to control separation, when applied upstream of the shock. Seebaugh and Childs [10] investigated experimentally the axisymmetric flow in the interaction region of the boundary layer inside a duct. Contrary to the conclusions of Strike and Rippy [9], suction within the interaction region was found to be more effective in suppressing the effects of separation.

Remlinger et al. [15] and Hamed et al. [16-20] modeled bleed by resolving the flow through the individual bleed ports. The advantage of this approach over that which simulates the hole roughness effects [13, 14] is that the bleed mass flux distribution, the bleed drag, as well as the boundary-layer characteristics downstream can be determined from the numerical solution. Comparative information regarding the effect of bleed hole sizes, slant angle and bleed location relative to the shock can be obtained using this approach to help resolve the controversy among the different experimental data concerning the effect of these parameters. Hamed et al. [17] investigated the effects of slot width, depth [18-20] and slot slant angle on the flow field in the interaction zone of an oblique shock/turbulent boundary layer interaction. The results obtained in these investigations for bleed through slots located across the shock impingement point indicate that turbulent boundary layer separation could be eliminated by removing 10 to 16 percent of the incoming boundary layer mass flow through slanted slots. The slots with low slant angle have higher discharge coefficients and start to bleed at higher plenum pressures. In addition they produce redeveloping boundary layer downstream with higher friction coefficient. The purpose of this study is to investigate the effect of bleed location relative to the shock on the flow field in the interaction region and downstream. For this purpose numerical simulations were conducted for

---

* Professor, Fellow AIAA
** Post Doctoral Assistant, Member AIAA
*** Student Member, AIAA

both normal and 20° slanted slots at three locations, upstream, across and downstream of the shock impingement point. The computed results for the different configurations are presented to demonstrate their effect on the flow field in the interaction zone and downstream of the interaction as well as the bleed flow inside the slot.

Computational Details

Numerical flow simulations were conducted for bleed applied through normal and slanted slots in the interaction region of an externally generated incident oblique shock and a turbulent boundary layer. The flow was considered to be turbulent throughout the calculation domain; no attempt was made to model transition and/or relaminarization. As in our previous studies [16-20], the solution domain used in the two dimensional flow simulations extends upstream of the flat plate leading edge, downstream of the interaction region and inside the bleed slot, where the specified plenum pressure at the bottom controlled the amount of bleed mass flow.

The upper solution domain boundary was set at 0.13 ft. from the flat plate with the lower solution domain at the bottom of the bleed slot. In the streamwise direction, the domain extended along the plate length of 1.13 ft. and the distance of 0.07 ft., upstream of the plate leading edge to the station where the uniform upstream conditions are applied. The incident oblique shock crosses the upper boundary, and all other wave systems including the reflected, and any separation and reattachment shocks, cross the outflow boundary. Uniform freestream flow conditions are applied at the inflow boundary and all variables are extrapolated at the outflow boundary. No slip adiabatic flow conditions are applied at the plate and bleed walls. The static pressure is specified and first order extrapolation is applied for the rest of the flow variables at the bottom of the bleed slot. The location of the incident shock is fixed at the upper boundary with free stream and post shock conditions specified upstream and downstream.

The PARC code [21] with a two-equation k-ε turbulence model was used in this bleed study. The turbulence model is based on Chien's low Reynolds number k-ε model [22] with Nichols [23] modifications to add compressibility effects. This code has been used in several supersonic and hypersonic inlet flow computations [7, 24].

The computations were performed using a 308x68 grid over the plate surface and an 89x68 grid inside the bleed slot. Variable grid spacing was used in both x and y directions for grid clustering around the bleed walls and at the plate surface, with $y_{min} = x_{min} = 0.2579410^{-4}$ ft. corresponding to $y^+ = 2.0$ at $x = 0.9$ ft. The computations for a typical bleed case required 5000 local time steps at 0.2 CFL number to reach steady state solution based on six orders of magnitude reductions in the averaged root mean square error in the flux at three different locations relative to the shock.

Results and Discussion

The computations were conducted at the incoming flow conditions of M = 2.96, Re = 1.2×10^7/ft, and an impinging oblique shock angle of 25.84° (wedge angle of 7.93°) corresponding to the test conditions of reference [25] for the separated flow case with no bleed. The flow characteristics inside the bleed slot, and throughout the interaction were determined for bleed through a normal and 20° slanted slot. The slot width for the normal bleed case was 0.01065 ft. which is equal to 0.8085 times the boundary layer thickness upstream of the interaction. To maintain comparable bleed mass flows among the normal and slanted bleed cases, the opening at the plate surface was maintained at 0.0106 ft. leading to a slot width which is 0.2766 times the boundary layer upstream for the 20° slanted slots. The effect of bleed location was investigated by studying the flow field with bleed applied upstream, across and downstream of the incident shock interaction with the plate surface. The slot opening center, X_{ref}, was located at 0.99468, 1.0 and 1.00532 ft. from the plate leading edge for the three cases respectively. This corresponds to the incident shock interaction point with the plate was situated at the downstream corner, the center and the upstream corner respectively for the three bleed locations.

Figure 1 presents the Mach number contours for the six different slot geometries at choked conditions. The wave system across the bleed opening consists of an expansion fan at the upstream slot corner then an oblique shock at the downstream corner of the slanted bleed slot or a bow shock that originates inside the normal slot. The recirculation flow region inside the slot at upstream wall occupies a large portion of the slot width in the normal bleed cases, but is much smaller in extent inside the 20° slanted slot. The two mechanisms controlling the formation of recirculation region inside the slot at the upstream wall are insufficient flow turning into the normal bleed slot, and the impinging oblique shock wave which originates at the downstream edge of the bleed slot in the 20° slanted bleed [20]. The corresponding Mach number and flow angle distribution across the slot opening are presented in Figures 2 and 3. The static pressure and friction coefficient distribution over the plate surface are presented in Figures 4 and 5. In all these figures, the results for the three different bleed locations were shifted such that they were all aligned around the center of the bleed opening, X_{ref}, in each case. According to these figures, the Mach number is initially higher in the upstream bleed case but approaches the same value towards the slot's downstream corner as the other two bleed locations. The flow angle is equal to the slot angle in the 20° slanted bleed but is less than 40° in the case of normal bleed. In the normal bleed slot cases, the flow angles are highest for the downstream bleed and lowest for the upstream bleed. The initial sharp flow overturning in the normal bleed case (Fig. 3) is caused by a small separation bubble on the plate

surface upstream of the slot which is confirmed by the negative friction in Fig. 5. According to Fig. 5 which presents the skin friction distribution over the plate surface, a small separated flow region is predicted at upstream of the slot and an even smaller one at downstream corner in all normal bleed cases. On the other hand, no flow separation was predicted over the plate surface with the 20° slanted bleed slot upstream and across of the shock. In the 20° slanted bleed downstream of the shock, the flow separates over the plate surface upstream of the slot opening. According to Figs. 4 and 5, the mass removal effects extend both upstream and downstream of the bleed slot and is reflected in both the surface pressure and friction coefficient. The pressure rise downstream of the bleed slot is faster in the normal bleed than the slanted bleed for all three locations. The change in the friction coefficient over the plate surface downstream of the interaction is characteristically that of boundary layer redeveloping in the case of bleed through the slanted slots [20]. However the skin friction distribution downstream of the interaction is very different in the case of normal bleed since the stagnation point is slightly inside the slot's downstream wall [20].

Figure 6 presents the variation in the discharge coefficient with the plenum pressure, P_b, normalized by the local pressure, P_{loc}. For the bleed locations upstream, across and downstream, P_{loc} represents the pressure before the incident shock ($P_{loc} = 1.0\ P_{inf}$), behind the incident shock ($P_{loc} = 1.7752\ P_{inf}$), and behind the reflected shock ($P_{loc} = 2.96\ P_{inf}$) respectively. The same data is represented in Fig. 7 in the form of bleed mass flow as a percentage of the boundary layer mass flow upstream of the interaction at x = 0.9 ft. According to these figures, the highest discharge coefficient is obtained with the upstream bleed through 20° slot and the lowest with downstream through normal slot. The slanted bleed discharge coefficient is very sensitive to the bleed location where higher discharge coefficients are obtained with upstream bleed, while the downstream bleed resulted in choked discharge coefficients lower than the across the shock bleed. The difference between the discharge coefficients for the upstream and across the shock normal bleed is very small. The highest bleed mass flow is obtained with normal bleed across the shock and with 20° slanted bleed downstream of the shock. The lowest choked bleed mass flow is obtained with the normal bleed upstream of the shock. In general bleed mass flow changes were gradual and choking occurred at lower plenum pressures in the case of normal bleed. This is consistent with the experimental hole bleed data presented by Syberg and Koncsek [2].

The effect of bleed mass flow on the boundary layer characteristics downstream of the interactions at X=1.13 ft. is presented in Figures 8 through 11 for all six configurations. According to these figures, all slot configurations produce nearly the same displacement thickness, $\delta^* = 0.0024$ ft. and momentum thickness, $\theta = 0.0007$ ft. at choking, but the bleed through the normal slot across the shock produces lower values ($\delta^* = 0.0020$ ft. and $\theta = 0.0006$ ft.) at a lower bleed mass flow rate (8% of the boundary layer). In general the transformed form factor downstream of the interaction did not change significantly over the bleed mass flow range. It had the smallest value ($H_x = 1.36$) for the normal slot at 15% bleed mass flow. This is consistent with the data presented by Fukuda et al. [3] for the scoop in the case of the forward centerbody interaction where the upstream edge Mach number was 2.09. However the friction coefficient is low for the normal bleed at these conditions. The small effect of the bleed configuration can be attributed to the small differences in the bleed slot locations (a maximum of 0.0106 ft. or 0.8085 times the boundary layer thickness upstream). Additional results were obtained for wider normal slots, whose centers were located at X=0.97872 ft., X=1.0 ft and X=1.04256 ft. from the leading edge. The resulting boundary layer characteristics for these wide slots (D/δ=3.234) are presented in Figures 12 and 13. According to the results in these figures, across the shock bleed produces larger reductions in both displacement and momentum thickness than both upstream and downstream bleeds. All these configurations produce the same effect at bleed mass flows equal to 28% of the incoming boundary layer. However these large bleed mass flow with the wider normal slots do not improve the downstream boundary layer characteristics compared to the smaller bleed mass flows through the narrow slots.

Conclusions

A numerical investigation was conducted to study the effect of 20° slanted and normal bleed slot location relative to the shock on the flow field in an oblique shock wave/turbulent boundary layer interaction. The results indicate that the slanted bleed slot discharge coefficient is more sensitive to bleed location. The highest discharge coefficient is obtained with the slanted bleed slot located upstream of the incident shock followed by the slot located across the shock. The normal bleed discharge coefficient is less sensitive to the bleed location but is lowest in the case of downstream bleed. Higher bleed mass flows are obtained however with the downstream bleed location. The boundary layer momentum and displacement thickness downstream of the interaction approached the same value for all bleed configurations at choked conditions, but otherwise varied with the bleed location in the case of normal unchoked bleed. The smallest reduction in the δ^* and θ were obtained with normal upstream bleed and the largest reduction with the across the shock unchoked normal bleed. However the friction coefficient was much higher for slanted bleed. The boundary layer characteristics were more sensitive to bleed location for larger bleed mass flows through wide normal slots. In general across the shock bleeds resulted in larger reductions in both δ^* and θ but all bleed locations were most effective and produced similar reductions when 26 percent of the incoming boundary layer was bled through the normal slots.

Acknowledgements

This work was sponsored by NASA Lewis Research Center, Mr. D. Saunders, Project Monitor. The computational work was performed on the CRAY YMP of the Ohio Supercomputer.

REFERENCES

1. Hamed, A. and Shang, J., "Survey and Assessment of the Validation Data Base for Shock Wave Boundary Layer Interactions in Supersonic Inlets," AIAA Paper 89-2939, July 1989.

2. Syberg, J. and Koncsek, J.L., "Bleed System Design Technology for Supersonic Inlets," AIAA/SAE 8th Joint Propulsion Specialist Conference, AIAA Paper No. 72-1138, 1972.

3. Fukuda, M.K., Hingst, W.R. and Reshotko, E., "Bleed Effects on Shock/Boundary-Layer Interactions in Supersonic Mixed Compression Inlets," J. Aircraft, Vol. 14, No. 2, pp. 151-156, February 1977.

4. Hamed. A.,"Flow Separation in Shock Wave-Bounday Layer Interactions at Hypersonic Speeds", NASA CR 4274. February 1990.

5. Martin, A.W., Koslin, L.C. and Sidney, D.M., "Dynamic Distortion at the Exit of a Subsonic Diffuser of a Mixed Compression Inlet," NASA CR-1644, December 1970.

6. Knight, D.D., "Improved Calculation of High Speed Inlet Flows. Part I: Numerical Algorithm," AIAA J., Vol. 19, No. 1, January 1981, pp. 34-41, and "Part II: Results," AIAA J., Vol. 19, No. 2, February 1981, pp. 172-179.

7. Weir, L.J., Reddy, D.R. and Rupp, G.D., "Mach 5 Inlet CFD and Experimental Results," AIAA Paper 89-2355, July 1989.

8. Carter, T.D. and Spong, E.D., "High Speed Inlet Investigation. Vol. I Description of Program and Results; Vol. II Data Summary," AFFDL-TR-77-105, November 1977.

9. Strike, W.T. and Rippy, J., "Influence of Suction on the Interaction of an Oblique Shock with a Turbulent Boundary Layer at Mach 3," AEDC-TN-61-129, October 1961.

10. Seebaugh, W. and Childs, M., "Conical Shock Wave Boundary Layer Interaction Including Suction Effects," Journal of Aircraft, Vol. 7, No. 4, 1970, pp. 334-340.

11. Benhachmi, D., Greber, I. and Hingst, W., "Experimental and Numerical Investigation of an Oblique Shock-Wave/Turbulent Boundary Layer Interaction with Continuous Suction," AIAA Paper 89-0357, January 1989.

12. Gubbison, R.W., Meleason, E.T. and Johnson, D.F., "Performance Characteristics from Mach 2.58 to 1.98 of an Axisymmetric Mixed Compression Inlet System with 60 Percent Internal Contraction," NASA TM X-1739, February 1969.

13. Fukuda, M.K., Hingst, W.G. and Reshotko, E., "Control of Shock Boundary Layer Interactions by Bleed in Mixed Compression Inlets," NASA CR 2595, 1975.

14. Wong, W.F., "The Application of Boundary Layer Suction to Suppress Strong Shock-Induced Separation in Supersonic Inlets," AIAA Paper No. 74-1063, October 1974.

15. Rimlinger, M.J., Shih, T.I-P and Chyu, W.J., "Three-Dimensional Shock-Wave/Boundary-Layer Interactions with Bleed Through a Circular Hole," AIAA Paper 92-3084, January 1992.

16. Hamed, A. and Lehnig, T., "An Investigation of Oblique Shock/Boundary Layer/Bleed Interaction," Journal of Propulsion and Power, Vol. 8, No. 2, 1992, pp. 418-424.

17. Hamed, A. and Lehnig, T., "The Effect of Bleed Configuration on Shock/Boundary Layer Interactions," AIAA Paper 91-2014, Sacramento CA, June 1991.

18. Hamed, A., Shih, S.H. and Yeuan, J.J., "An Investigation of Shock/Turbulent Boundary Layer/Bleed Interaction," AIAA Paper 92-3085, January 1992.

19. Hamed, A., Shih, S.H. and Yeuan, J.J., "A Parametric Study of Bleed in Shock Boundary Layer Interactions," AIAA Paper 93-0294, January 1993.

20. Hamed, A., Yeuan, J.J. and Shih, S.H., "An Investigation of Shock Wave Turbulent Boundary Layer Interaction with Bleed Through Normal and Slanted Slots," AIAA Paper 93-2155, June 1993.

21. Cooper, G.K., and Sirbaugh, J.R., "PARC

Code: Theory and Usage," AEDC-TR-89-15, 1989.

22. Chien, K-Y, "Prediction of Channel and Boundary-Layer Flows with a Low Reynolds Number Turbulence Model," AIAA Journal, Vol. 20, January 1982, pp 33-38.

23. Nichols, R. H., "A Two-Equation Model for Compressible Flows," AIAA Paper 90-0494, AIAA 28th Aerospace Sciences Meeting, Reno, NV, January 1990.

24. Reddy, D.R., Smith, G.E., and Liou, M.F., "Three-Dimensional Viscous Analysis of Hypersonic Inlet," AIAA Paper 89-0004, January 1989.

25. Law, C.H., "Supersonic Turbulent Boundary Layer Separation," AIAA Journal, Vol. 12, June 1974, pp. 794-797.

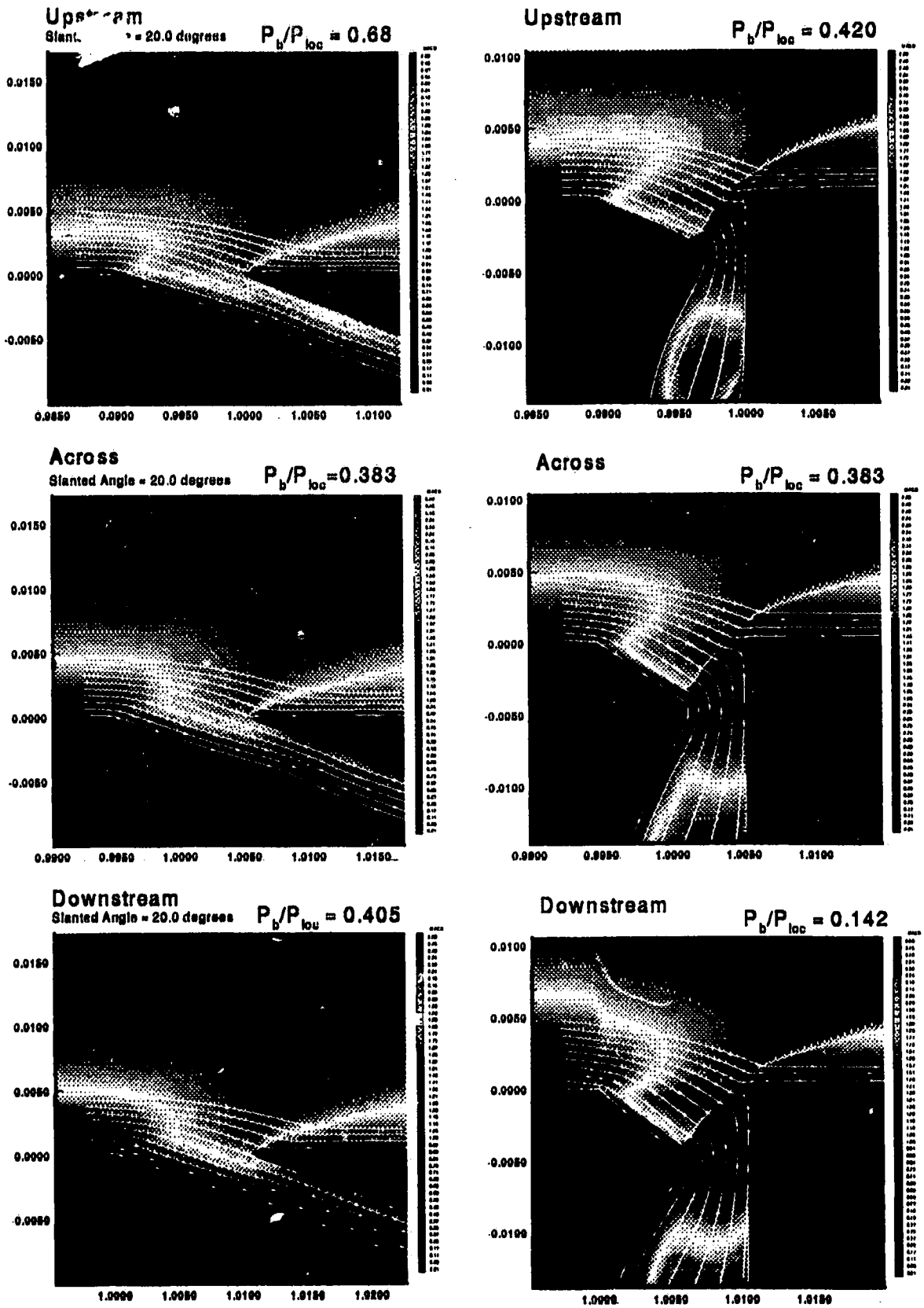

Fig. 1. Mach Number Contours for Six Different Slot Geometries at Choked Conditions

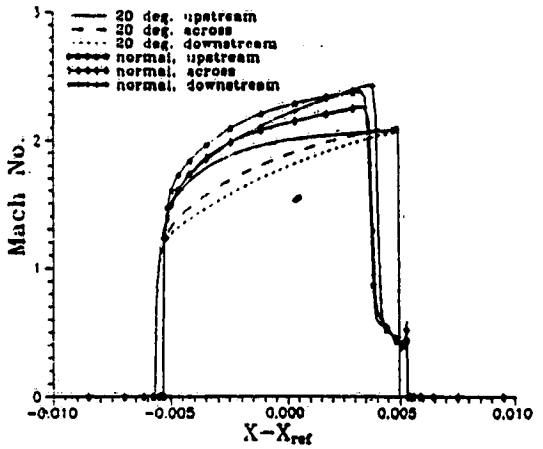

Fig. 2. Mach Number Distribution Across the Slot Opening at Choked Conditions.

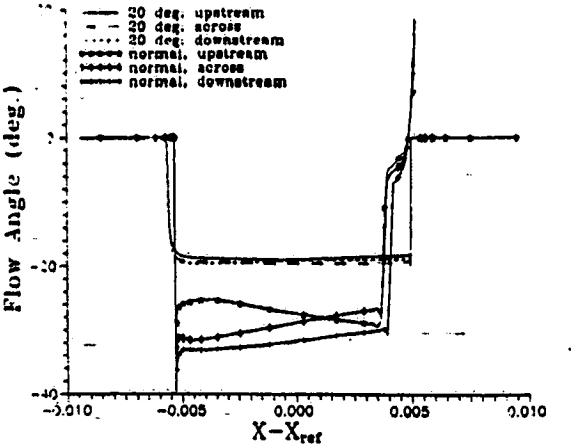

Fig. 3. Flow Angle Distribution Across the Slot Opening at Choked Conditions.

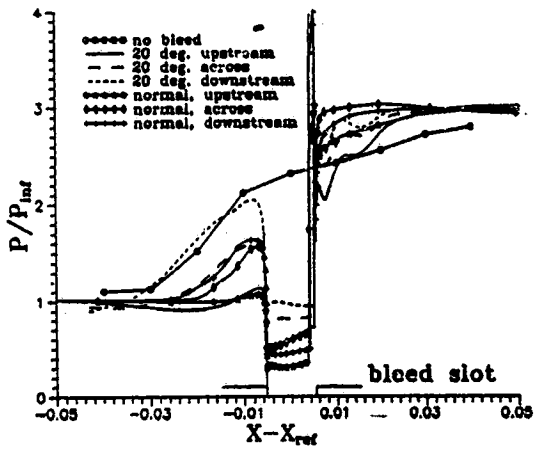

Fig. 4. Static Pressure Distribution Across the Slot Opening at Choked Conditions.

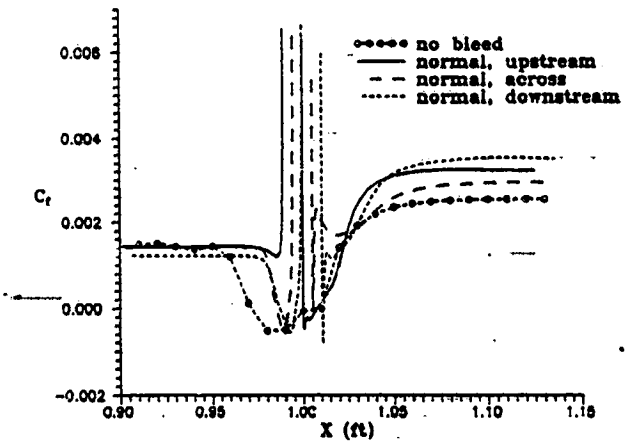

Fig. 5a. Friction Coefficient Distribution in the Interaction Region at Choked Conditions.

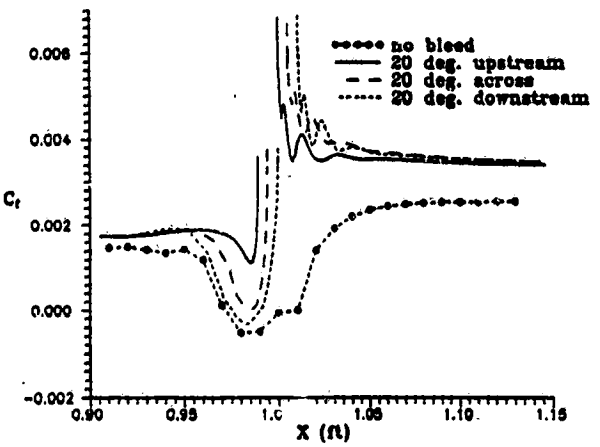

Fig. 5b. Friction Coefficient Distribution in the Interaction Region at Choked Conditions.

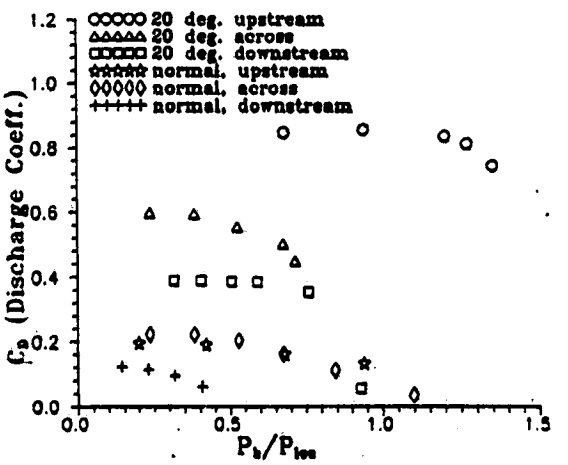

Fig. 6. Variation of Discharge Coefficient with the Bleed Plenum Pressure.

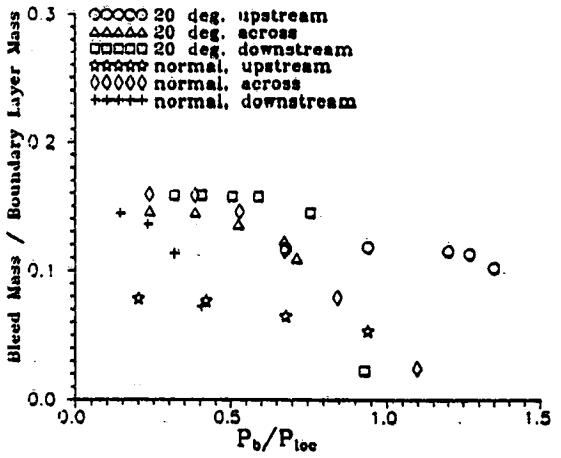

Fig. 7. Variation of Bleed Mass Flow Rate with the Bleed Plenum Pressure.

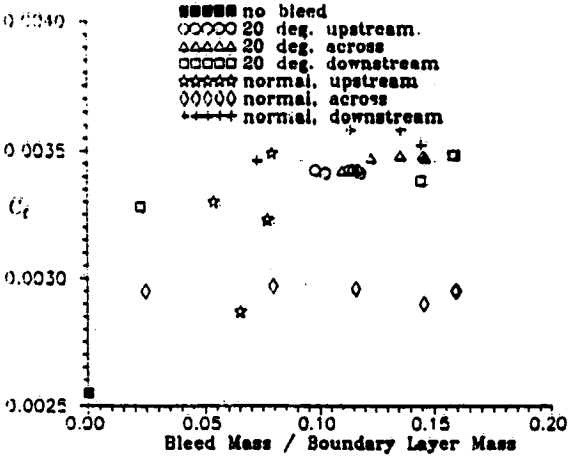

Fig. 8. Effect of Bleed Mass Flow on the Friction Coefficient Downstream of Interaction Region, at X = 1.13 ft.

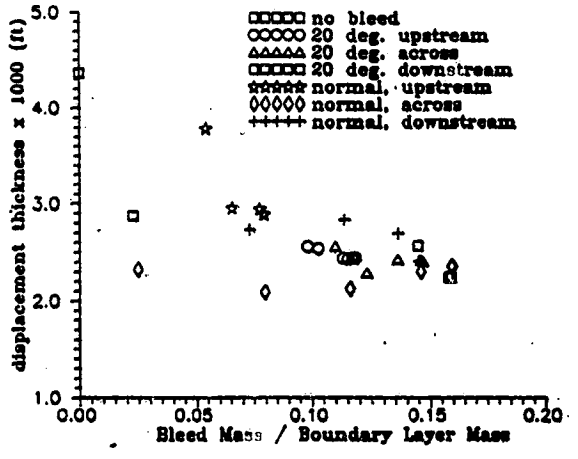

Fig. 9. Effect of Bleed Mass Flow on the Displacement Thickness Downstream of Interaction Region, at X = 1.13 ft.

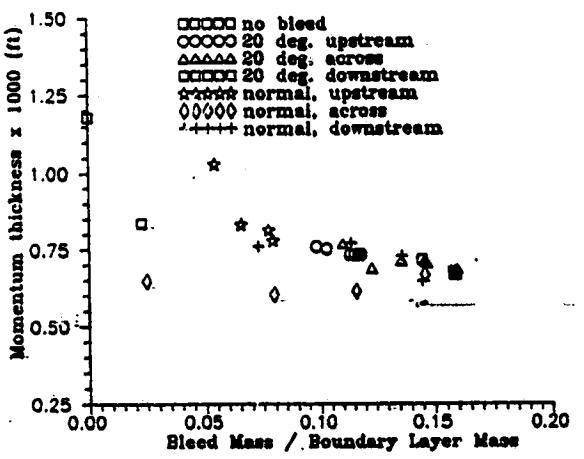

Fig. 10. Effect of Bleed Mass Flow on the Momentum Thickness Downstream of Interaction Region, at X = 1.13 ft.

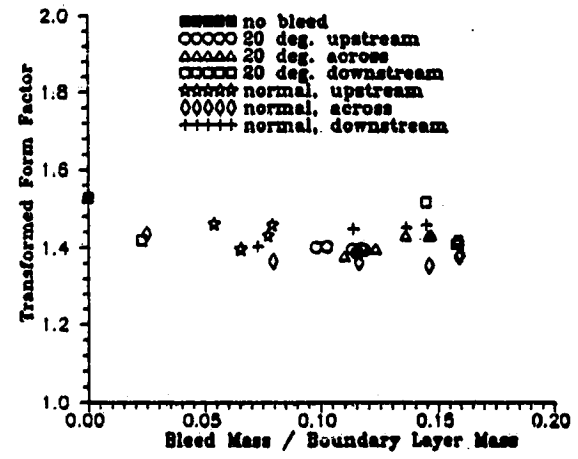

Fig. 11. Effect of Bleed Mass Flow on the Transformed Form Factor Downstream of Interaction Region, at X = 1.13 ft.

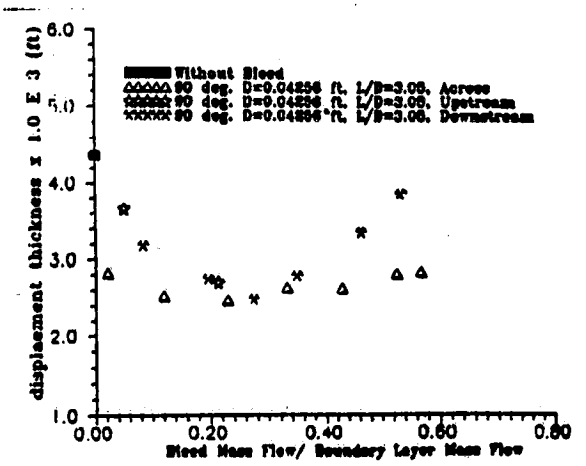

Fig. 12. Effect of (Bleed Mass Flow/B.L. Mass Flow) on the Displacement Thickness Downstream of Interaction Region, at X = 1.13 ft.

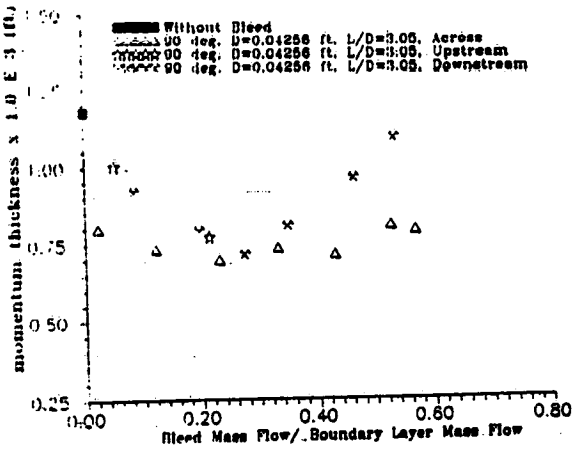

Fig. 13. Effect of (Bleed Mass Flow/B.L. Mass Flow) on the Momentum Thickness Downstream of Interaction Region, at X = 1.13 ft.

APPENDIX E

FLOW CHARACTERISTICS IN BOUNDARY LAYER BLEED SLOTS WITH PLENUM

A. Hamed*, J.J. Yeuan and Y.D. Jun*****
Department of Aerospace Engineering and Engineering Mechanics
University of Cincinnati
Cincinnati, OH 45221

Abstract

Numerical simulations were conducted to investigate the performance characteristics of bleed through normal slots and its effect on the turbulent boundary layer development under zero and strong adverse pressure gradient caused by incident oblique shock. The solution to the compressible Navier-Stokes and k-ε equations was obtained in a domain that includes the regions inside the bleed slot and plenum in addition to the external flow. The computational results demonstrate the interactions between the plenum, and bleed flow and the effect of incident shock on the boundary layer development downstream. The computed results agree with the experimentally measured pitot and static pressure distribution inside the slot. The bleed mass flow without incident shock was underpredicted over the range of plenum pressures. The computations predicted the measured increase in bleed mass flow with incident shock.

Introduction

Bleed is used in supersonic inlets to control the effects of flow separation associated with shock boundary layer interactions on ramps, cowls and side walls. In order to predict the effect of bleed on the boundary layer development and internal shock structure, few investigators [1-3] included ramp chambers, throat plenum and exit louvers in their supersonic inlet flow simulations. However, because of the enormous increase in computational time and grid generation complexity, most investigators simulated the global effects of bleed by changing the boundary conditions [4-7] and/or the turbulence models [8,9] in the bleed regions. The imposed mass flux in the bleed area was based on experimental measurements in some investigations [7] and on empirical correlation of the bleed discharge coefficient in others [4-6]. Even when the turbulence model was modified for mass removal at the porous wall [8] the effect of bleed on boundary layer development was not adequately predicted.

Reproducing the experimentally measured boundary layer profiles over the porous wall even required the implementation of blowing rather than suction in the turbulence model [8]. Paynter et al. [9] used a rough wall algebraic turbulence model to simulate the increase in the growth rate of boundary layer induced by bleed, by changing the roughness parameter in the numerical solutions to the Navier-Stokes equations until the boundary layer profiles matched the experimental measurements [10, 11]. They determined that roughness was a strong function of the upstream boundary layer mass flux removed, in the bleed rates between 3% and 15%. However Paynter et al. pointed out that the experimental set-up whose data they used to develop their model, may have produced non uniformity in the mean velocity distribution and nonequilibirum boundary layer in the bleed region. In general, bleed models are restricted by the particular flow conditions and any inadequacies in the experimental data used in their model development. According to Hamed and Shang [12], the conclusions regarding the effects of bleed hole size and bleed location relative to the shock were not consistent among several experimental studies.

Hamed, et al. [13-18] and Remlinger, Shih and Chyll [19-22] followed an alternative approach to investigating bleed effects. They conducted numerical simulations in which the viscous flow field was resolved inside the individual bleed holes and slots. This approach helps in understanding the important local phenomena that control the flow in the bleed regions, and how they are affected by the bleed configuration, and the external flow conditions. These type of investigations can and have been used in simple flow configurations to study the relative effects of bleed/slot angle, size and location. They revealed the presence of a separation bubble near the hole/slot entrance and a "bleed shock" that initiates inside the hole/slot and attaches to the downstream corner under certain conditions. The size of the separation bubble which controls the bleed discharge coefficient is strongly affected by bleed hole/slot slant angle and less by the free stream

---

* Professor, Fellow AIAA.
** Post Doctoral Assistant, Member AIAA.
*** Student Member, AIAA.

conditions and plenum pressure. The boundary layer development downstream was strongly influenced by the bleed angle and the bleed shock strength.

The purpose of present numerical study is to investigate the effects of external flow and plenum conditions on bleed performance. In the investigated configuration bleed is applied to a flat plate turbulent boundary layer through a normal slot. The numerical solution to the viscous flow inside the slot and plenum and over the plate surface were obtained for supersonic flow with and without impinging shock at the slot's upstream corner. The flow computations were conducted over a range of plenum pressures up to choked bleed conditions. The results, which are compared with experimental data, show the flow characteristics inside the bleed slot and the effect of bleed on the boundary layer development downstream with and without incident shock.

Flow Configuration and Computational Details

In the investigated flow configuration shown schematically in Fig. 1, bleed is applied through a normal slot to the turbulent boundary layer on a flat plate. The bleed slot whose width is one centimeter and its depth 2.54 cm is connected to a 41.4 cm x 63.5 cm plenum. Outside of the slot, the solution domain extended 12.2 cm above and 40.9 cm along the flat plate surface. The boundaries AB and CD were located at 28.2 cm upstream and 12.7 cm downstream of the slot's upstream corner to match the locations of experimental velocity profile measurements in reference [6].

The flow computations were conducted using the PARC code [23] with the compressible k-ε turbulence model of Chien [24] modified by Nichols [25] for compressibility effects. The change in bleed mass flow rate was achieved through changing the static pressure at the plenum's outflow boundary. Referring to Fig. 1, the upstream boundary conditions consisted of free stream Mach number, stagnation pressure and stagnation temperature and a computed boundary layer velocity profile for flat plate computations which was matched to the experimentally measured profile's displacement and momentum thickness. The pre-shock and post-shock conditions were specified along the upper boundary to locate the inviscid incident shock at the upstream corner of the slot and flat plate surface. Flow variables were extrapolated at the downstream boundary and at the plenum's outflow boundary where the static pressure was specified to control the bleed mass flow. The initial conditions were specified from the solution without bleed for a given free stream Mach number. Subsequently, the computed flow field with the bleed slot and plenum was used to initialize the solutions at higher bleed mass flow rates (lower plenum pressure settings).

The computational grid shown in Fig. 2 includes a 308x68 grid over the flat plate surface, 89x68 grid inside the bleed slot and 187x148 grid inside the plenum chamber. Variable grid spacing was used in both x and y directions for grid clustering around the bleed walls, plenum chamber walls and at the plate surface, with $x_{min} = 0.9446 \times 10^{-3}$ cm and $y_{min} = 0.4755 \times 10^{-3}$ cm corresponding to $y^+ = 0.959$ at the inflow turbulent boundary layer at 2.46 free stream Mach number.

Results and Discussion

Typical results of the computed flow inside the slot near choked conditions are presented in Fig. 3 and compared with the experimental results of Davis et al. [27] reproduced in Figures 4 for incident oblique shocks whose inviscid impact point coincides with the slot's upstream corner at x=0. The figures present the pitot and static pressure contours for a shock generation angle $\alpha = 8°$, at 2.46 free stream Mach number. The computations predict very well both the shape and magnitude of the pressure contours inside the slot, the location of flow separation, and the size of the separation bubbles on the slot walls. The computed Mach number and velocity vectors, which are shown in Fig. 5, indicate flow angles of 33° from the plate surface, and high Mach numbers of 1.8 in a triangular region at the center of the slot opening. Disagreements can be observed between the experimental and computational results in this region. Since the pitot probe was always parallel to the slot walls in the experiment, one should expect discrepancies in these regions where the probe is oriented at 67° angle to the Mach 1.8 flow. The sharp gradients in the pressure across "bleed shock" were also not resolved by the measurements. The experiment indicates reattachment of the flow on the slot's downstream wall near the exit, which was not predicted by the computations.

Effect of Incident Shock

The effect of incident shock at the slot's upstream corner is demonstrated by comparing the computational results with and without the shock. Figures 6 and 7 present the computed Mach number and pressure contours inside the slot and in the neighboring regions over the plate surface and inside the plenum. The Mach number contours inside the slot indicate that when there is no incident shock, the separated flow region along the slot's upstream wall is much larger while the separated flow region over the slot's downstream wall near the exit is much smaller. In addition, the Mach number contours indicate less flow turning into the slot when there is no incident shock. This coincides with a weaker expansion fan at the slot's upstream corner as can be seen from the pressure contours. Also without incident shock, the "bleed shock" which originates inside the slot is quickly weakened outside

through interactions with a second expansion fan at the slot's downstream corner.

The maximum computed bleed mass flow with and without incident shock was 5.1% and 2.35% of the incoming boundary layer for the slot geometry (D/δ = 0.38). The pressure and Mach number contours indicate a separation bubble on the plate surface upstream of the slot in the case of incident shock. This is confirmed by the skin friction coefficient distribution of Fig. 8. One can see from Fig. 8 that there is a large difference in the predicted friction coefficients with and without incident shock within two slot widths downstream of bleed. In order to understand the cause of this difference, the mass flux, flow angle, and Mach number distribution across the slot opening are presented in Figs. 9-11. In the case of no incident shock, the mass flows out of the slot in the subsonic region behind the "bleed shock" and the downstream slot wall. This flow turns around the slot corner and forms the boundary layer over the plate surface. In the case of incident shock the subsonic flow goes into the slot opening in the region behind the "bleed shock", and the flow over the plate surface downstream originates outside the slot.

According to the velocity profiles of Fig. 12, the effect of incident shock is seen to extend over two to three slot widths upstream and downstream of the slot, where the distorted velocity profiles are less full near the plate. The distortion upstream is associated with the shock induced pressure gradient and flow separation. The shape of the profiles downstream is affected both by the local flow conditions above the slot and by the strength of the "bleed shock" at the slot opening. Since the incident shock reduces the flow velocity, the profiles downstream of the slot are less full near the wall. The "bleed shock", has smaller effect on the downstream velocity profiles in the case with no incident shock because it is quickly weakened by the expansion fan at the slot's downstream corner.

Plenum Interactions

A considerable part of the computational effort was consumed in modeling the flow field inside the plenum. The increased computational effort was not only associated with the number of grid points inside the plenum (50.6% of the total) but also with the slower convergence of the flow at low subsonic plenum speeds. In order to determine the nature of the plenum interactions with the bleed and external flow fields, the bleed mass flux was monitored at the slot opening (bleed inflow) and exit (bleed outflow) during the computations. Fluctuations persisted in the bleed mass at both inflow and outflow boundaries when the computations were conducted using local time stepping. The amplitude of the bleed mass flow fluctuations was higher at higher plenum pressures and diminished near choking. Subsequently one time accurate flow simulation was performed with α=8° incident shock at choked bleed conditions. The computational results indicated no fluctuations in the bleed mass flow at the slot's inflow boundary in this case and much smaller fluctuations in the bleed mass flow at the outflow boundary compared to the local time stepping results. Additional numerical computations with local time stepping were then performed without the plenum. The bleed mass flow in these computations did not fluctuate and coincided with the time accurate bleed mass flow at the slot's inflow boundary.

The discharge coefficient, Q, and the flow coefficient, F, are used to present the bleed mass flow data in nondimensional form. They are defined as follows:

$$Q = m_b / A_b P_r \left(\frac{\gamma}{RT_{t_{inf}}}\right)^{\frac{1}{2}} \left(\frac{2}{\gamma+1}\right)^{\frac{\gamma+1}{2(\gamma-1)}}$$

When the stagnation free stream value $P_{t_{inf}}$ is used for the reference pressure, P_r, the discharge coefficient, Q, represents the ratio between the bleed mass flow and the ideal mass flow that could pass into the slot at sonic conditions if the flow was to expand isentropically to fill the bleed area A_b. On the other hand, the flow coefficient represents the ratio between the bleed mass flow and the mass flow that would pass through the bleed area at the flow conditions $\rho_e U_e$ outside the boundary layer

$$F = m_b / A_b \rho_{inf} U_{inf}$$

The predicted variation in the discharge coefficient with plenum pressure is presented in Fig. 13 with the experimental results of references [26] and [27]. The figure shows the computed bleed mass flow without plenum, as well as the range of bleed mass flow fluctuations in the computations with plenum using local time stepping. The computations without plenum agree with the experimental data in the case of incident shock, but under-predict the bleed mass flow without shock over the range of plenum pressures. The much higher discharge coefficient in the case of incident oblique shock can be caused by the increased static pressure above the slot and/or the velocity distortion upstream. In order to separate the two effects, a bleed discharge coefficient based on the local static pressure, P_{loc}, is presented in Fig. 14. The value of the local static pressure was taken as P_{inf} for no incident shock and P_1, the inviscid static pressure behind the incident shock (P_1/P_{inf} = 1.7). This figure indicates that the difference in the computed discharge coefficient with and without incident shock becomes smaller based on this normalization. The remaining

difference can be attributed to the incoming velocity profile distortion by the incident shock.

Conclusions

Numerical simulations were conducted for supersonic flow at Mach 2.46, with bleed applied through a normal slot with and without incident shock at the slot's upstream corner. The computed results agree with the experimental measurements inside the slot in the case of incident shock. The computations indicate higher flow angles at the slot opening and a narrower separation bubble on the slot's upstream wall in the case of incident shock which leads to higher discharge coefficient. The "bleed shock" which originates inside the slot and extends as an oblique shock outside is quickly weakened in the case with no incident shock by the interactions with an expansion fan at the slot's downstream corner.

The plenum caused fluctuations in the bleed mass flux at the slot exit but time accurate computations at choked conditions indicated that these disturbances did not affect the flow and mass flux at the slot opening. The fluctuations were associated with the lateral movement of the bleed flow between the two separation bubbles on the slot walls. The computed bleed mass flow without plenum coincided with the predicted steady value at the slot inlet in the time accurate numerical simulations with plenum. The experimental data for bleed mass flow agreed with the computations in the case of incident shock but were higher with no incident shock.

Acknowledgements

This work was sponsored NASA Grant NAG3-1213, Dave Saunders, Project Monitor. The computational work was performed on the CRAY YMP of the Ohio Supercomputer.

References

1. Forester, C.K., and Tjonneland, E., "New Guide for Accurate Navier-Stokes Solution of Two-Dimensional External Compression Inlet with Bleed," International Council of the Aeronautical Sciences 88-2.5.1, 1988.

2. Fujimoto, A., Niwa, N., and Sawada, K., "Numerical Investigation on Supersonic Inlet with Realistic Bleed and Bypass Systems," AIAA Paper 91-0127,. Jan. 1991.

3. Fujimoto, A. and Niwa, N., "Experimental and Numerical Investigation of Mach 2.5 Supersonic Mixed Compression Inlet," AIAA 93-0289, January 1993.

4. Abrahamson, K.W., "Numerical Investigation of a Mach 3.5 Axisymmetric Inlet," AIAA 93-0289, January 1993.

5. Benhachmi, D., Greber, I. and Hingst, W., "Experimental and Numerical Investigation of an Oblique Shock-Wave/Turbulent Boundary Layer Interaction with Continuous Suction," AIAA Paper 89-0357, January 1989.

6. Saunders, J.D. and Keith, T.G., Jr., "Results from Computational Analysis of a Mixed Compression Supersonic Inlet," AIAA 91-2581, June 1991.

7. Reddy. D.R., Benson, t.J., and Weir, L.J., "Comparison of 3-D Viscous Flow Computations of March 5 Inlet with Experimental Data," AIAA Paper 90-0600, Jan. 1990.

8. Lee, D.B. and Leblanc, R., "Interaction onde de Choc Oblique-Couch Limite sur Paroi Poreuse avec Aspiration," Paper 23, AGARD CP-365, "Improvement of Aerodynamic Performance Through Boundary Layer Control and High Lift Systems," August 1984.

9. Paynter, G.C., Treiber, D.A., and Keerling, W.D., "Modeling Supersonic Inlet Boundary Layer Bleed Roughness," J. of Propulsion and Power, Vol. 9, No. 4, 1994, pp. 622-627.

10. Schuehle, A.L., "Tabulation of the Boundary Layer Profile Data Taken for the SST Bleed System Development and Performance Test," Boeing METM-70-50. August 26, 1970.

11. Mayer, D.W., "Turbulent Supersonic Boundary Layer Flow in an Adverse Pressure Gradient Including the Effects of Mass Bleed," MSME Thesis, University of Washington, 1977.

12. Hamed, A. and Shang, J., "Survey of Validation Data Base for Shock Wave Boundary Layer Interactions in Supersonic Inlets," Journal of Propulsion, Vol. 7, No. 4, July 1991, pp. 617-625.

13. Hamed, A., Shih, S. and Yeuan, J.J., "Investigation of Shock/Turbulent Boundary-Layer Bleed Interactions," Journal of Propulsion and Power, Vol. 10, No. 1, Jan.-Feb. 1994, pp. 79-87.

14. Hamed, A., Yeuan, J.J. Shih, S.H., "An Investigation of Shock Wave Turbulent Boundary-Layer Interaction with Bleed through Slanted Slots," AIAA Paper No. 93-2992, July 1993.

15. Hamed, A., Yeuan, J.J. and Shih, S.H., "An Investigation of Bleed Through Normal and Slanted Slots in Shock Wave Turbulent Boundary Layer Interaction," AIAA Paper No. 93-2155, June-July 1993.

16. Hamed, A., Shih, S.H. and Yeuan, J.J., "A Parametric Study of Bleed in Shock Boundary Layer Interactions," AIAA Paper No. 93-0294, January 1993.

17. Hamed, A. and Lehnig, T., "Effect of Bleed Configuration on Shock/Laminar Boundary-Layer Interactions," *to appear in* J. of Propulsion & Power, Vol. 11, No. 1, Jan. Feb. 1995.

18. Hamed, A. and Lehnig, T., "Investigation of Oblique Shock/Boundary-Layer Bleed Interaction," J. of Propulsion and Power, Vol. 8, No. 2, March-April 1992, pp. 418-424.

19. Rimlinger, M.J., Shih, T.I-P and Chyu, W.J., "Three-Dimensional Shock-Wave/Boundary-Layer Interactions with Bleed Through Multiple Holes," AIAA Paper 94-0313, January 1994.

20. Shih, T.I-P, Rimlinger, M.J. and Chyu, W.J., "Three-Dimensional Shock-Wave/Boundary Layer Interactions with Bleed," AIAA Journal, Vol. 31, No. 10, 1993, pp. 1819-1826.

21. Chyu, W.J., Rimlinger, M.J. and Shih, T.I-P, "Effects of Bleed-Hole Geometry and Plenum Pressure on Three-Dimensional Shock-Wave/Boundary Layer/Bleed Interactions," AIAA Paper 93-3259, July 1993.

22. Rimlinger, M.J., Shih, T.I-P and Chyu, W.J., "Three-Dimensional Shock-Wave/Boundary-Layer Interactions with Bleed Through a Circular Hole," AIAA Paper 92-3084, July 1992.

23. Cooper, G.K., and Sirbaugh, J.R., "PARC Code: Theory and Usage," AEDC-TR-89-15, 1989.

24. Chien, K-Y, "Prediction of Channel and Boundary-Layer Flows with a Low Reynolds Number Turbulence Model," AIAA Journal, Vol. 20, January 1982, pp 33-38.

25. Nichols, R. H., "A Two-Equation Model for Compressible Flows," AIAA Paper 90-0494, AIAA 28th Aerospace Sciences Meeting, Reno, NV, January 1990.

26. Willis, B., Davis, D. and Hingst, W., "Flow Coefficient Behavior for Boundary-Layer Bleed Holes and Slots," AIAA Paper 95-0031, 33rd Aerospace Sciences Meeting, Reno, Nevada, January 9-13, 1995.

27. Davis, D., Willis, B. and Hingst, W., "Flowfield Measurements in Slot-Bled Oblique Shock-Wave and Turbulent Boundary-Layer Interaction," AIAA Paper 95-0032, 33rd Aerospace Sciences Meeting, Reno, Nevada, January 9-13, 1995.

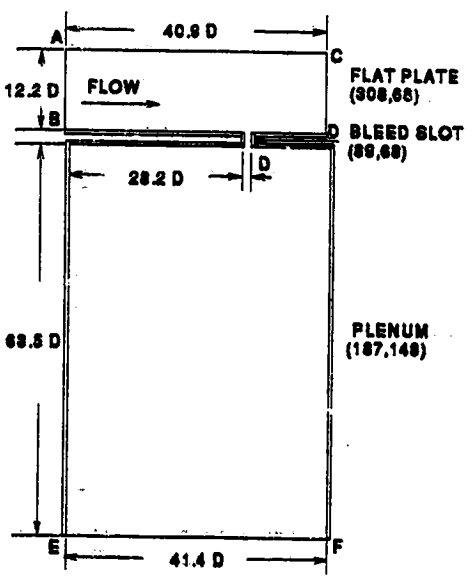

Fig. 1. Schematic of Computational Domain.

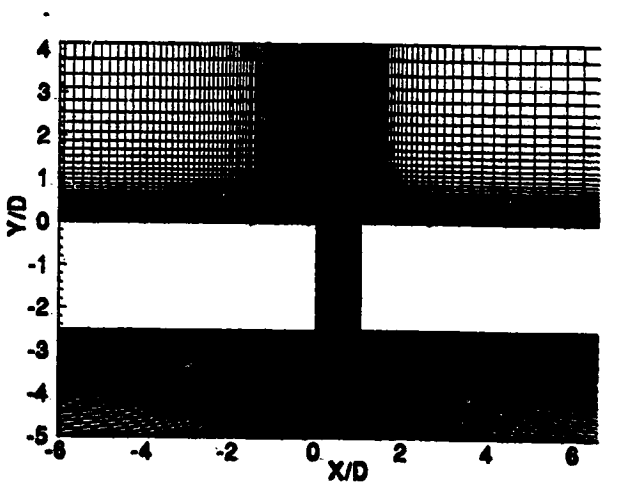

Fig. 2. Computational Grid Near Bleed Slot.

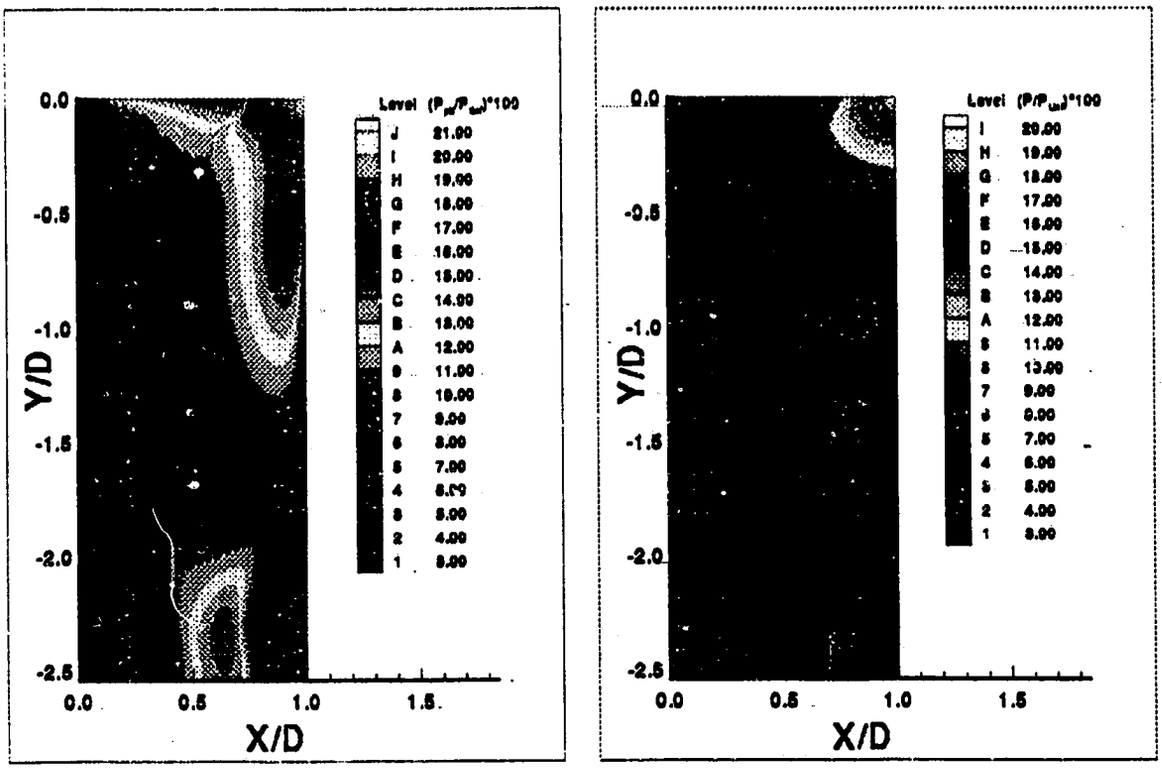

Fig. 3. Pitot and Static Pressure Contours Inside Slot (Computational Results) M = 2.46, α = 8°.

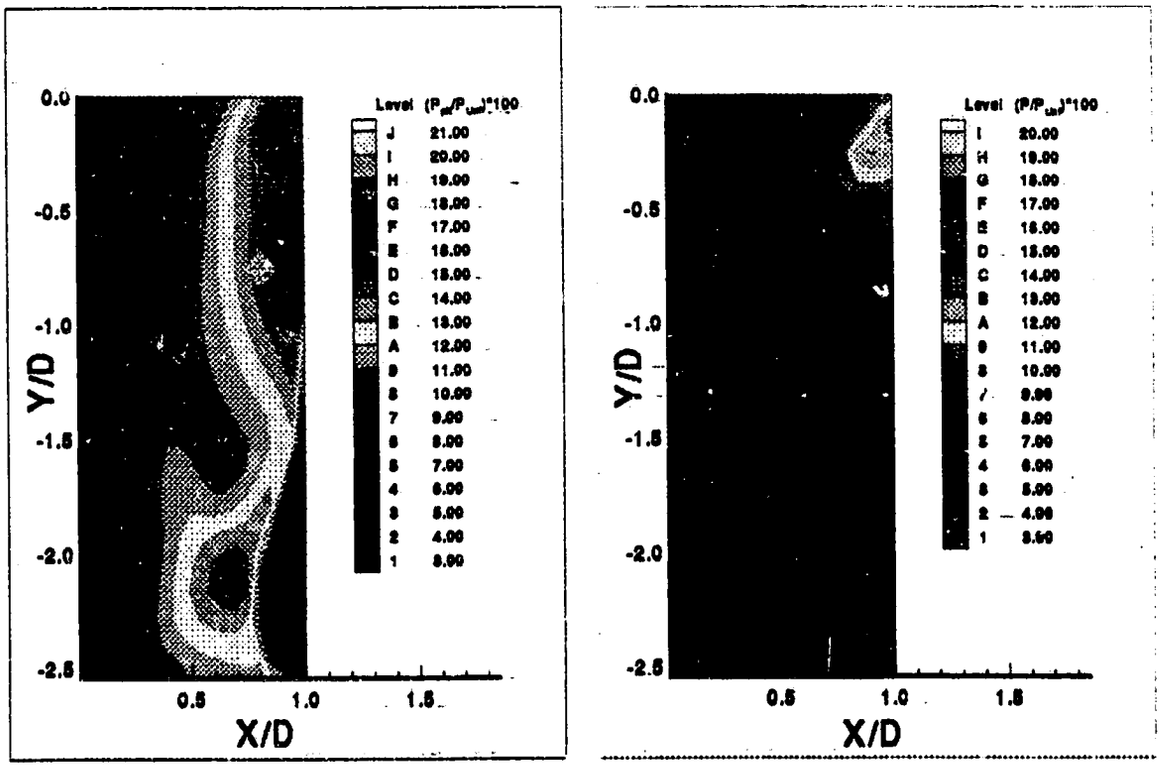

Fig. 4. Pitot and Static Pressure Contours Inside Slot (Experimental Results [27]) M = 2.46, α = 8°.

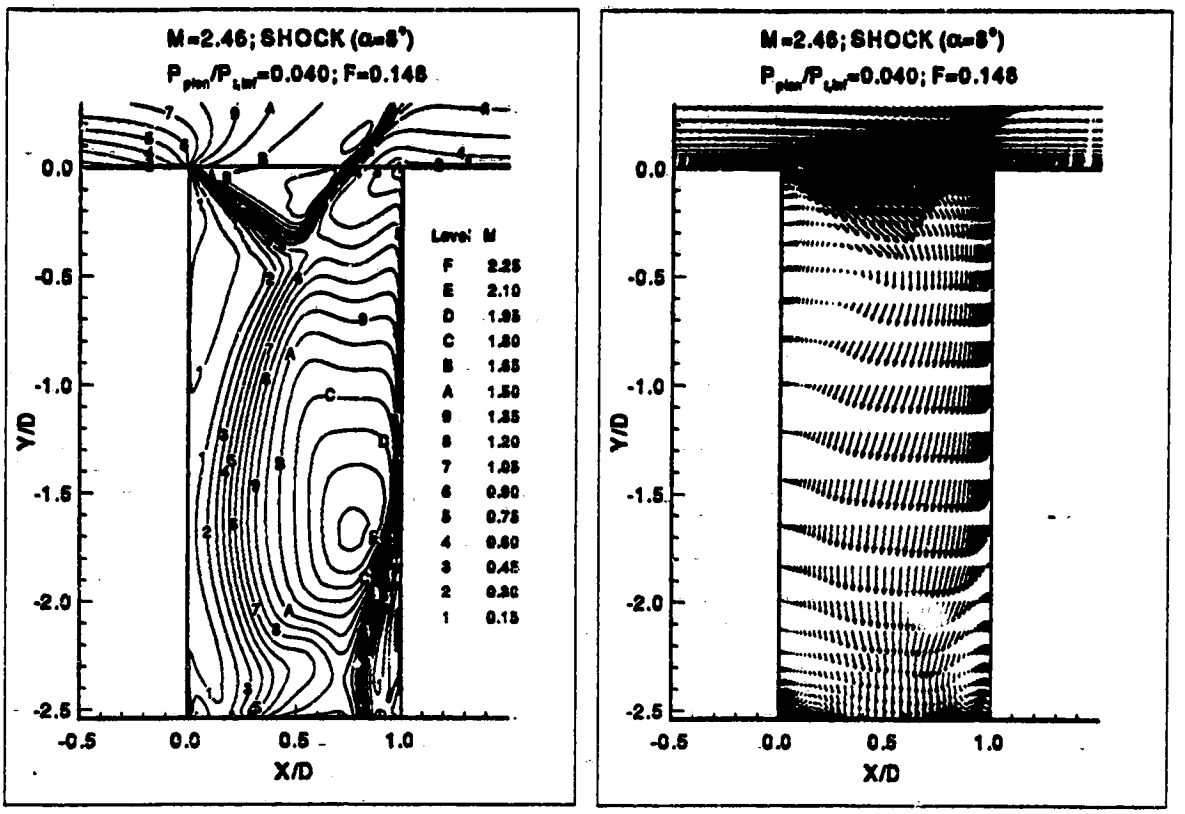

(a) Mach Number Contours (b) Velocity Vectors

Fig. 5. Velocity Field Inside Slot

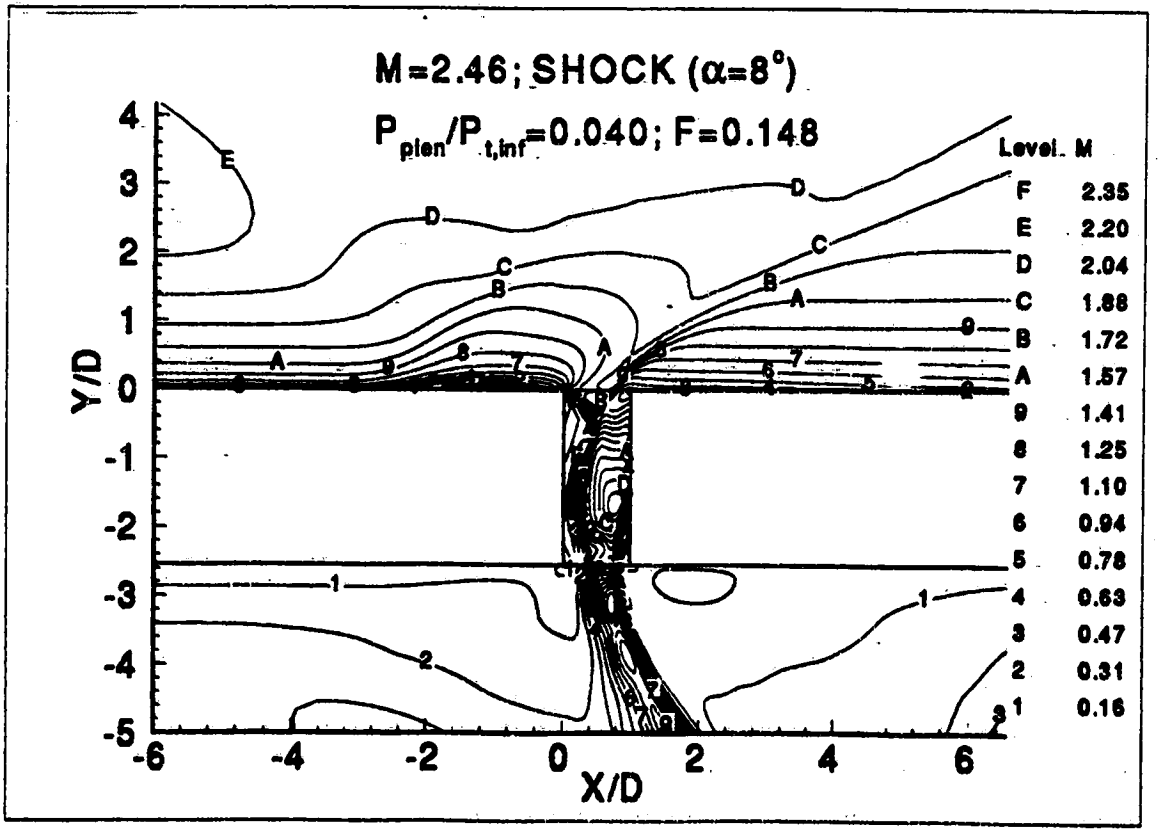

(a) With Incident Shock

Fig. 6. Comparison of the Mach Number Contours With and Without Incident Shock

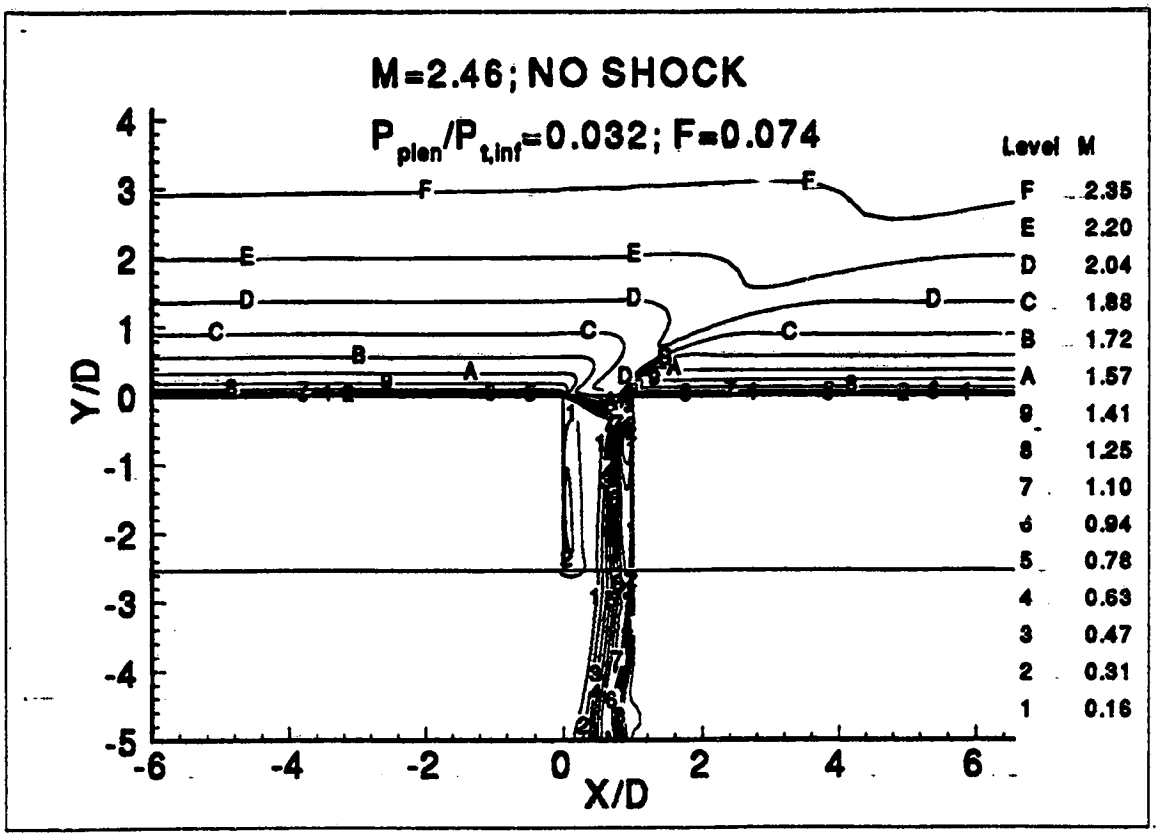

(b) Without Incident Shock

Fig. 6. Comparison of the Mach Number Contours With and Without Incident Shock

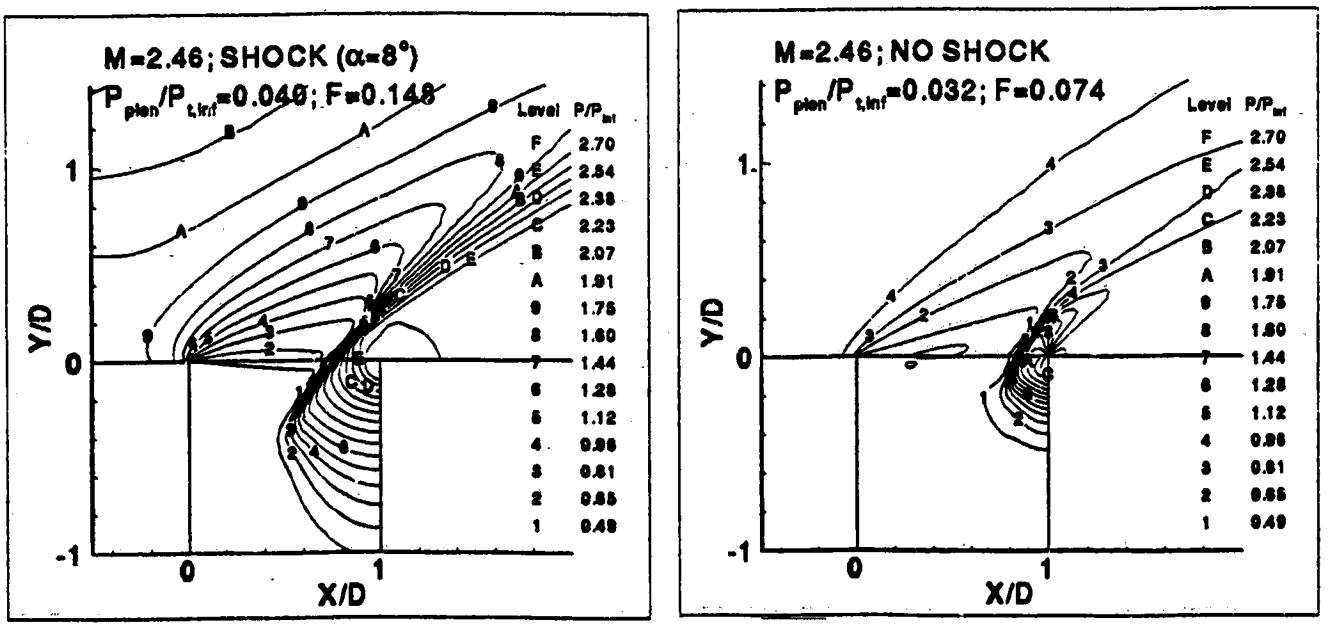

(a) With Incident Shock

(b) Without Incident Shock

Fig. 7. Comparison of the Pressure Contours With and Without Incident Shock

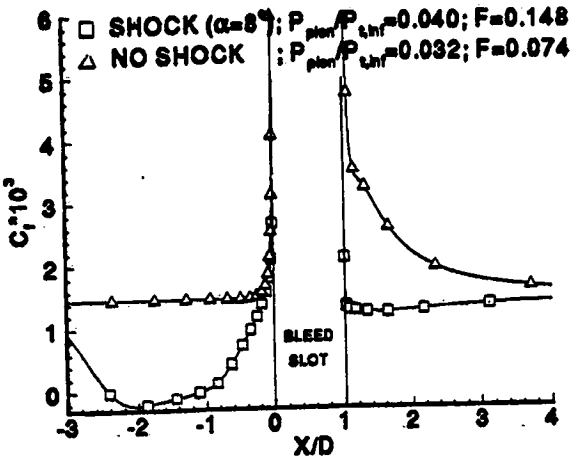

Fig. 8. Skin Friction on the Plate Surface.

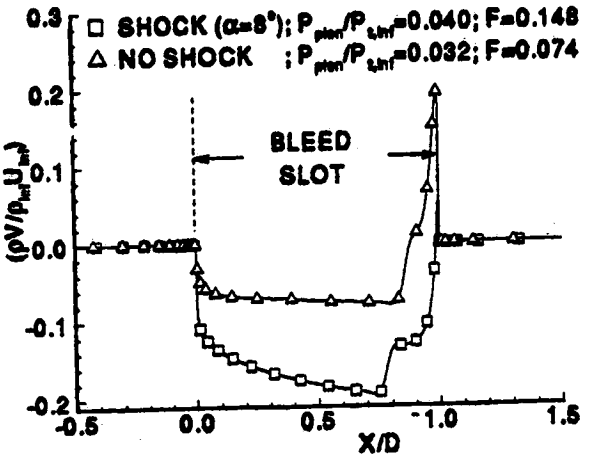

Fig. 9. Bleed Mass Flux Across Slot Opening

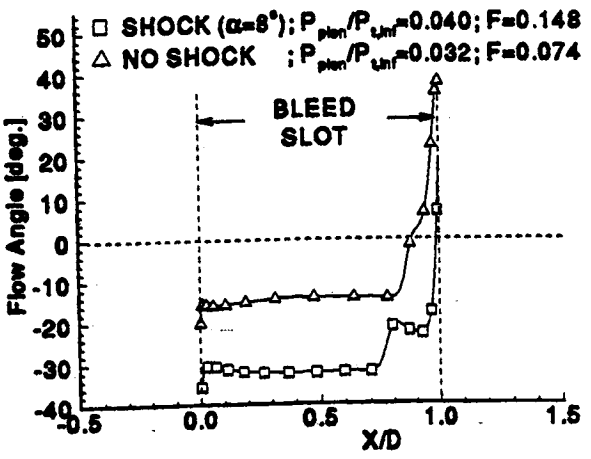

Fig. 10. Flow Angle Across Slot Opening.

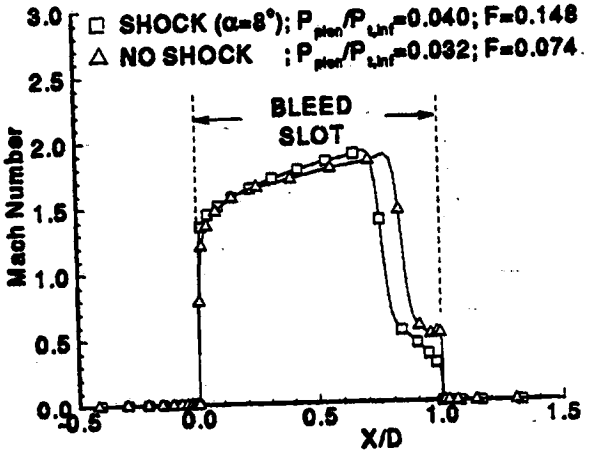

Fig. 11. Mach Number Across Slot Opening.

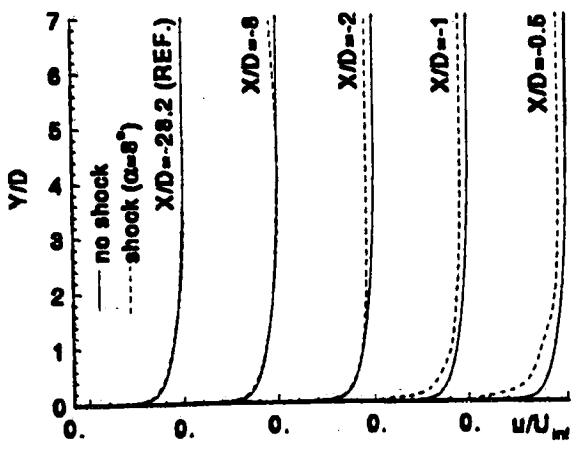

(a) Upstream of Bleed Slot

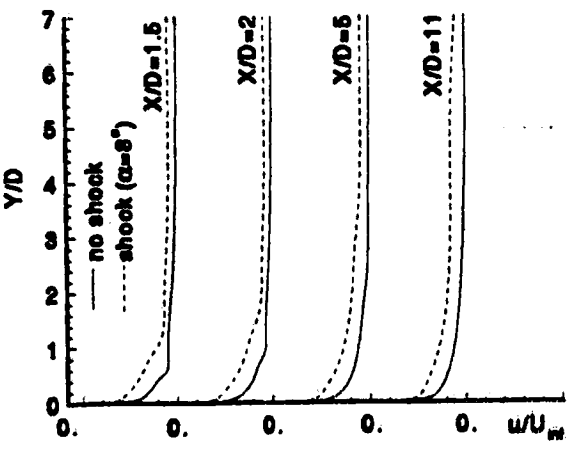

(b) Downstream of Bleed Slot

Fig. 12. Boundary Layer Velocity Profiles

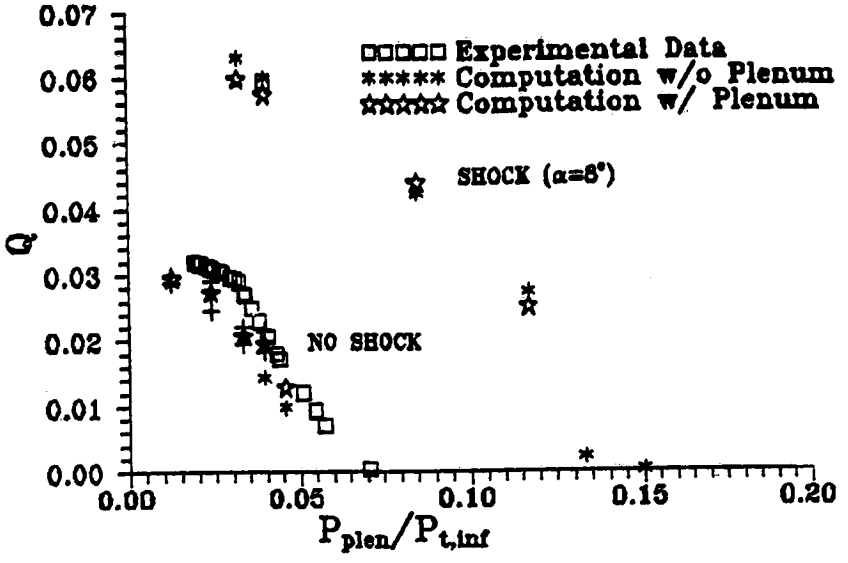

Fig. 13. Bleed Discharge Coefficient Based on $P_{t_{inf}}$

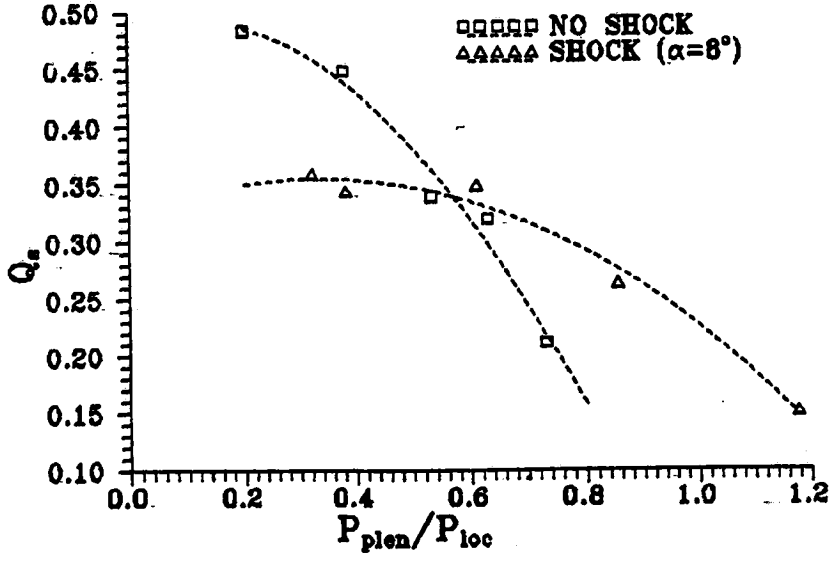

Fig. 14. Bleed Discharge Coefficient Based on P_{loc}